Univerzita Karlova v Praze
Přírodovědecká fakulta
Ústav hydrogeologie, inženýrské geologie a užité geofyziky

Studijní program: Aplikovaná geologie
Studijní obor: Užitá geofyzika

Václav Kuna

Výskyt teleseismicky zaznamenaných zemětřesení a subdukcí vyvolané magmatické procesy pod ostrovními oblouky

Teleseismic earthquake occurrence and subduction-induced volcanic activity along island arcs

DIPLOMOVÁ PRÁCE

Vedoucí závěrečné práce: RNDr. Aleš Špičák CSc.

Praha, 2013

Prohlašuji, že jsem závěrečnou práci zpracoval samostatně a že jsem uvedl všechny použité informační zdroje a literaturu. Tato práce ani její podstatná část nebyla předložena k získání jiného nebo stejného akademického titulu.

V Praze, 17.8.2013 Václav Kuna

Poděkování

Rád bych poděkoval všem, kdo se podíleli na vzniku mé diplomové práce. Zejména chci poděkovat vedoucímu práce RNDr. Aleši Špičákovi CSc. a konzultantu RNDr. Jiřímu Vaňkovi DrSc. za cenné rady v průběhu práce a velmi trpělivé korektury. Děkuji taktéž všem členům oddělení Tektoniky a geodynamiky za vytvoření přátelského pracovního prostředí. Dále bych rád poděkoval doc. RNDr. Tomáši Fischerovi, Ph.D. za kurz aplikované seismologie, který mi umožnil základní seznámení se seismostatistikou a který ve svém důsledku tuto práci nasměroval.

Contents

1. Introduction

The world's largest earthquakes, the most destructive tsunamis and the most explosive volcanism are generated at subduction zones at convergent plate margins. These areas are often highly populated, with important mineral resources accumulated over geologic time. Despite of the high societal and economic importance of subduction zones, many processes and problems still remain poorly understood and unresolved. Many research institutions and projects around the world have concentrated on the investigation of convergent plate margins, e.g., the *National Oceanic and Atmospheric Administration* (NOAA), *Integrated Ocean Drilling Program* (IODP), *Japan Agency for Marine-Earth Science and Technology* (JAMSTEC), long-lasting projects of the *US National Science Foundation MARGINS* and *GeoPRISMS, etc.* The investigation of subduction zones is demanding both due to high expenses of instrumental equipment and complexity of the field research.

The plate tectonics group of the *Institute of Geophysics of the Academy of Sciences of the Czech Republic* has been exploring the processes at convergent plate margins since early 70's. Due to the limited resources available, field exploration cannot be conducted and the research is based on the analysis of the open data sources, such as global earthquake catalogues. The following phenomena have been studied at the Institute of Geophysics in particular: disastrous earthquakes (e.g. Vaněk et al., 2000; Špičák et al., 2007), accumulation of metals (e.g. Hanuš et al., 2000), complexity of the process of subduction (Hanuš and Vaněk, 1985; Špičák and et al., 2004, 2005), and recently namely seismo-volcanic interactions (e.g. Špičák et al., 2005, 2008, 2011, 2013a, b). This thesis continues in the investigation of seismo-volcanic interactions.

Seismicity pattern beneath volcanoes is usually examined in order to understand processes in magmatic chambers and to predict volcanic activity (e.g. Konstantinou and Schlindwein, 2002; Roman and Cashman, 2006). Seismicity reflects mechanical properties of the rock environment, too. Earthquake occurrence points to a brittle behavior whereas the absence of earthquakes may reflect partial melting of the environment. Seismicity pattern beneath volcanoes is specific by frequent occurrence of earthquake swarms. Earthquake swarms are thought to be triggered by magma intrusions into the prestressed brittle medium. This idea

can be applied to submarine parts of volcanic arcs where our knowledge of recent volcanic activity is rather poor. In this case specific seismicity pattern may point to recent magma ascent at these areas hidden from the direct observations of magmatic/volcanic processes. For example, a recently active submarine volcano was found in the Andaman-Nicobar volcanic arc by Kamesh Raju at al. (2012), after an analysis of a remarkable seismic sequence. Specific earthquake occurrence probably accompanied recent magmatic activity of the Suyio, Mokuyo and Doyo seamounts in the Izu-Bonin volcanic arc (Yuasa et al., 1991; Špičák et al., 2009).

The above mentioned investigations into the seismo-volcanic interactions at convergent plate margins were focused on particular regions. The aim of this diploma thesis is to establish a statistical apparatus appropriate for analyzing earthquake occurrence at subduction zones globally and to apply this apparatus to constrain areas of possible magma migration in the crust.

At the beginning of the thesis I shortly summarize basic concepts of volcanism at convergent plate margins and basic seismological principles. In the next chapters I describe the data used and regions of investigation. Two following chapters comprise the description of analyses applied in the thesis – the fractal dimension analysis and the b-value analysis. The results of the analyses and the interpretations are then presented for individual regions of interest.

2. Volcanism at convergent plate margins

The large portion of world's volcanism occurs at convergent plate margins with ongoing subduction. Subduction-related volcanoes usually form linear or curved belt chains called volcanic arcs. These arcs are positioned on the overlying plate, parallel to the plate margin that is usually morphologically expressed by a deep trench at the sea floor. An arc can be placed either on the oceanic or continental lithosphere.

The first case occurs when an oceanic lithosphere subducts under another oceanic lithosphere. Volcanoes form islands and the volcanic arc is called *island arc*. This type of arc can be found in the western Pacific: Aleutians, Kuriles, Izu-Bonins, Marianas, New Hebrides or Tonga-Kermadec. If the production of magma along the arc is sufficiently high, volcanic islands interconnect and form an extensive area of land built on the oceanic lithosphere. Such an environment forms in New Zealand, Japan, Kamchatka, the Cascades and Java (Davidson, J. P., 1991).

If the oceanic lithosphere subducts under the continental one, volcanic arcs are formed on the continental lithosphere. This type of volcanic arcs is represented by Andean South America (Davidson, J. P., 1991).

2.1. Types of subduction zones

Subduction of oceanic lithosphere is partly driven by the density difference between the lithosphere and the underlying mantle. Density of the oceanic lithosphere is largely controlled by its age (Uyeda and Kanamori, 1979; Uyeda, 1982; Conrad and Lithqow-Bertelloni, 2002). Lithosphere close to a spreading center is thin, hot, and therefore buoyant. As it moves away from the spreading center, it becomes thicker and colder and its density grows.

A relatively old and dense slab sinks rapidly, subsiding at a steep angle, around 60° for Mariana subduction (Syracuse an Abers, 2006), causing the process known as slab rollback (Heuret and Lallemand, 2005). The slab sweeps back through the mantle and pulls the upper plate along, which can lead to a spreading in a backarc area and formation of the

backarc basin. This type of arcs is referred to as the *Mariana type* and is common in the western Pacific.

If the lithosphere is young and buoyant, the slab sinks at a gentle angle. This type of behavior is observed e.g. in Chilean subduction zone (the subduction dip is about 25°) and it is called the *Chilean type*. The lower angle of subduction causes an increase in compressional stresses that are transmitted to the upper plate. Therefore, this process may lead to compressional deformations of the crust, such as folding and thrust faulting. The convergence rate also influences the angle of subduction – a higher rate leads to shallowing of subduction (Uyeda and Kanamori, 1979; Uyeda, 1982).

2.2. Magma source and composition

The trigger of the magmatic processes is depth- or pressure-dependent. It implies that the depth of the subducting slabs beneath the volcanic arcs is always the same, independent on the slab dip. The distance between the volcanic arc and the trench is variable and depends on the slab dip (Syracuse and Abers, 2006).

According to one of the theories, magma is generated within the mantle wedge above the subducting slab (e.g. Schmidt, 1998). In such a case, melting of the mantle is thought to be a consequence of hydration of the wedge by the volatiles released from the subducted slab. The volatiles cause lowering of the solidus of the wedge. This hypothesis of magma generation is supported by thermal models of subduction zones. Thermal models assume that the temperature of the subducting slab at depths between 100 and 150 km is below the solidus due to a lack of volatiles at these depths (Schmidt, 1998).

Another assumption, based on the analysis of spatial distribution of earthquakes at subduction zones, has been proposed by Hanuš and Vaněk (1985). They noted the absence of teleseismic earthquakes in the Wadati-Benioff zone (WBZ) at depths between 100 and 200 km. In addition to this, strong seismicity in the wedge above this aseismic zone was reported by Špičák et al. (2004, 2005) beneath some volcanoes. The absence of earthquakes in the WBZ is thought to be a consequence of the change of rheological properties of the rock environment, probably due to partial melting. Contrarily, strong seismicity beneath some volcanoes points to the fact that the rock environment beneath them is capable of brittle failure and thus probably not melted. This led to the conclusion that the magma source areas could be placed directly within the subducting slab.

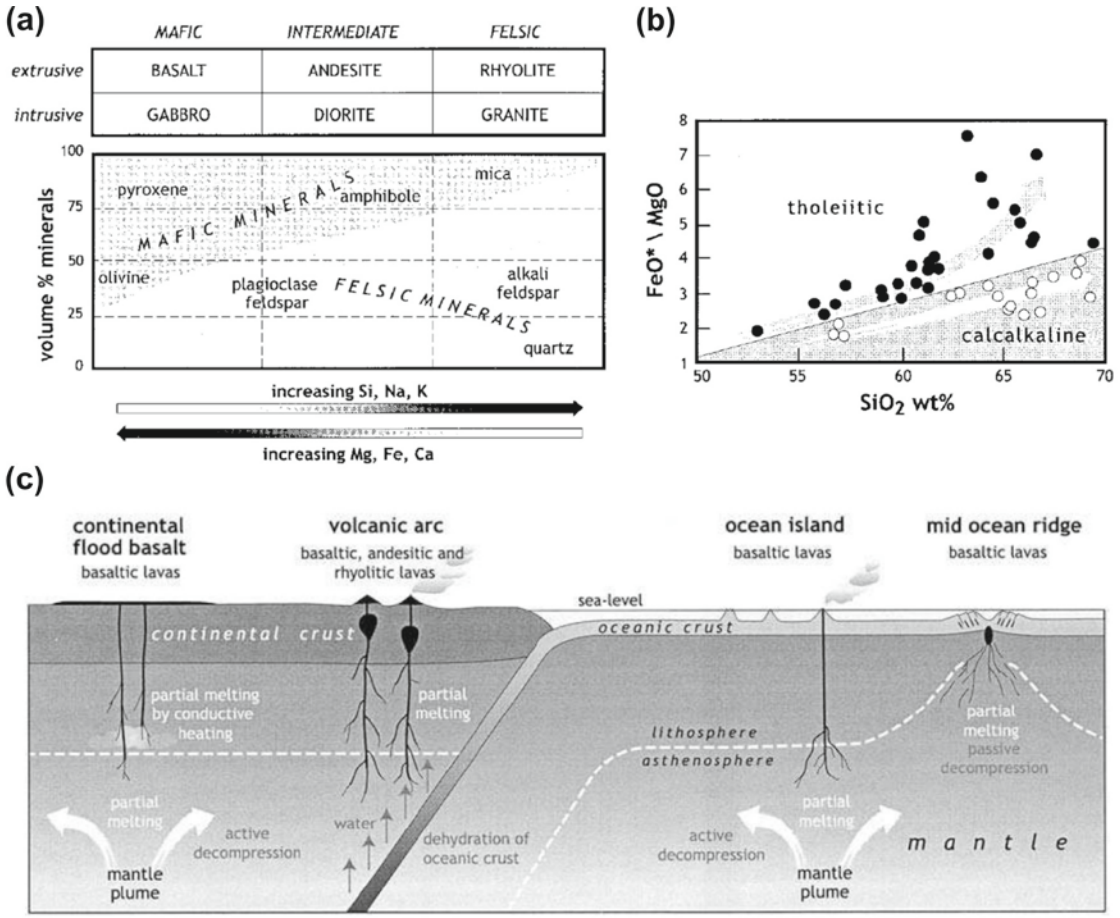

Fig. 1. Magma composition. (a) Mineralogy and the general compositional characteristics of the most common igneous rock types. (b) The difference between calc-alkaline and tholeiitic rocks expressed by contrasting FeO/MgO ratios. (c) A schematic vertical section through a continent and ocean showing crust and mantle lithosphere and melting mechanisms for Mid-Ocean Rift Basalts , Ocean Island Basalts, island arcs, and continental flood basalts. Reprinted from Sigurdsson (2000).

Magma composition depends on the tectonic position of its source and influences volcanic processes at the surface. Explosivity of eruptions grows with the growing viscosity of the magma, controlled by the content of felsic minerals and fluids in the magma. The most common rock type at volcanic arcs at subduction zones is calc-alkaline andesite (about 60 % of SiO_2, high content of calcium, potassium and sodium, depleted in magnesium and iron) (Fig. 1a). The calc-alkaline character makes calc-alkaline magma distinct from the volcanic rocks at mid-ocean ridges that are of tholeitic character (poor in sodium and potassium) (Fig. 1b). Eruptions at island arcs are usually of Plinian character producing ejecta in the form of ash and dust. Occurrence of basaltic or rhyolitic rocks is sparse at

volcanic arcs and depends on the rate of fractional crystallization of the ascending magma. Basalts may occur at oceanic arcs, they are usually represented by pillowed basalts and large volumes of hyaloclastic tuffs and breccias (Condie, 1997). Dacites sometimes occur at the continental convergent margins (Fig. 1c) (Sigurdsson, 2000).

3. The seismological background

An earthquake is a sudden release of energy accompanied by generation of seismic waves. Earthquakes are almost always related to faults – internal surfaces in the Earth along which blocks of rocks move. Earthquakes are explained by the elastic rebound theory (Reid, 1910), according to which the blocks on both sides of a fault move with respect to each other, but friction locks the fault for a certain time interval (years, decades, or even more) and prevents movement. After the stress accumulated in the medium reaches the value of friction forces, the fault slips and releases energy in the form of seismic waves (Michelson, 1917). This behavior of rocks is described as brittle-elastic; rocks behave in this way at low temperatures and high strain rates (Park, 1983). Earthquakes cannot occur in a medium with an elevated temperature and a low confining pressure (e.g. in melted or partially melted rocks) because such a medium behaves in a plastic or viscous manner. In such an environment, mechanical energy cannot be accumulated.

3.1. Earthquake parameters

Three basic parameters are used for the description of earthquakes: location, origin time, and magnitude. In the case of the felt, and particularly disastrous earthquakes, intensity is an additional parameter for describing their consequences.

3.1.1. Location and origin time

Location is the essential parameter in the earthquake description. It is comprised of three space components – latitude and longitude of the epicenter and depth of the hypocenter. The location parameters are determined by the travel-time curves (the dependence of time of wave propagation on epicentral distance) and the location itself is based on the readings of first onsets of individual seismic waves. Location is closely connected with the calculation of another essential parameter – the earthquake origin time.

3.1.2. Magnitude

Magnitude characterizes the strength of an earthquake. It reflects energy of seismic waves released during an earthquake and depends on the size of the fault that moves, and on the triggering stress. Magnitude determination is based on reading of the maximum amplitude of seismic waves recorded on the seismogram. All magnitude scales have a general form:

$$M = \log_{10}\left(\frac{A}{T}\right) + F(h, \Delta) + C, \quad (1)$$

where A is the maximum amplitude of the signal, T is its dominant period, F is the calibrating function for the variation of the amplitude with the epicentral distance Δ and the earthquake depth h, and C is the regional scale factor. Magnitude scales are logarithmic – an increase in one unit of magnitude corresponds to a ten-fold increase of the seismic wave amplitude (Lowrie, 2007).

Principles of magnitude determination were introduced by Beno Gutenberg and Charles Richter in 1935 (Richter, 1935). They used magnitude scale for description of local earthquakes in California. Their method was based on measuring of the surface wave maximum amplitude on the Wood-Anderson seismograph in the epicentral distance of 100 km. Because the waves are measured in a short epicentral distance by this method, the magnitude scale is described as the *local magnitude* M_L (or simply "*Richter scale*").

For epicentral distances larger than 20° several methods of magnitude estimation were developed. The surface-waves magnitude is defined by the *International Association for Seismology and Physics of the Earth's Interior* (IASPEI) as:

$$M_s = \log_{10}\left(\frac{A_s}{T}\right) + 1.66\log_{10}(\Delta) + 3.3, \quad (2)$$

where A_s is the vertical component of the ground motion in micrometers (μm) determined from the maximum Rayleigh wave amplitude, T is the wave period (commonly around 20 s), Δ is the epicentral distance in degrees ($20° \leq \Delta \leq 160°$). As the amplitude of the surface waves strongly depends on the focal depth of the earthquake, the surface-wave magnitude is considered as a reliable parameter only for earthquakes with focal depths less than 50 km.

In order to exclude the depth-dependency of the magnitude, Gutenberg (1945) proposed an equation that calculates magnitude from the maximum amplitude of the ground motion related to P-waves - the body-wave magnitude (m_b). Amplitude of body waves depends

only on the distance from the earthquake focus and is independent on the focal depth. The relation is defined as:

$$m_b = \log_{10}\left(\frac{A_p}{T}\right) + Q(\Delta, h), \tag{3}$$

where A_p is the maximum amplitude of the P-wave having the period (T) of less than 3 s, $Q(\Delta, h)$ is an empirical correction for the signal attenuation due to the epicentral distance (Δ) and the focal depth (h).

The surface-wave magnitude M_s and the body-wave magnitude m_b often differ for larger ($M \geq 5$) earthquakes. This is caused by the different methods of magnitude determination – while surface-wave magnitude is derived from low-frequency signal ($f \sim 0.05\ Hz$), body-wave magnitude uses waves with higher frequencies ($f \sim 1\ Hz$) (Lowrie, 2007).

A serious problem of magnitude determination, in particular for very large earthquakes ($M \geq 7$), is the effect of saturation. From a certain level of energy released during an earthquake, amplitudes of seismic wave cannot be amplified and the magnitude became saturated. The effect of saturation starts to influence the magnitude estimation around the magnitude 5 (if body waves are measured) and 7 (for surface waves). From the saturation level the magnitude does not correctly reflect the earthquake strength and underestimates the real amount of energy released.

An alternative way to determine magnitude of very large earthquakes is based on the analysis of the long-period spectrum of the seismic wave. The method, introduced by Hanks and Kanamori (1979), uses a quantity called seismic moment for magnitude determination. Seismic moment M_0 well represents measure of the energy released during an earthquake. It is defined as

$$M_0 = \mu S D, \tag{4}$$

where S is the area of the segment of the fault plane fractured during an earthquake, D is the displacement of the rock blocks that slipped, and μ is the rigidity modulus of the rocks adjacent to the fault. The moment magnitude is defined using the seismic moment:

$$M_W = \frac{2}{3}(\log_{10} M_0 - 9.1), \tag{5}$$

where M_W is expressed in Nm (SI units). The moment magnitude is possible to determine only for well-recorded large events of $M_W \geq 5$..

3.1.3. Macroseismic intensity

Macroseismic intensity is a descriptive measure of effects of shaking. Its value is linked to the position of an observer and not to the earthquake itself. There is an empirical relation between the intensity and the magnitude. Intensity estimation is based on macroseismic observations and not on instrumental observations. Macroseismic intensity does not depend only on the strength of an earthquake, but also on the distance from the epicenter and on the geological structure of the shaken area. The most commonly used intensity scales are the Modified Mercalli intensity (MMI) scale, the European Macroseismic Scale (EMS) ranging from I (nearly unfelt) to XII (destructive earthquake) (Lowrie 2007) or Medvedev–Sponheuer–Karnik (MSK) scale.

3.2. Seismic sequences

Earthquake occurrence is a complex natural phenomenon. It varies in time, space and magnitude. Despite of this complexity earthquake occurrence is not always a purely random process. Individual earthquakes can be linked together both in time and in space, and their spatial distribution is linked to tectonic structures at all scales – e.g. single faults, fault systems or plate boundaries.

Among the non-random manifestations of seismicity, earthquake sequences are the most studied phenomena. Seismic sequence is defined as an accumulation of earthquakes in a relatively short time interval and a relatively small area. Seismic sequence may be of various character according to number of events, their magnitudes, seismicity pattern (swarm, foreshock-mainshock-aftershock sequence). Majority of seismic sequences occur within an area of the order of thousands square kilometers (up to 100 x 100 km), commonly in the course of days or weeks, rarely months. The spatial distribution of earthquakes within sequences shows that they occur at fault planes or at interconnected fault systems. Character of a sequence depends on the structure of the earth's crust, namely its fracturing, and on spatial distribution of the tectonic stress.

Systematic research into seismic sequences was conducted by Mogi (1967) who defined three basic types of sequences:

(i) A dominant earthquake without foreshocks followed by aftershocks. This type of sequence occurs in a homogenous medium under a nearly uniform applied stress and is

represented by a majority of strong tectonic earthquakes. (ii) A dominant earthquake with foreshocks followed by numerous aftershocks. Such a sequence occurs in moderately fractured regions, where the spatial distribution of stress is not uniform. Only a minority of large earthquakes occur in this way. (iii) No dominant earthquake occurs in the sequence. The strongest earthquake in the swarm does not exceed the others of more than one grade at the magnitude scale. This type of sequence is called seismic or earthquake swarm. It is supposed to occur in highly fractured regions (Mogi, 1967).

Seismic sequences occur as a consequence of the mutual triggering of earthquakes. When an earthquake occurs, the elastic stress is released in the hypocenter, and, simultaneously, stress is increased at the neighboring parts of the fault. The elastic stress, which is suddenly increased at the fault, exceeds the friction forces and triggers another earthquake. This mechanism is referred to as the co-seismic stress transfer, based on the elastic behavior of the crust (Bhattacharyya and Chakrabarti, 2006).

A post-seismic stress transfer mechanism can influence earthquake occurrence, too. This mechanism is associated with the viscous stress transfer in the lower levels of the earth crust and the upper part of the mantle and is referred to as quasi-static. The quasi-static stress transfer and associated triggering of a next earthquake does not occur in a short time interval as in the case of the co-seismic mechanism; it is supposed to take month to years and operate to long distances. Viscous stress transfer remains a controversial topic in Earth sciences, discussed both in the framework of numerical modeling and in the statistical analysis of seismic data (Hill et al., 1993; Harris, 1998).

3.3. Seismo-volcanic interactions

Analysis of parameters and properties of earthquakes and earthquake sequences may contribute to understanding magmatic processes beneath active volcanoes. Weak (magnitude < 4) and shallow (depth < 10 km) seismicity almost always accompanies movements of magma in magmatic chambers. These earthquakes are observed by local seismic networks in order to predict volcanic activity. It is a well-recognized topic with a worldwide application potential (e.g. Konstantinou and Schlindwein, 2002; Roman and Cashman, 2006). In post-volcanic areas, local earthquake monitoring substantially helps to understand processes at seismogenic faults, such as a possible role of fluids in triggering of seismic swarms (Špičák and Horálek, 2001; Heinicke et al., 2009).

Besides the locally and regionally observed seismicity, teleseimic earthquakes of much higher magnitude class occurring deeper in the crust are observed beneath some volcanoes (Fig. 2). Even the weakest earthquakes recorded by teleseismic network are relatively strong, with body wave magnitude m_b greater than 4. Teleseismic earthquakes beneath volcanoes often occur in swarms. Origin time of these earthquakes sometimes correlates with volcanic eruptions.

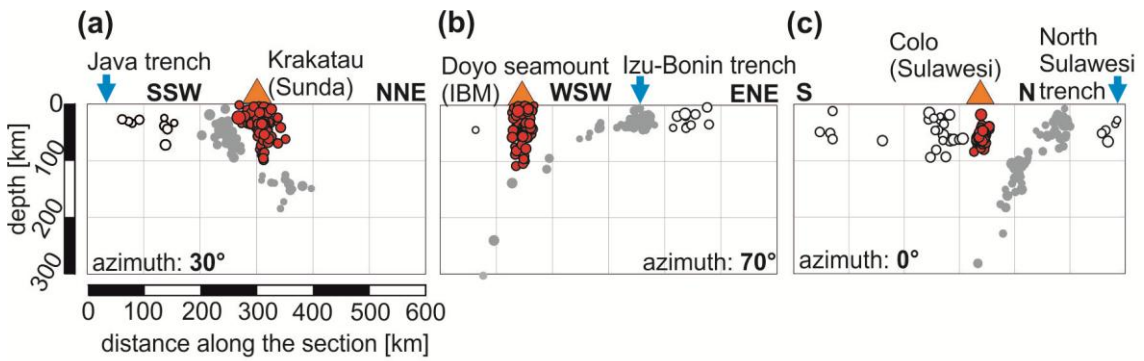

Fig. 2. Seismo-volcanic interactions (teleseismic earthquakes). (a) Krakatau volcano, Sunda Strait, Indonesia: earthquakes occur as single events, do not accompany volcanic eruptions (Špičák et al., 2002); (b) Doyo seamount, Izu-Bonin, Japan: earthquakes occured in a seismic sequence without any obvious time relation to volcanic eruption (Špičák et al., 2009); (c) Colo volcano, Tomini Gulf, N. Sulawesi, Indonesia: earthquakes occurred in a sequence that accompanied the devastating 1983 Volcanic Explosivity Index (VEI) 3 volcanic eruption.

3.4. Earthquake occurrence at subduction zones

The most distinct feature of earthquake occurrence at subduction zones is the Wadati-Benioff zone (WBZ). The WBZ (#1 in Fig. 3) is the inclined zone of seismicity delineating the subducting oceanic plate surrounded by aseismic mantle. At some subduction zones (Tonga, Java) the WBZ reaches the boundary between the upper and lower mantle at depths of about 660 km. A detailed investigation of the inclination of the WBZs in relation to position of volcanic arcs has been done by Syracuse and Abers (2006).

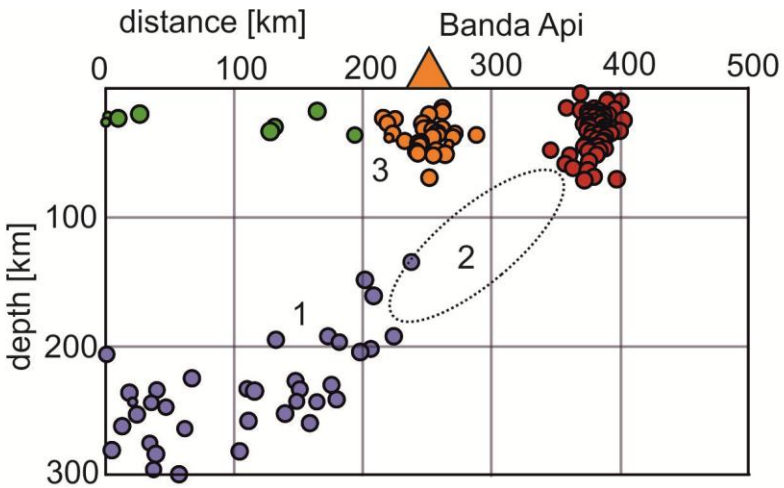

Fig. 3. Schematic cross-section through a volcanic arc. Earthquakes are denoted by circles (blue - Wadati-Benioff zone (1), red - upper part of the subducting plate, orange - beneath the volcanoes (3), green - in the overlying wedge). The aseismic gap in the subducting slab (2) is marked by the dashed ellipse. The Banda Api volcano is denoted by orange triangle.

Hanuš and Vaněk (1985) observed that at depths between 100 and 200 km beneath volcanic arcs (#2), a region without teleseismically observable earthquakes often occurs in the Wadati-Benioff zone. They entitled the region Intermediate Depth Aseismic Gap (IDAG) and explained its existence as a consequence of specific material properties at respective depths of the subducting slabs, namely the loss of ability of brittle failure which is a necessary condition for a strong earthquake occurrence. The IDAG probably reflects partial melting of the slab at the relevant depths; it often occurs beneath volcanic arcs.

A specific seismicity pattern has been observed in the mantle wedge above the WBZ beneath some volcanoes (#3) and denoted as Seismically Active Column (SAC) by Špičák et al. (2004, 2005, 2009). The presence of numerous teleseismically recorded earthquakes beneath volcanoes casts doubt on presence of extensive magmatic reservoirs at relatively shallow depths (up to 30-40 km) beneath volcanoes. Contrarily, SACs point to the brittle character of the medium within the overlying wedge. Seismicity of this type is supposed to be related to magma transport through the pre-stressed fractured medium.

4. Regions of our interest, data and data preparation

4.1. Areas of investigation

The aim of this thesis is to recognize areas with a specific seismicity pattern that could reflect magma migration and ascent towards the surface. I concentrated on subduction zones with submarine parts of volcanic arcs where such analysis could contribute to better knowledge of hitherto poorly studied submarine volcanic provinces. Seventeen regions, mostly constituting the "Ring of fire" in the Pacific, have been studied (Fig. 4). These are (counterclockwise): Aleutian Island Arc (1), Kuril Island Arc (2), Ryukyu Island Arc (3), Izu-Bonin Island Arc (4), Mariana Island Arc (5), Yap and Palau Island Arcs, Andaman-Nicobar Island Arc (6), Philippine-Halmahera Island Arc (7), Banda and Seram Island Arc (8), Bismarck Island Arc, Solomon Island Arc (9), New Hebrides Island Arc (10), Tonga Island Arc (11), Kermadec Island Arc (12), the region of Auckland Islands, Scotia Island Arc (13) and Lesser Antilles Island Arc (14).

4.2. Data

The EHB database of hypocentral determinations was used as the primary source for the analysis. The EHB database is based on data of the International Seismological Center (ISC) during the 1964-2008 period, relocated by the algorithm of Engdahl et al. (1998). Information on volcanoes has been taken from the Catalogue of the Active Volcanoes of the World (Neumann Van Padang, 1951) and from the Smithsonian Global Volcanism Program database (Siebert et al., 2002-, Ventzke et al., 2002-).

The way of creation of the EHB seismic database is shortly described below.

4.2.1. EHB database

The EHB database contains nearly 140,000 events that occurred during the period 1964 to 2008 and are well-constrained teleseismically by arrival-time data reported to the

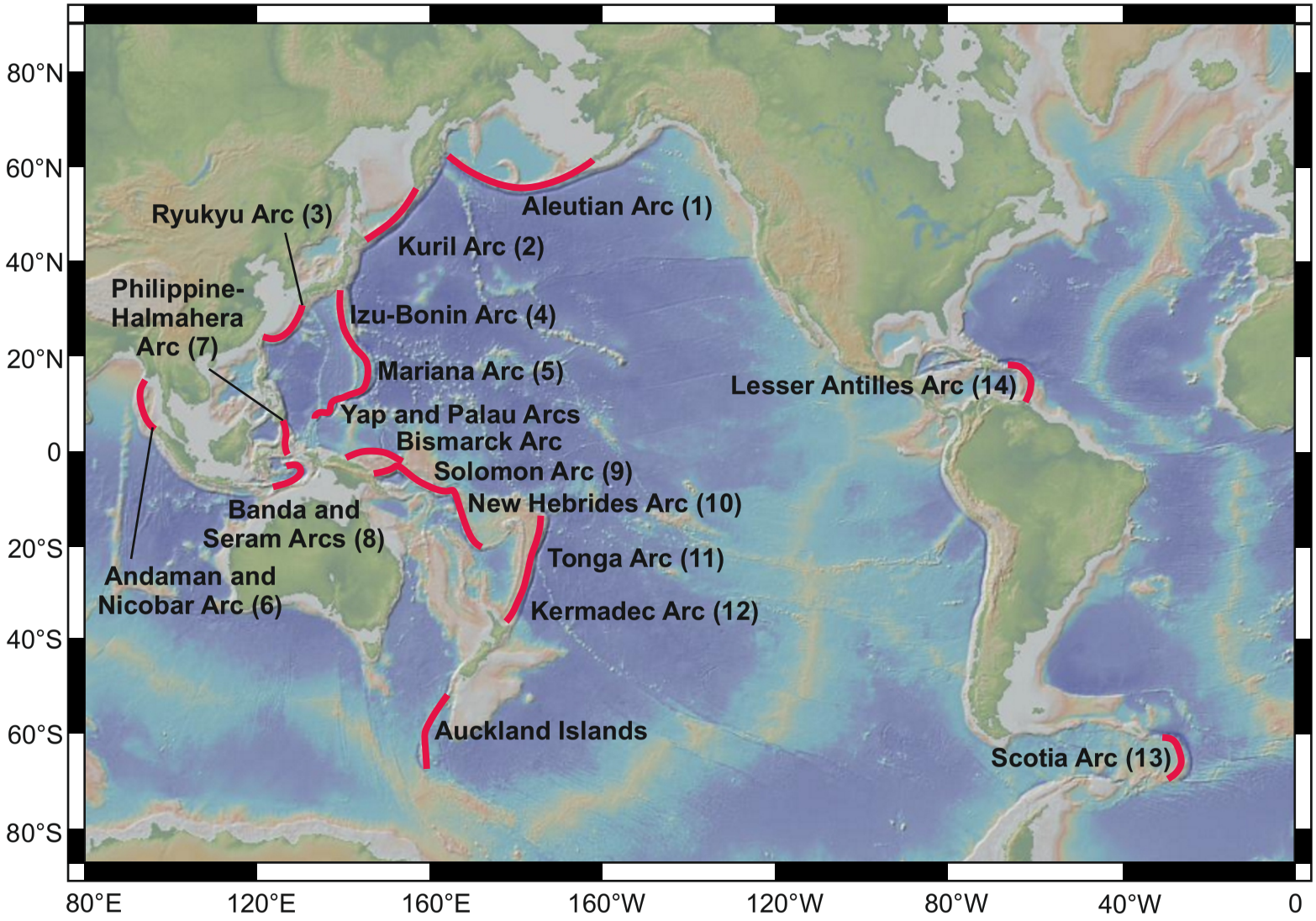

Fig. 4. Map of studied regions.

International Seismological Centre (ISC) and to the *U.S. Geological Survey's National Earthquake Information Center* (NEIC). The ISC and NEIC hypocenter determinations are based on the readings of P and S waves, whereas the EHB relocation procedure uses additional arrival times of PKiKP, PKPdf; and the teleseismic depth phases pP, pwP, and sP. For independent identification of the depth phases a global probability model was developed by Engdahl et al. (1998). Many of weak earthquakes tabulated in the ISC or the USGS databases are not contained in the EHB database as the EHB relocation procedure is applied only to teleseismically well-constrained events. The results obtained by the EHB relocation procedure are more accurate for both epicenter and focal depth determination. Due to the usage of the depth phases (pP, pwP, sP) the improvement of accuracy is significant particularly for the focal depth determination (Engdahl et al., 1998). The EHB dataset became suitable for worldwide studies of the Wadati-Benioff zones, tomographic imaging etc. A comparison between the magnitude completeness of EHB and ISC database is depicted in Fig.5.

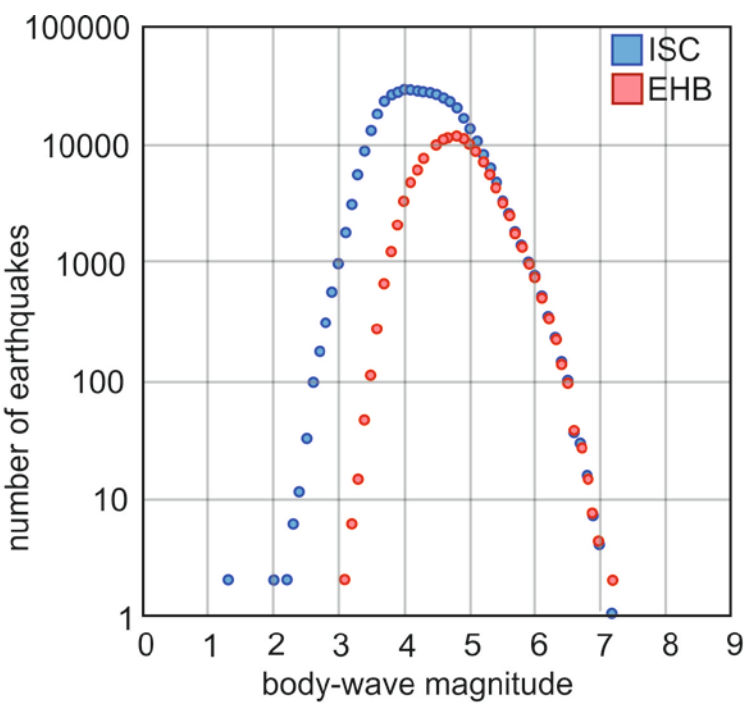

Fig. 5. The magnitude completeness. The magnitude completeness for EHB and ISC databases.

The accuracy of hypocentral determinations is essential for the following data analysis. The standard error of the epicentral determination ranges from 5 to 25 km and of the depth determination from 2 to 15 km in the EHB database.

The relatively high accuracy of data, robustness of their determinations, global geographical coverage and a relatively long time interval of almost 50 years make the EHB database suitable for statistical analysis and for structural analysis of the Earth interior.

4.3. Processing of data

The seismic as well as the volcanological data had to be prepared for the analysis. The data preparation is summarized in the following paragraphs.

4.3.1. Seismic data

As described above, earthquakes beneath volcanic arcs occur both in the subducting plate and in the overlying lithospheric wedge. Only earthquakes occurring within the lithospheric wedge can be linked to the process of magma migration and are relevant for further analysis. To distinguish the events occurring in the Wadati-Benioff zone from those in the overlying plate, the region of our interest has been covered by relatively narrow swaths (swath width 0.5 degree – approximately 55 km), perpendicular to the plate boundary (Fig. 6). Earthquakes belonging to a particular swath were displayed in a vertical section along the swath and the earthquakes belonging to the wedge in the given swath was delimited and analyzed.

The numbers of earthquakes in individual regions are summarized in Tab. 1.

After this introductory analysis three regions (region of Auckland Islands, Bismarck Island Arc and Yap and Palau Island Arc) have been excluded due to a lack of seismicity.

4.3.2. Data on volcanoes

The basic data on volcanoes in the individual regions under study are summarized in Tab. 2. The period of the volcanic activity between 1964 and 2008 is of particular importance because it enables to correlate volcanic eruptions with the EHB earthquake catalog.

An important parameter for describing intensity of a volcanic eruption is the Volcanic Explosivity Index (VEI). It integrates quantitative data and sets a 9-grade scale of eruption explosivity. The VEI was established by Newhall and Self (1982); the criteria for defining

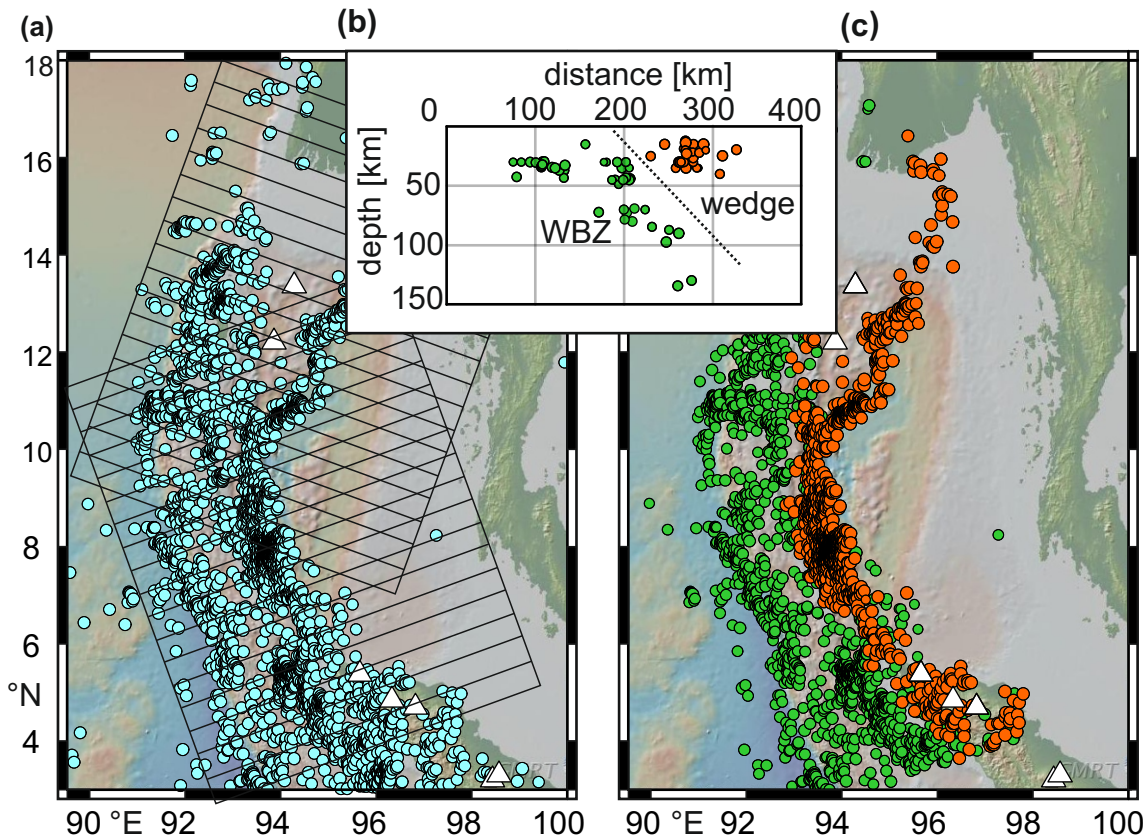

Fig. 6. Delimitation of earthquakes in the WBZ and in the overlying lithospheric wedge in individual island arcs. The process comprises three phases: (a) The region is covered by swaths perpendicular to the plate boundary; (b) vertical cross-sections containing the earthquakes belonging to particular swaths are displayed. Cross-sections enable to distinguish between earthquakes occurring in the WBZ and those in the lithospheric wedge. (c) Epicentral map of earthquakes classified according to their affiliation to the WBZ (denoted by green color) and the overlying wedge (orange color) can be displayed after all the cross-sections are processed.

Tab. 1. Earthquake occurrence in the studied regions. Column 1: number of the volcanic arc; 2: name of the arc; 3: length of the arc in kilometers; 4: total number of earthquakes in period between 1964 and 2008; 5: number of swaths used for analysis; 6: number of earthquakes occurring in the overlying lithospheric wedge; 7: percentage of wedge earthquakes, 8: number of earthquakes in subducting plate. Data in column 6, 7, and 8 was not possible to determine for three island arcs (Auckland Islands, Bismarck, and Yap and Palau), because the seismicity in these regions is shallow and it is not possible to construct the tectonic boundary between the converging plates precisely.

1	2	3	4	5	6	7	8
No.	Region	Length [km]	Total No. of eq.	No. of swaths	No. of eq. in wedge	% of eq. in wedge	No. of eq. in subd. Plate
1	Aleutian Island Arc	2600	5335	57	406	8	4929
2	Kuril Island Arc	1200	7259	30	83	1	7176
3	Ryukyu Island Arc	1200	2420	23	498	21	1922
4	Izu-Bonin Island Arc	1200	5146	28	926	18	4220
5	Mariana Island Arc	2200	5029	56	720	14	4309
x	Yap and Palau Island Arcs	1000	101	22	-	-	-
6	Andaman-Nicobar Island Arc	1300	2770	35	1256	45	1514
7	Philippine-Halmahera Island Arc	500	4292	10	305	7	3987
8	Banda and Seram Island Arc	900	2512	21	359	14	2153
x	Bismarck Island Arc	1300	96	24	-	-	-
9	Solomon Island Arc	2000	5967	45	855	14	5112
10	New Hebrides Island Arc	1600	5250	35	426	8	4824
11	Tonga Island Arc	1400	10193	31	275	3	9918
12	Kermadec Island Arc	1600	6341	38	272	4	6069
x	region of Auckland Islands	1100	197	26	-	-	-
13	Scotia Island Arc	900	1900	16	124	7	1776
14	Lesser Antilles Island Arc	1000	765	37	97	13	668
	Total number	23000	65573	534	6602	10	58971

Tab. 2. Data on volcanoes in individual island arcs. Column 1: number of the volcanic arc; 2: name of the arc; 3: number of volcanoes in the arc; 4: number of volcanoes active in period between 1964 and 2008; 5: number of eruptions of volcanoes in period between 1964 and 2008; 6: number of dormant volcanoes in the arc (last eruption before 1964).

1	2	3	4	5	6	7
No.	Region	No. of volcanoes	No. of volcanoes active 1964-2008	No. of eruptions 1964-2008	No. of dormant volcanoes	No. of submarine volcanoes
1	Aleutian Island Arc	47	6	60	41	1
2	Kuril Island Arc	74	17	64	57	4
3	Ryukyu Island Arc	16	4	27	12	3
4	Izu-Bonin Island Arc	30	18	147	12	11
5	Mariana Island Arc	25	11	37	14	21
x	Yap and Palau Island Arcs	0	0	0	0	0
6	Andaman-Nicobar Island Arc	2	1	6	1	0
7	Philippine-Halmahera Island Arc	10	5	28	5	2
8	Banda and Seram Island Arc	7	2	2	5	0
x	Bismarck Island Arc	2	0	0	2	0
9	Solomon Island Arc	39	11	84	28	4
10	New Hebrides Island Arc	18	11	85	7	2
11	Tonga Island Arc	20	12	21	8	9
12	Kermadec Island Arc	23	5	45	18	13
x	region of Auckland Islands	0	0	0	0	0
13	Scotia Island Arc	9	3	13	6	1
14	Lesser Antilles Island Arc	16	5	17	11	1
	Total number	338	111	636	227	72

the index are summarized in Tab. 3. The numbers of eruptions according to their VEI are in Fig. 7.

Tab. 3. The criteria for Volcanic Explostivity Index assignment. According to Siebert and Simkin (2002-).

VEI	0	1	2	3	4	5	6	7	8
General Description	Non-Explosive	Small	Moderate	Moderate-Large	Large	Very Large			
Volume of Tephra (m3)		$1x10^4$	$1x10^6$	$1x10^7$	$1x10^8$	$1x10^9$	$1x10^{10}$	$1x10^{11}$	$1x10^{12}$
Cloud Column Height (km) Above crater Above sea level	<0.1	0.1-1	1-5	3-15	10-25	>25			
Qualitative Description	"Gentle"	"Effusive"	"Explosive"		"Cataclysmic"	"Paroxysmal"	"Colossal"		
					"Severe"	"Violent"	"Terrific"		
Eruption Type		Strombolian			Plinian				
	Hawaiian			Vulcanian		Ultra-Plinian			
Duration	<1 hour				>12 hours				
			1-6 hours						
				6-12 hours					
Tropospheric injection	Negligible	Minor	Moderate	Substantial					
Stratosphheric injection	None	None	None	Possible	Definite	Significant			
Historical eruptions	755	963	3631	924	307	106	46	4	0

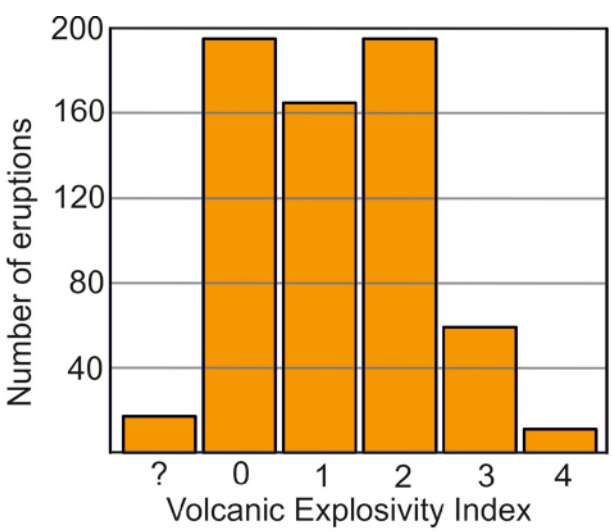

Fig. 7. Histogram of eruptions according to their Volcanic Explosivity Index in period between 1964 and 2008.

5. Seismic sequence recognition

Seismic sequence is determined by i) the maximum distance between two neighboring events, ii) the ultimate time delay of subsequent events and iii) the minimum number of earthquakes forming a seismic sequence. To constrain these parameters for both the co-seismic and the post-seismic stress transfer mechanisms, the analysis of fractal dimension of seismicity was used.

5.1. Dimension, fractal and fractal dimension

In this chapter, the basic terms that are needed for understanding the fractal analysis are explained. The definitions presented here are simplified; accurate mathematical definitions are beyond the scope of this thesis.

The *topological dimension* of a shape can be described as the minimum number of coordinates that are needed to define any point in the given shape (Kornreich, 1999). The topological dimension of a point is zero; the topological dimension of a line is one; the rectangle has a topological dimension of two and the cube of three (Fig. 8). The dimension three is the maximum topological dimension of the space we live in – the number three is called *embedding dimension of space* (Bhattacharyya and Chakrabarti, 2006). Analogically, one is the embedding dimension of time.

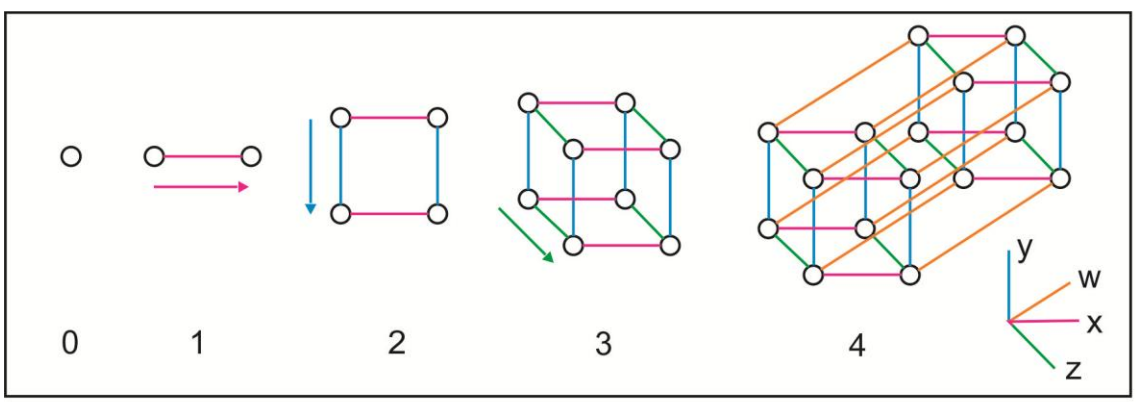

Fig. 8. Topological dimensions of space. The last column labels the coordinates used in the shapes. The number denotes the topological dimension of the shape.

Fractals are patterns that look "the same from the near as from the far" (Gouyet, 1996). This feature of fractals is called self-similarity and means that the pattern does not change with the change of scale. Fractal patterns have a fractal dimension that usually exceeds their topological dimension (Mandelbrot, 2004). The fractal dimension of an entity is usually not an integer (Mandelbrot, 1982). According to the computational algorithm, several different types of fractal dimensions are defined (e.g. Correlation Dimension, Hausdorff Dimension etc.). Several fractals with their dimensions are depicted in Fig. 9.

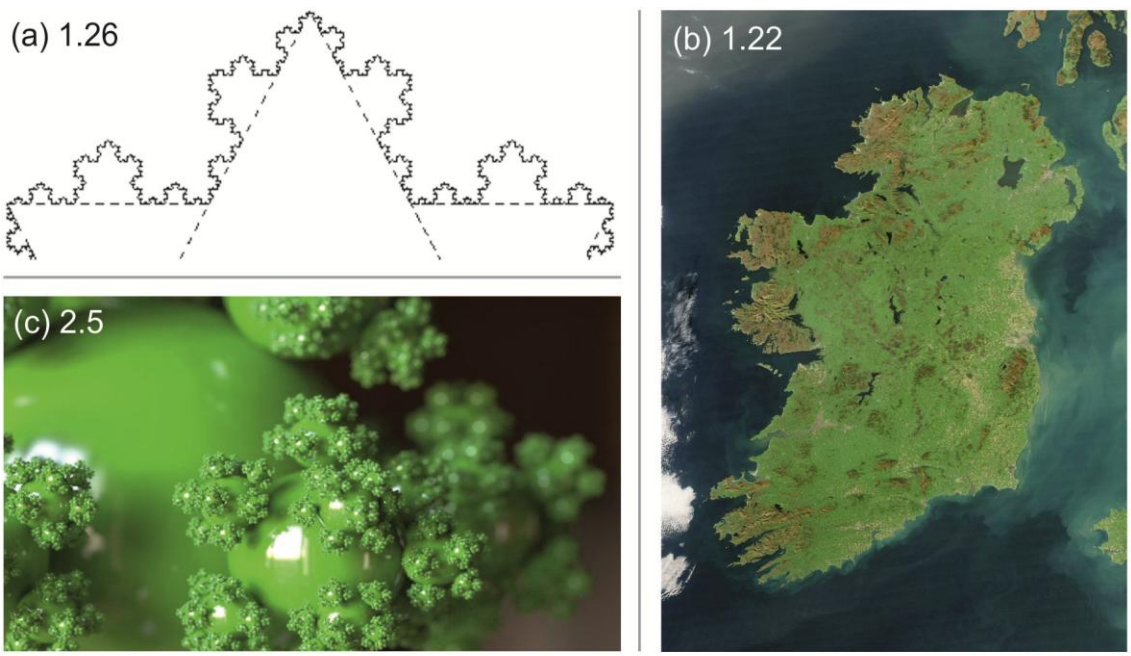

Fig. 9. Examples of fractals and their Hausdorff dimensions. (a) The Koch curve (snowflake); (b) Coastline of Ireland; (c) surface of the Haines sphereflake.

Fractal theory can be also useful in the study of the real-world structures that show a self-similarity within a certain interval of scales. Nowadays, the application of these concepts is rapidly spreading out in a wide range of research fields, such as physiology, neuroscience, medicine or image analysis. A fractal dimension can be ascribed to many common objects and structures. For example, the Hausdorff fractal dimension of the coastline of Ireland is 1.22 (McCartney et al., 2010) and that of the coastline of Norway is 1.52 (Feder, 1988), note fjords in Norway. The fractal dimension of the surface of the human brain is 2.79, similar as of a broccoli (Kapelner, 2002), and of the lungs 2.97 (Sapoval, 2001).

5.2. Space-time Combined Correlation analysis

Earthquake distribution shows a self-similarity at certain scale intervals, both in the space and time domains; it is thus possible to determine the corresponding fractal dimension. The fractal dimension of a set of points randomly distributed in space is close to its topological dimension (i.e. 3), while a clustered set of points (like a seismic sequence) displays a much lower value of the fractal dimension.

Several methods can be used to determine the fractal dimension of an entity. For our purposes, the suitable way is to compute the so called co*rrelation dimension*. To achieve this and to determine mutual relations between earthquakes, the *combined space-time correlation dimension* must be computed first. Individual steps of the procedure are described in the following paragraphs.

5.2.1. Scale invariance in Space

Earthquakes occur in particular spatial patterns reflecting either plate boundaries, fault systems, or – at smaller scales – volcanic structures (Kagan and Knopoff, 1980). These patterns show scale invariance and many authors in the past have already concentrated on describing them by means of their fractal dimension (De Rubeis and Dimitriu, 1993; Kagan and Knopoff, 1980). The fractal dimensions of various patterns are different.

A frequently used and efficient tool for determining the scale invariance in the analysis of seismicity is the *correlation integral* (Grassberger and Procaccia, 1983; Bhattacharyya and Chakrabarti, 2006), defined as:

$$C(l) = \frac{2}{N(N-1)} \sum_{i=1}^{N-1} \sum_{j=i+1}^{N} \theta(l - \|\boldsymbol{x}_i - \boldsymbol{x}_j\|), \tag{6}$$

where $C(l)$ is the correlation integral, l is the distance in space, N is the total number of events, $\boldsymbol{x}$ is the coordinate vector and θ is the *Heaviside step function*. Heaviside step function, or the unit step function is a discontinuous function. Its value is equal to 0 for negative arguments and 1 for positive arguments. Its value at 0 depends on the particular definition and can be equal either to 0, ½ or 1.

The correlation dimension D is defined as:

$$d(l) = \frac{\delta \log C(l)}{\delta \log(l)} D = \lim_{l \to 0} d(l), \quad (7)$$

where $d(l)$ is the local slope. The correlation dimension D is equal to the value of the local slope in the interval, where the local slope $d(l)$ is aproximatelly constant. It can be displayed by plotting the value of the local slope $d(l)$ vs. $\log(l)$.

When applied to real earthquakes in a three-dimensional space, the correlation integral (Grassberger and Procaccia, 1983; Bhattacharyya and Chakrabarti, 2006) is defined as:

$$C(r) = \frac{2}{N(N-1)} \sum_{i=1}^{N-1} \sum_{j=i+1}^{N} \Theta(r - \|\boldsymbol{x}_i - \boldsymbol{x}_j\|), \quad (8)$$

where $\boldsymbol{x}_i$ and $\boldsymbol{x}_j$ are the position vectors (vectors of the space coordinates of the points). Distances between all pairs of earthquakes are measured in three dimensions connecting the points of the pair with a straight line. The value of the correlation integral $\mathrm{C(r)}$ shows how many pairs of points within the dataset are closer to each other than the distance of *r*.

The correlation dimension *D* (Fig. 10) changes with increasing distance. At short distances ($0 < r < 3\ km$) it is equal to zero, reflecting the absence of earthquakes at these distances. Intermediate distances ($3\ km < r < 30\ km$) are characterized by a relatively high value of the local slopes, setting the correlation dimension to value of $D \cong 2$. Because the correlation dimension of randomly distributed points in a plane is $D = 2$, such value in context of earthquake distribution suggests that the earthquakes at this distance interval occur at a fault plane. The value of the local slope at shorter distances of the interval is strongly influenced by the standard error of earthquake localization, which can increase the value of the local slope (up to the maximum value of the embedding dimension $D = 3$). At longer distances ($30\ km > r > 300\ km$), the influence of the plane distribution decreases and the local slopes descent from a value of $d(l) \cong 2$ to a value of $d(l) \cong 1.2$, suggesting the dominant effect of quasi-linear setting of earthquakes along large faults or plate boundaries. The correlation dimension cannot be determined in this interval. At high distances ($300\ km < r$) the effect of fault plane setting is negligible, the local slopes are constant again and the correlation dimension is $D \cong 1.2$.

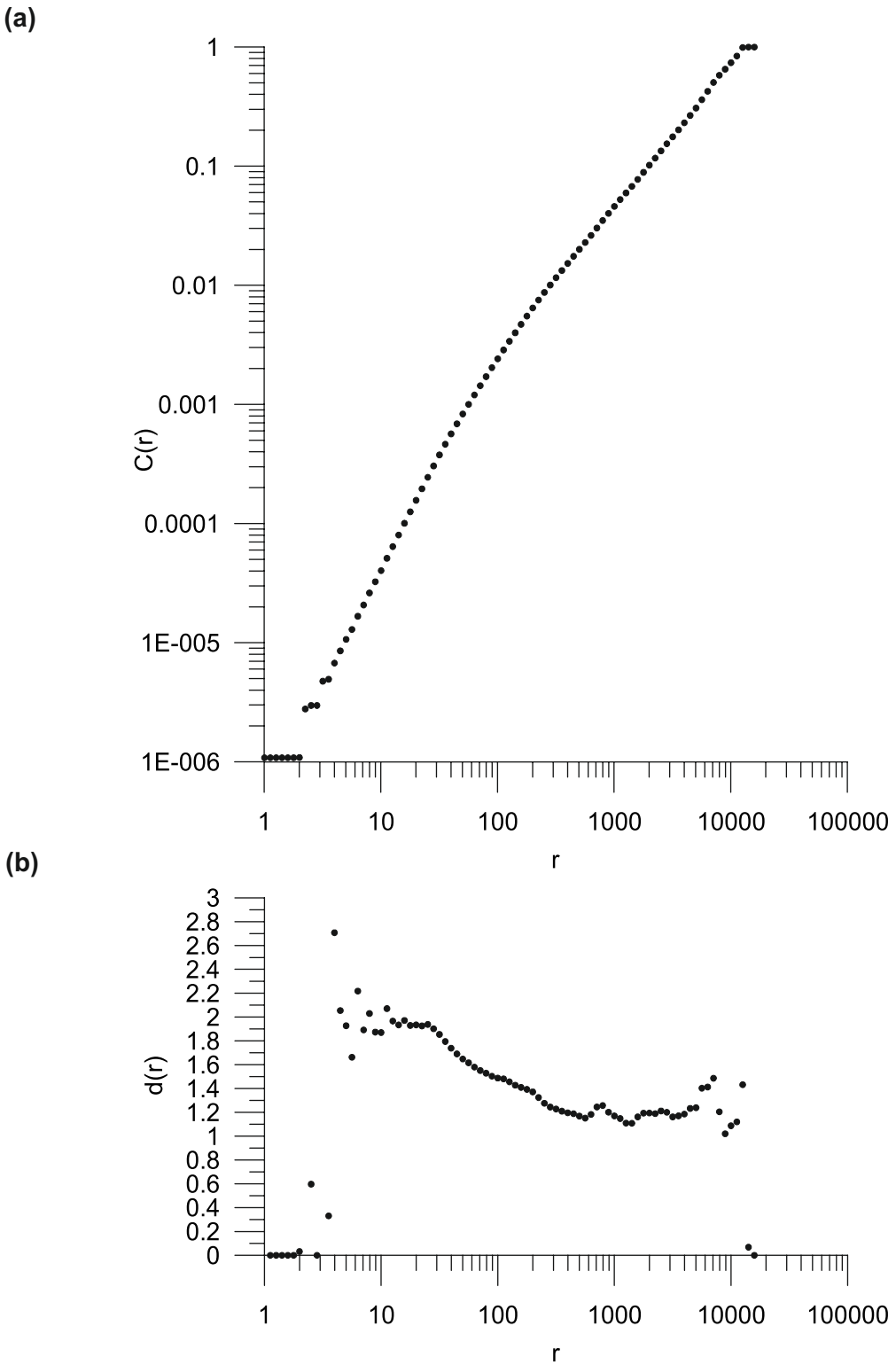

Fig. 10. Space correlation dimension. (a) Correlation integral (C(r)) of global seismicity (minimum magnitude 5) in space. r is the distance between hypocenters in kilometers. (b) Local slopes of the correlation integral at distances r. Reprinted from Bhattacharyya and Chakrabarti (2006).

5.2.2. Scale invariance in Time

The same method can be applied to the distribution of earthquakes in time. The correlation integral (Grassberger and Procaccia, 1983; Bhattacharyya and Chakrabarti, 2006) is expressed as:

$$C(\tau) = \frac{2}{N(N-1)} \sum_{i=1}^{N-1} \sum_{j=i+1}^{N} \theta(\tau - \|t_i - t_j\|), \tag{9}$$

where τ is a time interval (delay), t_i and t_j origin times of earthquake occurrence.

The time correlation dimension D is defined as:

$$d(\tau) = \frac{\delta \log C(\tau)}{\delta \log(\tau)} D = \lim_{l \to 0} d(\tau) \tag{10}$$

Contrary to the space correlation integral, the time correlation integral (Fig. 11.) shows a stable increase in the wide interval of delays and the local slope is constant in this interval. It results in a well-defined value of the correlation dimension D. The value of D is close to 1, which is the embedding dimension for time. This is evidence that the temporal distribution of global seismicity is nearly random.

5.2.3. Space-Time Combined Correlation Integral

Results of the space and time dimension analysis bring information on spatial and temporal distribution of earthquakes and confirm the known fact that earthquakes occur at fault planes and plate boundaries. On the other hand, it is apparent that the complex seismicity features (e.g. seismic sequences) could remain unreflected if only these methods are used. The patterns of complex features have to be recognized both in time and space domain together. The aim at detecting a non-random content of the data available for certain time and distance intervals needs combination of the space and time correlation integrals into a single combined correlation integral.

The space-time combined correlation integral (Bhattacharyya and Chakrabarti, 2006) is defined as

$$C_c(r,\tau) = \frac{2}{N(N-1)} \sum_{i=1}^{N-1} \sum_{j=i+1}^{N} [\theta(r - \|\boldsymbol{x}_i - \boldsymbol{x}_j\|) * \theta(\tau - \|t_i - t_j\|)], \tag{11}$$

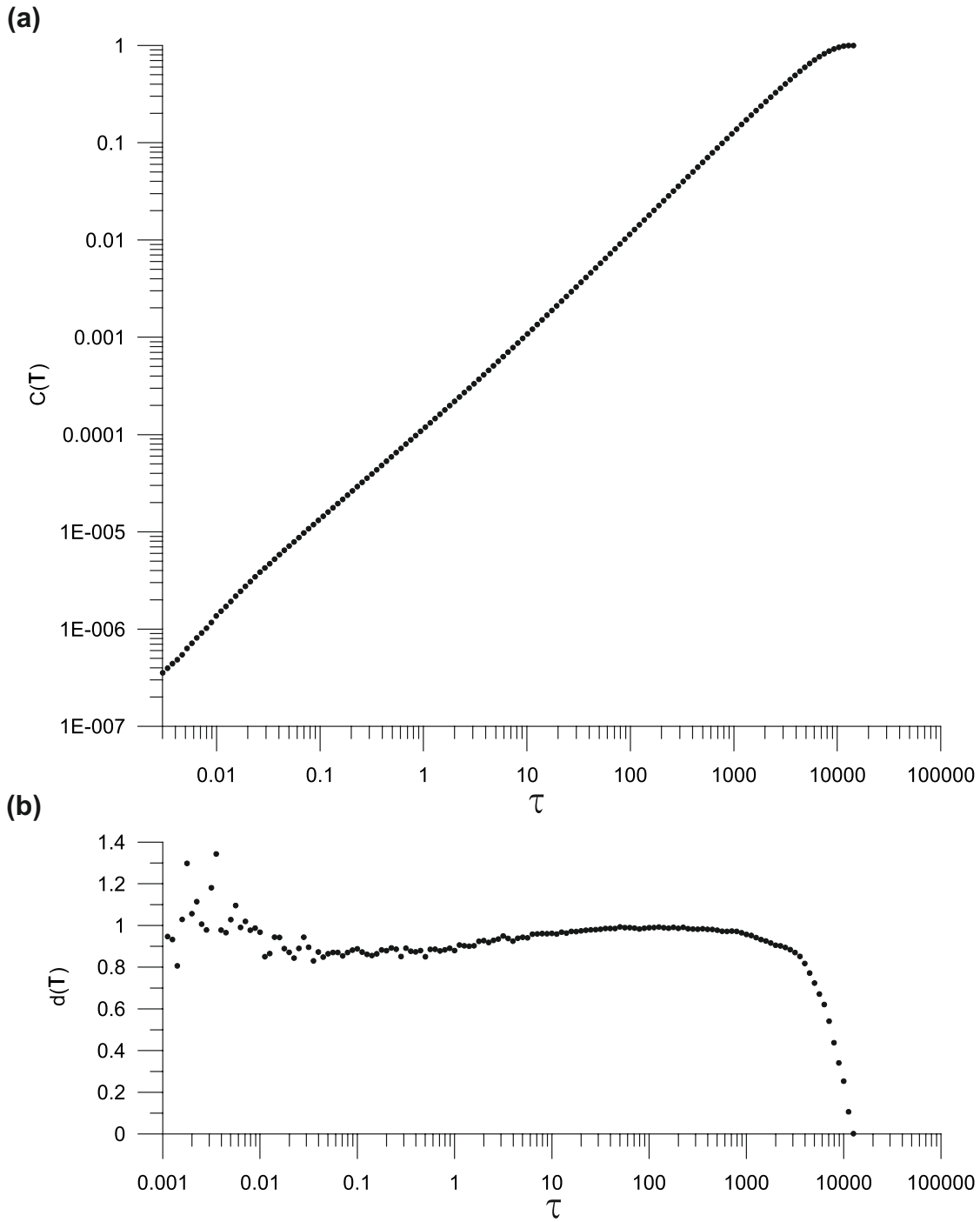

Fig. 11. Time correlation dimension. (a) Correlation integral of global seismicity in time. τ is the time interval (delay) in days; (b) local slopes of the correlation integral. Reprinted from Bhattacharyya and Chakrabarti (2006).

It is important to note that the equation (4.6) includes the space correlation integral (4.3) when $\tau = \tau_{max}$ and the time correlation integral (4.4) when $r = r_{max}$.

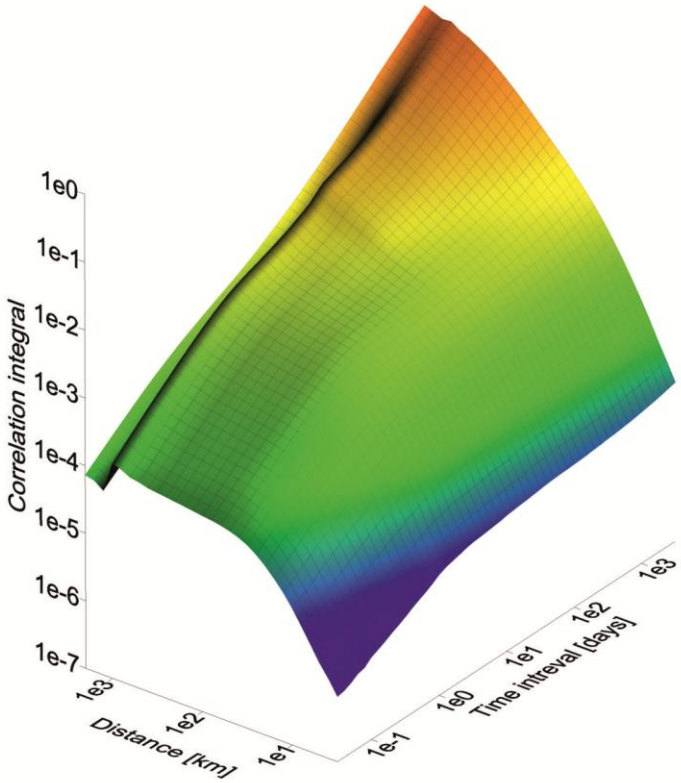

Fig. 12. Space-time combined correlation integral *C(r,τ)*. **For** *τ* **equal to the maximum time distance the plot reduces to space correlation integral (Fig. 10). Analogously, the plot reduces to time correlation integral (Fig. 11) when** *r* **is equal to the maximum distance between points in a dataset. The color depends on values on the vertical axis.**

The time correlation dimension D_t with its local slope d_t is defined as:

$$d_t(r,\tau) = \frac{\partial \log C_c(r,\tau)}{\partial \log \tau} \; D_t(\tau) = \lim_{\tau \to 0} d_t(r,\tau), \tag{12}$$

and the space correlation dimension D_s with its local slope d_s as:

$$d_s(r,\tau) = \frac{\partial \log C_c(r,\tau)}{\partial \log r} \; D_s(r) = \lim_{\tau \to 0} d_s(r,\tau), \tag{13}$$

For a random distribution of events in space and time, the d_t and d_s values are constant for the whole interval τ and r. Constant value of the local slopes implies absence of space-time correlations. The space-time combined correlation integral is depicted in Fig. 12.

Only seismicity occurring beneath the island arcs under study was analyzed by the space-time combined correlation integral. Nevertheless, the results would have been similar if global data with no respect to tectonic environment were used.

5.2.4. Time Combined Correlation Dimension

The time correlation dimension ranges from 0 to 1 (1 is the value of the embedding dimension for time). The time correlation dimension directly expresses a measure of clustering. If points are randomly distributed on a line, without any particular pattern, the values of the local slope of the correlation integral are equal to 1. When points are distributed in patterns, the values of local slope decrease. When all points are placed in the same position, the randomness is fully suppressed and the value of the local slope is equal to zero.

The plot of $d_t(r, \tau)$ in Fig. 13 shows patterns of various values. The most evident zone of the low correlation dimension is situated in the time interval between $3 * 10^{-1}$ days (about 8 hours) and 2 000 days (about 5.5 years). At the beginning of this time interval, the zone of the low correlation dimension corresponds to approximately 800 km, whereas it falls down to about 80 km at the end of the time interval. This suggests that earthquakes within this space-time interval are linked together (one of them probably triggered the other). Outside the time interval, the correlation dimension is high enough to assume that the points under study are mutually independent.

The so called *reshuffling procedure* was applied to check the validity of the result. The principle of the reshuffling procedure is mixing the values of the origin times of the events while keeping their original locations (Tab. 4.). Such a procedure destroys the natural mutual relations between the time and space values, although it does not change the statistical properties of the dataset in time and space domains separately. The computation was then repeated using the new, reshuffled dataset.

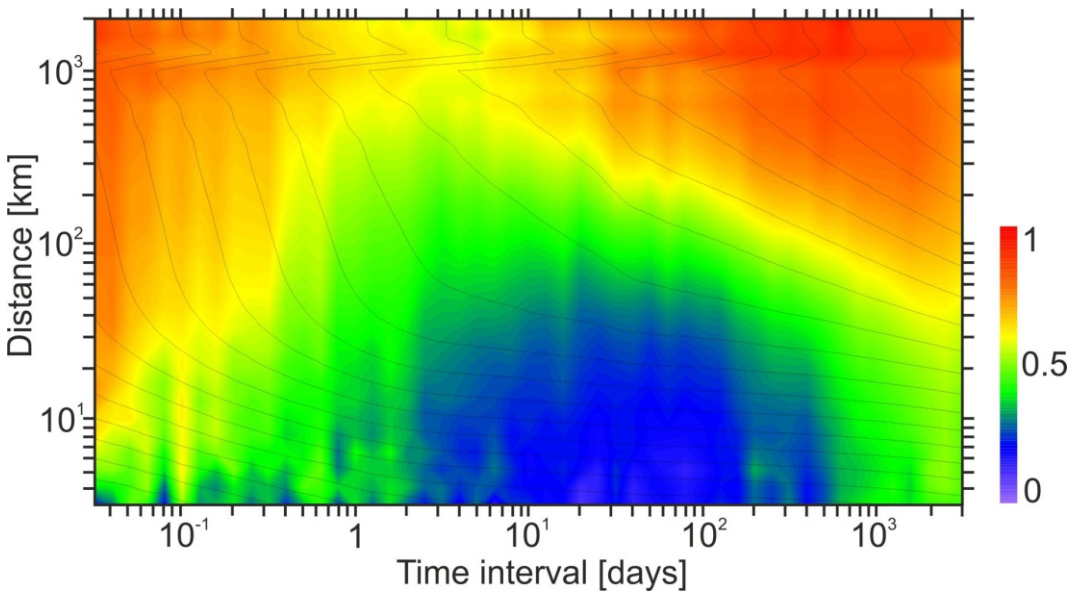

Fig. 13. Time correlation dimension. Local slopes of time correlation dimension $d_t(r,\tau)$ (color scale). Values of combined correlation integral $C_C(r,\tau)$ are denoted by grey isolines. Distance in kilometers is a measure of the vertical axes, time interval in days at horizontal axis. Both axes are logarithmic scaled.

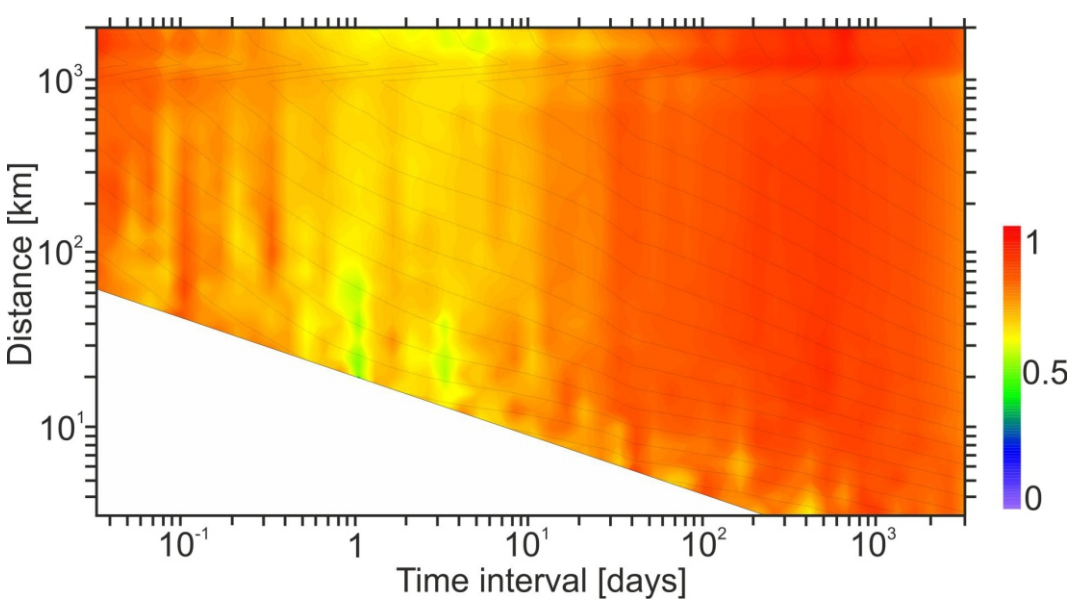

Fig. 14. Time correlation dimension for reshuffled dataset. Local slopes of time correlation dimension $d_t(r,\tau)$ (color scale) for reshuffled data. Values of combined correlation integral $C_C(r,\tau)$ are denoted by grey isolines.

Table 4. Reshuffling procedure. Left: original catalogue, right: reshuffled catalogue. The origin times are randomly assigned to another event.

Event #	Latitide	Longitude	Orig. time
1	1	1	2000/Jan/1
2	2	2	2000/Jan/2
3	3	3	2000/Jan/3
4	4	4	2000/Jan/4
5	5	5	2000/Jan/5

Event #	Latitide	Longitude	Orig. time
1	1	1	2000/Jan/3
2	2	2	2000/Jan/1
3	3	3	2000/Jan/5
4	4	4	2000/Jan/2
5	5	5	2000/Jan/4

Fig. 14. shows the distribution of $d_t(r,\tau)$ values for the reshuffled dataset. It indicates no patterning similar to that in Fig. 13. The correlation dimension lies close to 1 within the whole space and time interval, suggesting thus a random distribution of points in time. In the bottom left corner corresponding to low values of space and time intervals the white area indicates a lack of data for the calculation of $d_t(r,\tau)$. It is connected to a break-up of seismic sequences and, therefore, a low density of events within this space-time interval.

Two results arise from the comparison between Figures 13 and 14. First, the low values of the local slopes in Fig. 13 are not meaningless, but they reflect true relations in space-time distribution of events. Second, the absence of local slopes at short time and space ranges brings the evidence of the presence of seismic sequences at these intervals in Fig. 14. This analysis has made possible to define a time zone in the time combined correlation integral determining the limits of the time correlation between two events. The limit of this zone of time correlation is dynamically varying in time.

The values of the local slopes $d_t(r,\tau)$ in Fig. 13. are continuously varying between 0 and 1. As stated above, the values close to 1 correspond to random distribution of points in time, whereas the values close to zero reflect clustering. In order to exclude the certainly unconnected events, it is necessary to determine the minimum value of $d_t(r,\tau)$ where events occur randomly. To achieve this, the parameters of the Gaussian distribution of $d_t(r,\tau)$ for the reshuffled database were determined. The average value of $d_t(r,\tau) = 0.78$ was calculated with the standard deviation of $\sigma = 0.08$. Setting the limit to 2σ level, the lowest level of randomness was determined as $\mu - 2\sigma = 0.61$. This limit was applied to $d_t(r,\tau)$ values of the real data set in the interval from 1 day to 3 000 days, within which the distribution of threshold values of $d_t(r,\tau)$ can be convincingly approximated by a straight line in a log-log scaled plot (Fig. 15).

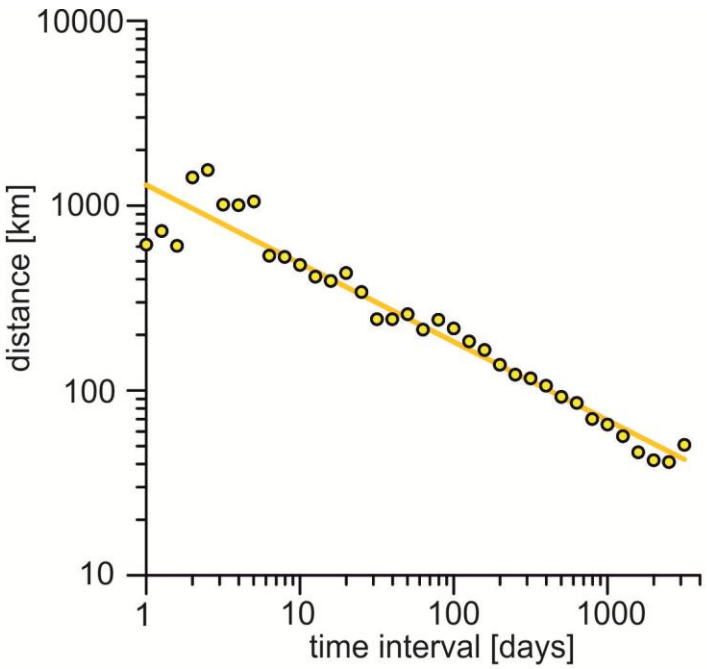

Fig. 15. Time correlation zone delimitation. Points mark values $d_t(r,\tau) = 0.61$, the line is the least square fit of points (equation $\log r = -0.42 \log \tau + 3.11$). τ - time intervals and r - inter-distances. The plot is log-log scaled.

The interpolation results in the equation:

$$\log R_I = -0.42 \log \tau + 3.11, \tag{14}$$

where R_I is the maximum distance between clustered points in kilometers and τ is the time interval between their origin times. The equation defines the limit of the correlation zone – the spatial zone, in which the two earthquakes are time-clustered.

The results may be influenced by an implementation of a magnitude threshold. If only earthquakes with higher magnitudes are used, the limit of the correlation zone shifts to higher distances but the slope of the limit remains unchanged. The magnitude threshold changes only the absolute term of the equation, not the linear term.

5.2.5. Space Combined Correlation Dimension

The space combined correlation dimension d_s has been calculated from the space-time combined correlation dimension C_c analogously to d_t. The value of d_s can vary from 0 to 3 (embedding dimension for space). However, the observed values usually do not reach the

maximum value. The first reason is that earthquakes occur at depths lower than 670 km which causes lowering of $d_s(r,\tau)$ at larger inter-distances. The second reason is that earthquakes tend to occur in either planar patterns - at faults, or in (quasi)linear patterns - at plate boundaries.

The pattern of $d_s(r,\tau)$ (Fig. 16) clearly differs from that of $d_t(r,\tau)$. Elevated local slope values ($d_s(r,\tau) \in \langle 2, 2.6 \rangle$) occur within the time interval between several minutes to 100 days at short distances (around 10 km). The local slope descends under 1 at larger distances (above 40 km). At time intervals larger than 100 days the $d_s(r,\tau)$ values are larger than at shorter time intervals.

A reshuffling procedure was also applied to coordinates of earthquakes in order to check the validity of the results. The origin times of the events were kept while the coordinates of events were randomly mixed. Similarly to the reshuffled $d_t(r,\tau)$, the calculation shows that the $d_s(r,\tau)$ values do not differ for different time intervals and show pure randomness in the whole space-time interval (Fig. 17). Moreover, the absence of the local slopes can be seen at the zone of the short time and short distance intervals.

The highest $d_s(r,\tau)$ values ($1 < d_s(r,\tau) < 3$) in the short distance interval (about 40 km) reflect the occurrence of earthquakes at seismogenic faults. The localization errors can make the values of $d_s(r,\tau)$ higher, especially in the short distance intervals. However, because the zone of high values of the local slope increases gently at larger time intervals and the localization error can be considered constant over the whole span of distance intervals, the results do not seem to be influenced by standard error of localization. The broadening of the zone of high correlation dimension is probably related to a real seismic process. To delimit this zone of high correlation dimension, the minimum value of $d_s(r,\tau)$ was set to 1. The behavior of the limit at the time interval between 15 minutes to 100 days can be convincingly approximated by a straight line in a log-log scaled plot (Fig. 18).

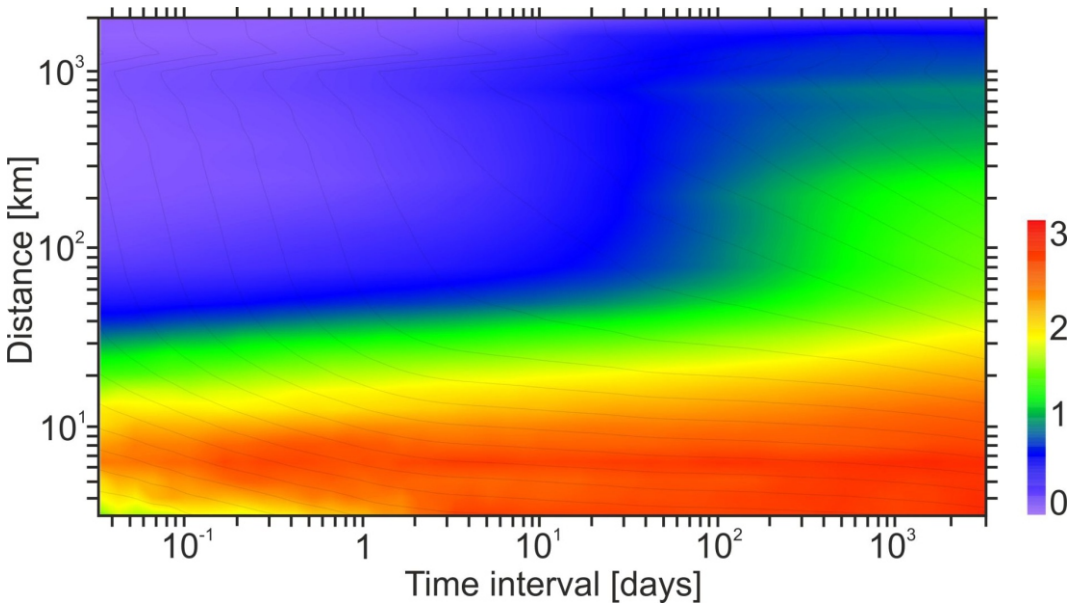

Fig. 16. Time correlation dimension. Local slopes of time correlation dimension $d_s(r,\tau)$ (color scale). Values of combined correlation integral $C_C(r,\tau)$ are denoted by grey isolines. Distance in kilometers is a measure of the vertical axes, time interval in days at horizontal axis. Both axes are logarithmic scaled.

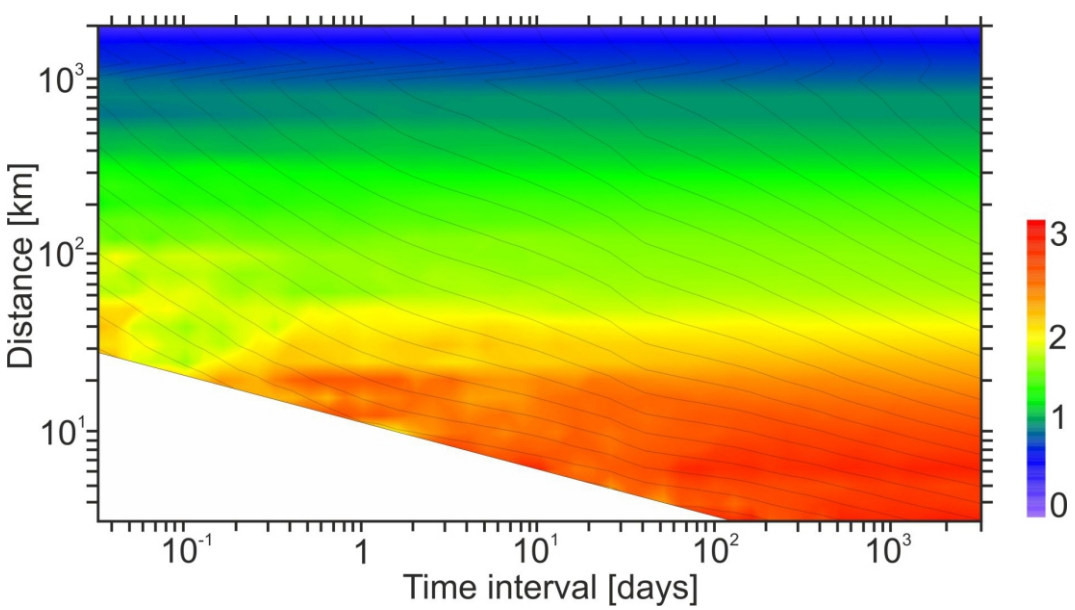

Fig. 17. Time correlation dimension for reshuffled dataset. Local slopes of time correlation dimension $d_s(r,\tau)$ (color scale) for reshuffled data. Values of combined correlation integral $C_C(r,\tau)$ are denoted by grey isolines.

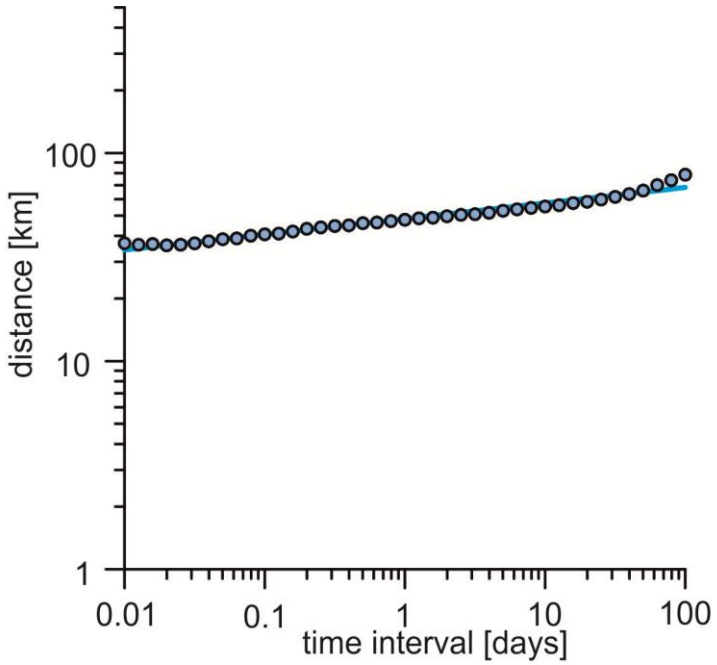

Fig. 18. Time correlation zone delimitation. Points mark values $d_s(r,\tau) = 1$, the line is the least square fit of points (equation $\log r = 0.075 \log \tau + 1.68$). τ - time intervals and r - inter-distances. The plot is log-log scaled.

The applied procedure resulted in the equation:

$$\log R_S = 0.075 \log \tau + 1.68, \tag{15}$$

The equation defines the short-range correlation domain that can be interpreted as the area of distribution of earthquakes in seismic sequences. The moderate spatial expansion of the zone of correlation in time (Fig. 19) is in agreement with the empiric law stating that the aftershocks spread out sub-diffusively away from the mainshock during the seismic sequence progression.

5.2.6. Correlation dimension analysis – conclusions

The analysis of the combined space-time correlation dimension has been used to set up a definition of seismic sequences, both in the time and space domains. This approach considers every event in a dataset as a potential first triggering element of a seismic sequence. The definitions formulated in this thesis set the space and time limits, in which earthquakes do not occur randomly. These definitions should serve as a robust tool for identifying mutually triggered events.

As for the space domain, the definition describes the window where earthquakes are clustered in space and do not occur randomly. The space domain is defined in the time interval of 45 minutes to 100 days. At the beginning of this interval it extends to 34 km while later it expands fluently to about 70 km. Because the space extent of the space domain is relatively narrow, this zone is also called the *near field domain*. As mentioned above, each earthquake induces two kinds of stress transfer – co-seismic and post-seismic transfer. As the co-seismic transfer is related to the elastic properties of the rock environment, the near field domain seems to be convenient to describe the space distribution of earthquakes triggered by the co-seismic stress transfer.

As for the time domain, a spatial window has been defined, where earthquakes are time-clustered, not occurring randomly. The range of the window of time correlation is much wider for short time intervals than the near field domain (Fig. 19). Because of this reason the domain can be also referred to the *far field domain*. The far field domain is defined by the interval of 1 to 2 000 days, extending to nearly 1 300 km at the beginning of the interval while shortening to only 50 km at its end. The far field domain seems to be related to the post-seismic stress transfer and it delimits the zone where the post-seismic processes such as a slow viscous relaxation of the lower part of the crust and upper mantle can trigger an earthquake.

5.3. Seismic sequences

The correlation dimension analysis provided criteria for the search of seismic sequences. The results of the sequence analysis in individual areas of our interest are presented in Tab. 5 and Fig. 20. The total number of 762 sequences occurred in the studied regions in the lithospheric wedge beneath volcanic arcs. Nearly 80% (606 sequences) of all seismic sequences are of the swarm character

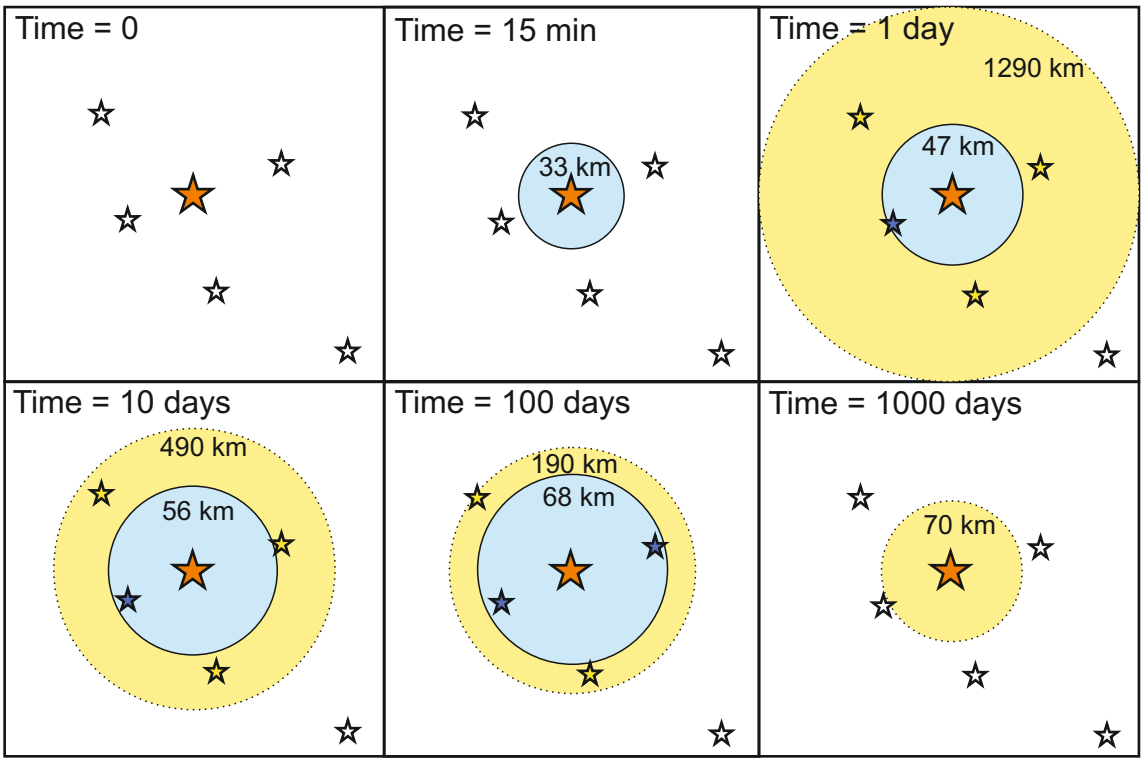

Fig. 19. Seismic sequence evolution. Cartoon showing the main steps of space-time evolution of a standard sequence. When an earthquake occurs (time=0), no earthquakes are space or time correlated; 15 minutes after the first event earthquakes are space correlated up to a spatial range of 33 km, no earthquakes are time correlated; 1 day after the space correlation radius grows to 47, earthquakes are time correlated until a spatial range of 1290 km from the mainshock; 10 days from the main event earthquakes are time correlated until a spatial range of 490 km from the mainshock; space randomness is around an area of 56 km in radius. After 100 days from the main event time correlation area decreased to 190 km from the mainshock; space randomness area has slowly increased to 68 km. After 1000 days from the main event time correlation area has reduced to 70 km.

Tab. 5. Seismic sequences in the studied regions. Column 1: The number of the region; 2: the name of the region; 3: the total number of earthquakes occurring in the region; 4: the number of earthquakes in lithospheric wedge; 5: percentage of earthquakes occurring in the wedge; 6: number of earthquakes in sequences in wedge; 7: percentage of wedge earthquakes occurring in sequence; 8: number of sequences found in wedge; 9: number of swarms (from the total number of seismic sequences).

1	2	3	4	5	6	7	8	9
No.	Region	# of eq. in region	# of eq. in wedge	% of eq. in wedge	# of eq. in seq.	% of wedge eq. in seq.	# of seq. in wedge	# of swarms in wedge
1	Aleutian Island Arc	5335	406	8	256	63	52	44
2	Kuril Island Arc	7259	83	1	29	35	12	9
3	Ryukyu Island Arc	2420	498	21	386	78	72	63
4	Izu-Bonin Island Arc	5146	926	18	809	87	61	55
5	Mariana Island Arc	5029	720	14	545	76	78	10
6	Andaman-Nicobar Island Arc	2770	1256	45	1100	88	95	83
7	Philippine-Halmahera Island Arc	4292	305	7	218	71	40	34
8	Banda and Seram Island Arc	2512	359	14	254	71	43	39
9	Solomon Island Arc	5967	855	14	660	77	116	98
10	New Hebrides Island Arc	5250	426	8	272	64	75	69
11	Tonga Island Arc	10193	275	3	119	43	46	38
12	Kermadec Island Arc	6341	272	4	192	71	50	45
13	Scotia Island Arc	1900	124	7	49	40	17	15
14	Lesser Antilles Island Arc	765	97	13	54	56	5	4
	Total	65179	6602	10	4943	75	762	606

In the following two paragraphs, I determine the space-temporal correlations between volcanic eruptions and seismic sequences (5.3.1.) and spatial correlations between locations of volcanoes and seismic sequences (5.3.2.).

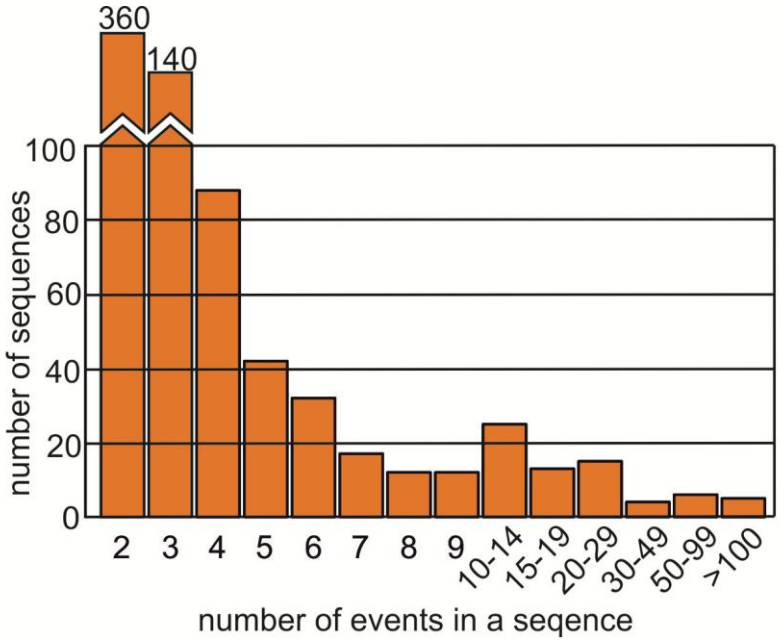

Fig. 20. Number of earthquakes in seismic sequences. The histogram shows number of seismic sequences with number of earthquakes contained in a sequence. Small sequences predominate, but there is also an important number of the very large ones. True number of events in sequence is usually substantially higher but many earthquakes remain undetected or are excluded during the relocation procedure.

5.3.1. Seismic sequences and volcanic eruptions

Some volcanic eruptions are accompanied by teleseismic earthquake sequences. The limits within which sequences can be related to eruptions have to be fixed. These are i) the ultimate distance between a sequence and a volcano, and ii) the ultimate time delay between a sequence and an eruption.

The correlation dimension analysis cannot be used in this case due to the lack of data. The limits have been thus estimated intuitively. Concerning the distance limit, the deepest seismic events beneath volcanoes occur at depths about 80 kilometers. Therefore, the zone of correlation around and beneath a volcano can be defined as a circle of a radius of 80 km. This means that every seismic sequence within a distance less than 80 km from a volcano can be considered as space-correlated. Concerning the temporal limit, the sequences may shortly precede the volcanic eruption or may occur during the eruption period. According to the order of magma ascent velocities (Sigurdsson, 2000) the maximum delay between a

sequence and an eruption was set to 30 days. Possible temporal relations of a sequence and a volcanic eruption are illustrated in Fig. 21.

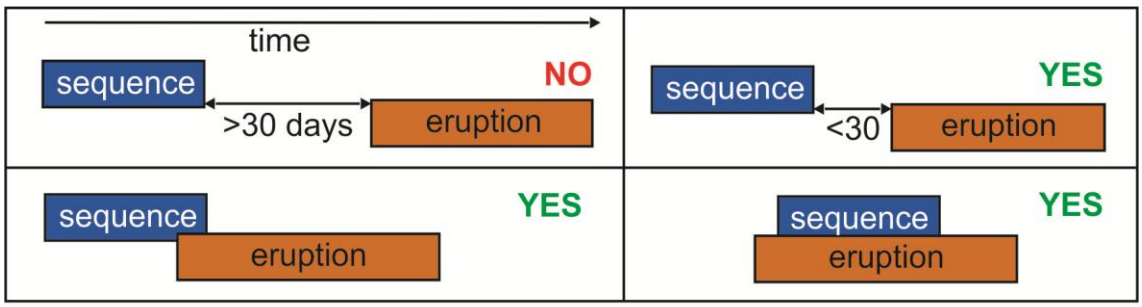

Fig. 21. Possible temporal correlations of a sequence with a volcanic eruption.

After applying these correlation limits, 86 sequences were found to be linked to 52 volcanic eruptions. To check if the space-time relations are not random, the explosivity characteristics of the related eruptions have been taken into account, too. It is reasonable to assume that the eruptions with higher Volcanic Explosivity Index (VEI) are more likely accompanied by strong earthquakes than the eruptions with lower VEI.

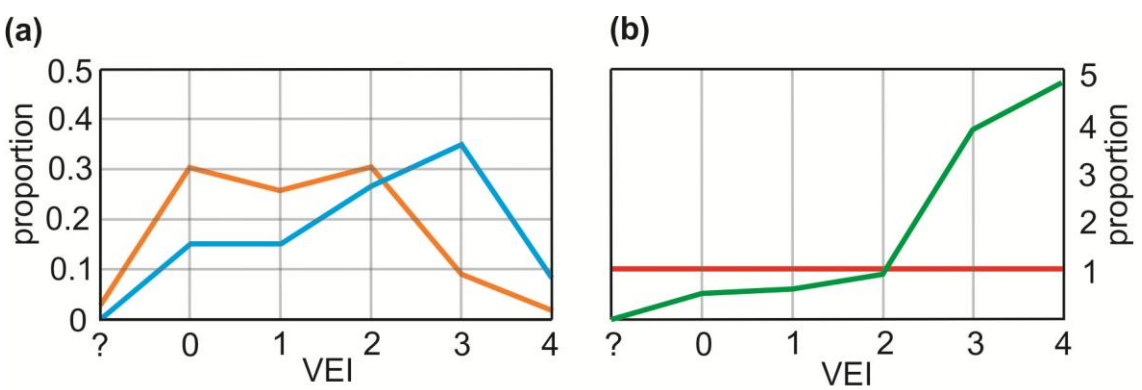

Fig. 22. Classes of VEI of eruptions and seismic sequences. (a) Orange curve shows proportion of the number of eruptions of individual classes of VEI to all eruptions occurring between 1964 and 2008 (P_I) (same as in Fig. 7.); blue curve denotes proportion of number of seismic sequences related to eruptions in individual VEI classes to total number of seismic sequences related to any eruption (P_C). (b) P_C/P_I ratio. If the distribution of correlated eruptions were random, the ratio would be approximately equal to 1. It can be seen that the eruptions with VEI higher than 3 are significantly more often correlated than the weaker ones.

If the available data relations are random, the observed correlations between the stronger eruptions and seismic sequences would have about the same frequency as the correlations between the sequences and all other eruptions. Such an assumption is, however, in a strong contradiction with the observed facts. Eruptions with VEI index equal to 3 or 4 are significantly more often accompanied by seismic sequences than weaker eruptions (Fig. 22b).

5.3.2. Seismic sequences and volcanoes

Seismic sequences occurring in the vicinity of volcanoes but without any direct link to volcanic eruptions probably reflect magmatic processes without any manifestation at the earth surface. This assumption is supported by the previous analysis of correlations between sequences and eruptions.

The spatial correlation between position of volcanoes and seismic sequences is determined for the same distance limit of 80 km. A total of 469 seismic sequences (62% of all the sequences occurring in the lithospheric wedges) are situated in the vicinity of a volcano. Some of the sequences are also related to more than one volcano. Large percentage of sequences is assigned to only a relatively small number of volcanoes. Nearly 25 % of 469 sequences can be linked to 5 volcanoes; 50 % of sequences to 15 volcanoes etc. Nearly 30 % of sequences belong to one of 13 volcanoes with eruption of the VEI class ≥ 3.

5.3.3. Seismic sequences and eruptions – conclusions

Seismic sequences beneath volcanic arcs at convergent plate margins are probably often triggered by magma migration. Seismic sequences beneath volcanic arcs tend to cluster; their clustering could serve as an indicator for recognition of active volcanic centers. The spatial density of seismic sequences is probably a more important factor than the number of earthquakes in a sequence. Although many seismic sequences are probably directly connected to magmatic activity, some sequences are a consequence of other tectonic processes than magma migration. However, seismic sequences can be used – if combined carefully with other indicators –as one of signs of the magmatic or even volcanic activity. On the other hand, seismic sequences do not occur beneath all active volcanoes and a lack of seismicity beneath a portion of a volcanic arc cannot be taken as a manifestation of absence of magmatic processes.

5.3.4. Earthquakes and seismic sequences in lithospheric wedge

Within individual regions, the percentage of earthquakes belonging to seismic sequences slightly grows with the increase of percentage of earthquakes occurring in the lithospheric wedge (Fig. 23). Although it is not a robust relation, the Pearson correlation coefficient is equal to 0.75 making a certain level of dependency probable.

Such a relation may reflect a degree of fracturing of the lithospheric wedge. With an increasing rate of fracturing of the wedge the proportion of wedge-related earthquakes should increase because the wedge easily releases stress produced by convergence. Simultaneously, the proportion of sequence-related earthquakes increases.

This finding is beyond the scope of this thesis, but it is worth to investigate it in detail in future.

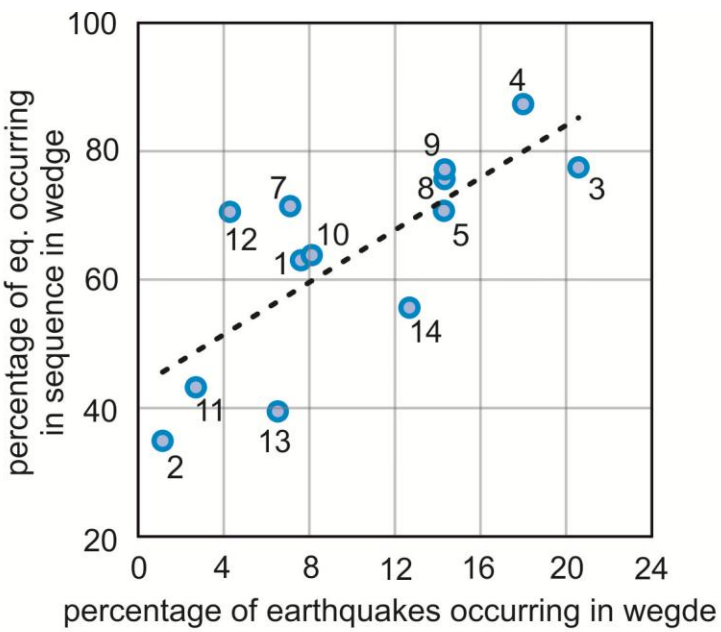

Fig. 23. Wedge seismicity and seismic sequences. Relation between the percentage of earthquakes occurring in the lithospheric wedge (horizontal axis) and percentage of earthquakes belonging to seismic sequences (vertical axis). The data from the Andaman-Nicobar Island Arc (region 6) are strongly affected by the large Sumatran earthquake in 2004 (see chapter 7.6) and are excluded. Data are marked by numbers of individual regions.

6. *b*-value analysis

Magma ascends to the earth surface through lithospheric wedges. On the way up, it has to overcome extreme lithostatic pressures, intruding primarily to areas of the lowest resistance. It is possible to assume that magma ascends preferably through a fractured medium than through a compact rock. This assumption is tested by the Gutenberg-Richter law in the following paragraphs.

6.1. Gutenberg-Richter Law

According to the United States Geological Survey, about 1 300 000 earthquakes within the magnitude range of 2 – 2.9 on average occur every year; about 13 000 earthquakes in the magnitude range of 4 – 4.9 and only 15 in the magnitude range of 7 – 7.9. The annual frequency of earthquakes rapidly decreases with the increasing magnitude. The relationship between the annual frequency (N) and the magnitude (M) called Gutenberg-Richter law (Gutenberg, 1945) is given by the following equation:

$$\log_{10} N = a - bM, \tag{16}$$

or

$$N = 10^{a-bM}, \tag{17}$$

where a and b are constants (Lowrie, 2007). The constant a is of less scientific interest; the constant b varies in dependence on properties of rock environment in the area under study. Globally, the *b*-value is equal to 1 which means that for every earthquake of magnitude 5 there are 10 earthquakes of magnitude 4, 100 earthquakes of magnitude 3 etc. *b*-value higher than 1 reflects geological complexity of the area, material heterogeneity and high crack density. *b*-value lower than 1 is typical for areas with a low degree of heterogeneity and with large faults with high stresses and strains (Bayrak, 2012). The *b*-value grows during earthquake swarms occurrence. The Gutenberg-Richter law and determination of *b*-value is illustrated in Fig. 24.

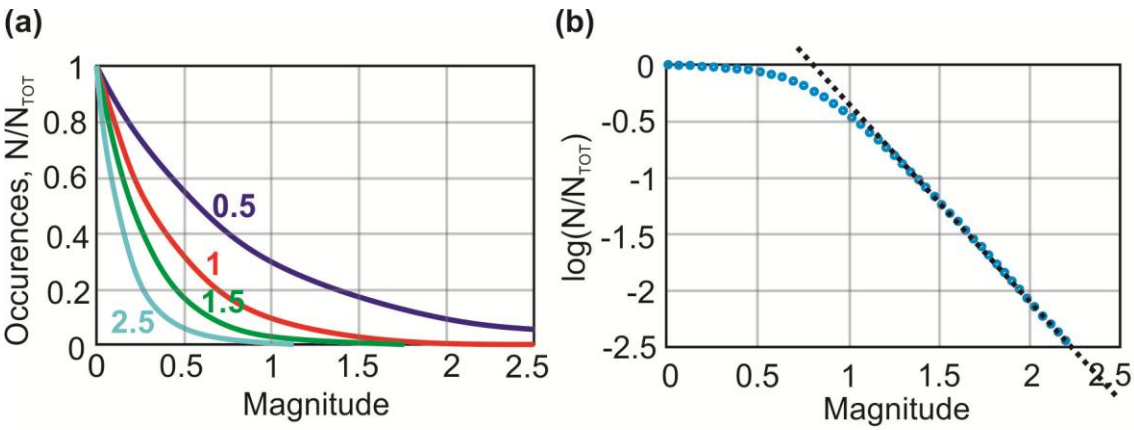

Fig. 24. Illustration of the Gutenberg-Richter law. (a) Decrease in number of earthquakes with increasing magnitude and related b-values. (b) The b-value determination. The b-value is equal to the slope of the line interpolated in the linear part of the diagram.

High b values are usually observed in areas around volcanoes. There are two possible explanations of this phenomeneon: i) magma ascents to the surface through a thick lithospheric wedge. To make the ascent most effective, magma intrudes preferably in zones weakened by a higher crack density (Murru et al., 2005); ii) frequent occurrence of seismic sequences beneath volcanoes.

Although the cause of the increased *b*-value around volcanoes is still questionable, the *b*-value can be used as one of the indicators of magmatic/volcanic processes.

6.2. Calculation of *b*-values

To determine the b value, a reliable determination of the earthquake magnitude is necessary. The EHB hypocentral determinations contain body-wave magnitude m_b for 99 % of earthquakes, surface-wave magnitude M_S for 36 % of events and moment magnitude M_W for 22 % of earthquakes. The EHB dataset was adjusted by the following steps to be suitable for the *b* value analysis:

i. The events without any magnitude determination were excluded (less than 1 % of data).
ii. In order to eliminate the effect of the magnitude saturation, the surface-wave magnitudes M_S or the moment magnitudes M_W were used wherever available (see Fig. 25a.).

iii. Body-wave magnitude m_b was used for all other earthquakes.

b-value express the slope of the line interpolated in the straight part of the log-log scaled cumulative histogram of magnitudes. The following steps were done in order to obtain the *b*-value:

i. The cumulative histogram of magnitudes in a log-log scale was plotted (Fig. 25b).
ii. The minimum magnitude for the interpolation of the line is the magnitude completeness of the dataset. The magnitude completeness of the dataset is the value of the most numerous magnitude. This value is obtained from the normal histogram of magnitudes.
iii. Using linear regression, the b-value was obtained as the slope of the interpolated line.

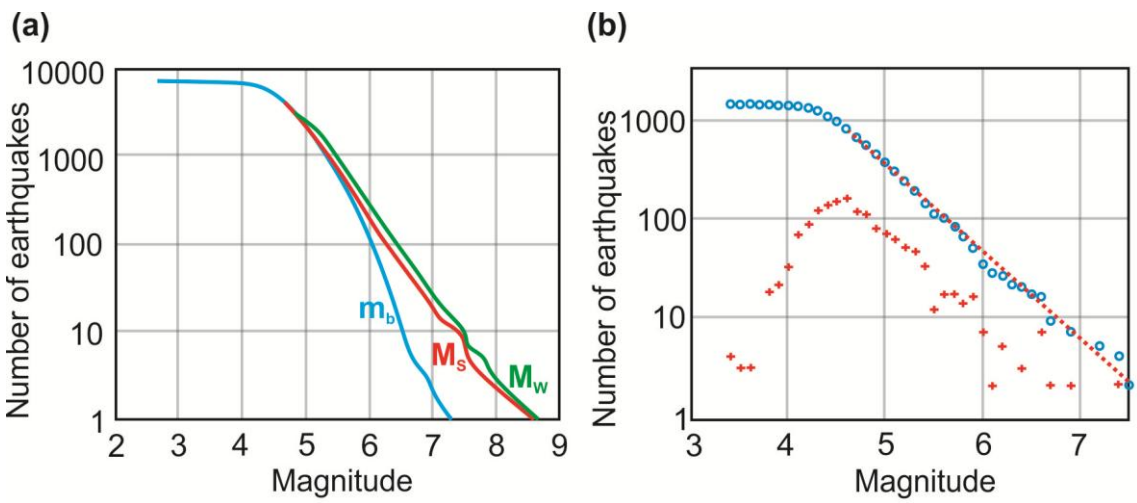

Fig. 25. b-value determination. (a) The effect of magnitude saturation for body wave magnitude m_b and surface wave magnitude M_s; (b) determination of b-value. The cumulative histogram of earthquake magnitudes is denoted by blue circles; normal histogram is denoted by red crosses; the red dashed line is the line obtained by linear regression of the cumulative histogram.

b-values are determined in a mesh of points for every analyzed region separately. Every b-value is calculated from the set of earthquakes that are situated within the circle of radius *r* from the calculation point (Fig. 26a). The problem of this approach is a low number of points arriving into the calculation which can cause increase in the error of the *b*-value calculation. The resolution of the resulting map depends on the number of points in a mesh and radius r.

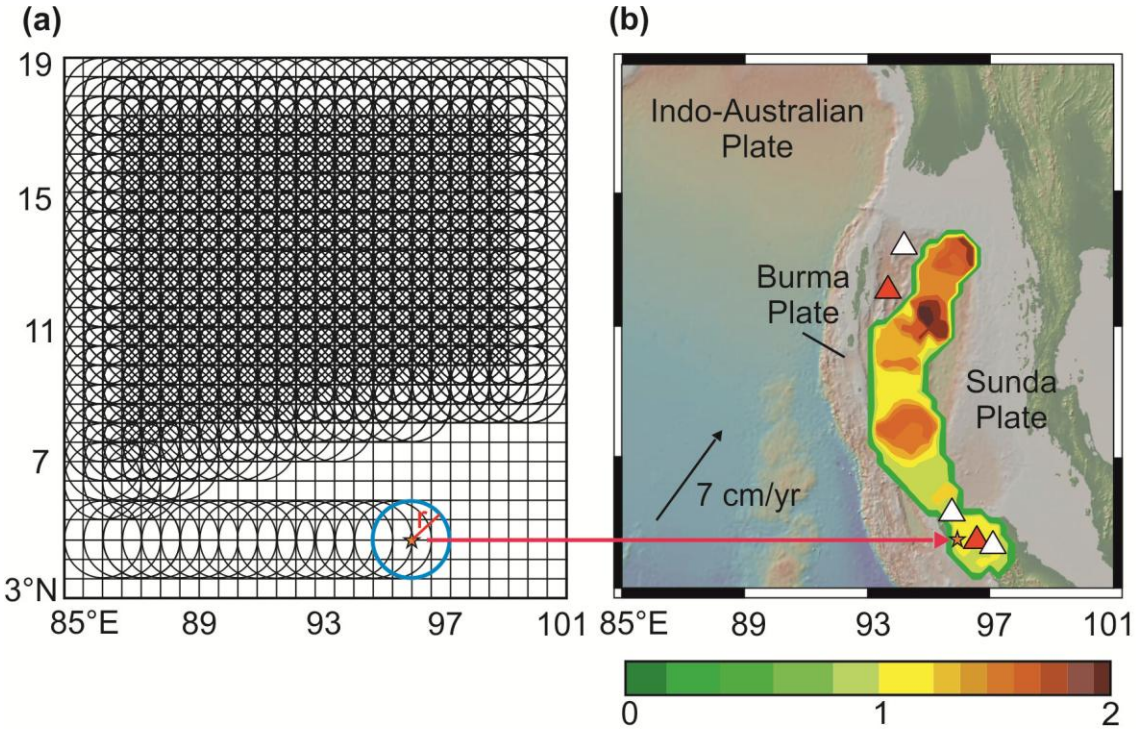

Fig. 26. Example of determination of b-values in a region. (a) Layout of mesh and radius of calculation *r*. The b-value was calculated from the set of earthquakes that are situated within the circle of radius *r* from the calculation point. (b) Example of the result in the Andaman-Nicobar volcanic arc.

7. Analysis and discussion of earthquake occurrence in individual domains

One of the aims of this diploma thesis was to detect areas with specific seismicity pattern that may reflect migration of magma in the crust and possible volcanic activity at the seafloor. The specific seismicity pattern is characterized by increased number of seismic swarms and, sometimes, increased *b*-value. The other feature that may indicate recently active magmatic/volcanic processes is the occurrence of a submarine morphological elevation at the seafloor above the seismicity pattern.

In the following paragraphs, the results of seismic sequence density analysis and analysis of *b*-value are presented and discussed. 14 subduction zones with active volcanic arcs were investigated. The study was concentrated on the submarine portions of the volcanic arcs, where only few active volcanoes included in the Smithsonian Global Volcanism Program database are situated.

7.1. Aleutian Arc

The Aleutian volcanic arc is situated in the northern Pacific Ocean. It is formed by 47 subaerial volcanoes and one submarine volcano. Six volcanoes were active between 1964 and 2008. The volcanic arc results from the subduction of the Pacific plate beneath the North American plate. The velocity of convergence varies from 7 to 8 cm/yr (Bird, 2003). The 3,400 km long Aleutian Trench extends from the intersection with the Queen Charlotte Fault system in the east to the triple junction of the Ulakhan Fault and Kuril-Kamchatka Trench in the west (Addicott and Richards, 1984).

The EHB database contains over 5,300 earthquakes occurring in the region. 92 % of earthquakes belong to the Wadati-Benioff zone and to the horizontal part of the Pacific plate in front of the trench. 8 % of earthquakes (over 400 events) occurred in the overlying wedge beneath the volcanic arc.

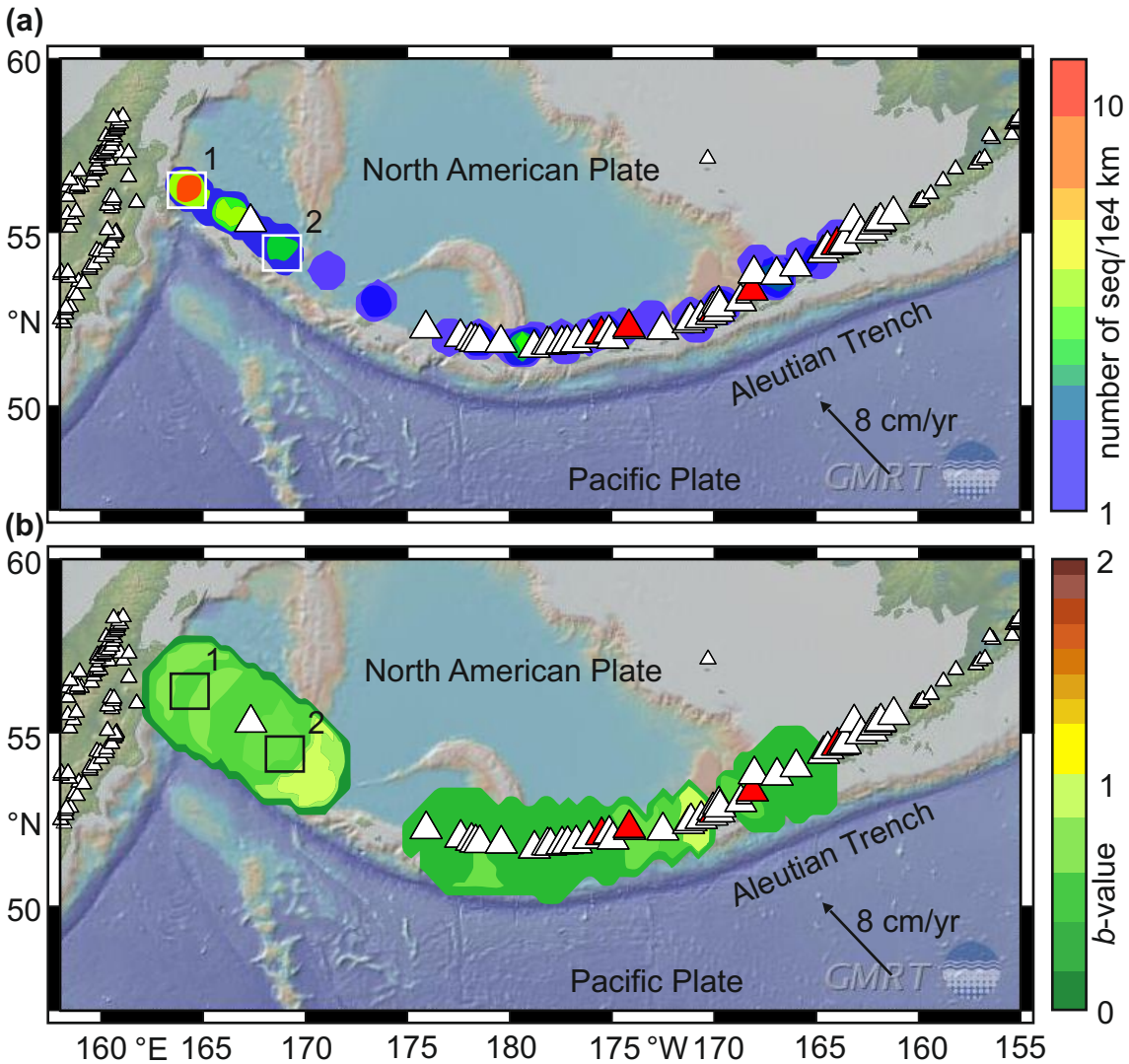

Fig. 27. Results of analyses for Aleutian volcanic arc. (a) Analysis of seismic sequence density. (b) Environment heterogeneity analysis. Volcanoes are denoted by triangles (volcanoes active between 1964 and 2008 are denoted by red color, volcanoes not belonging to the Aleutian arc are denoted by smaller symbols). The direction of convergence is indicated by the arrow. The areas 1, 2 highlighted by rectangles are presented in detail in Figs. 28 and 29, respectively.

The results of the analyses (seismic sequence density analysis, environment heterogeneity analysis) show several discrete spots of increased values (Fig. 27.). Some of them are situated in the vicinity of the volcanoes in the eastern part of the arc. Because this thesis is aimed at the areas without any volcano listed in the Smithsonian database, these spots of increased values are not discussed in detail. Two of the spots are placed in the western part of the arc without any link to a particular volcano. No remarkable seamount has been found either in the area 1 (Fig. 28a) or in the area 2 (Fig. 29a). Both these areas are situated in the region where the plates move horizontally along the plate boundary and the convergent component of the movement is small. Only shallow seismicity occurs here (Fig. 28b; Fig. 29b). The WBZ is absent, the process of subduction, the essential condition for magmatic processes at the volcanic arc, is not in progress. The increased values of the seismic sequence density probably reflect a complicated tectonic structure in the vicinity of the triple junction area.

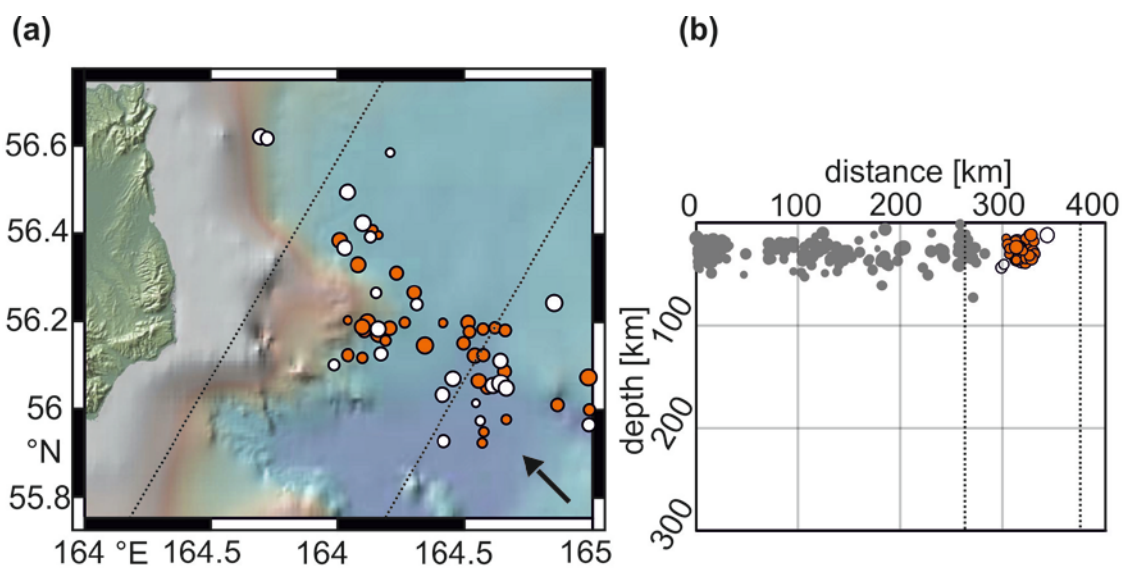

Fig. 28. Seafloor morphology and tectonic position of the area 1 in Aleutian volcanic arc. (a) Map showing seafloor morphology of the area 1. Black arrow indicates the direction of the subducting plate movement; the dotted lines show the position of the cross-section. (b) Seismic cross-section showing the tectonic position of the studied area. The position of the area of interest is denoted by the dotted vertical lines. Seismicity occurring in the horizontal part of subducting plate is denoted by grey dots, wedge earthquakes are colored in red, other wedge earthquakes are white.

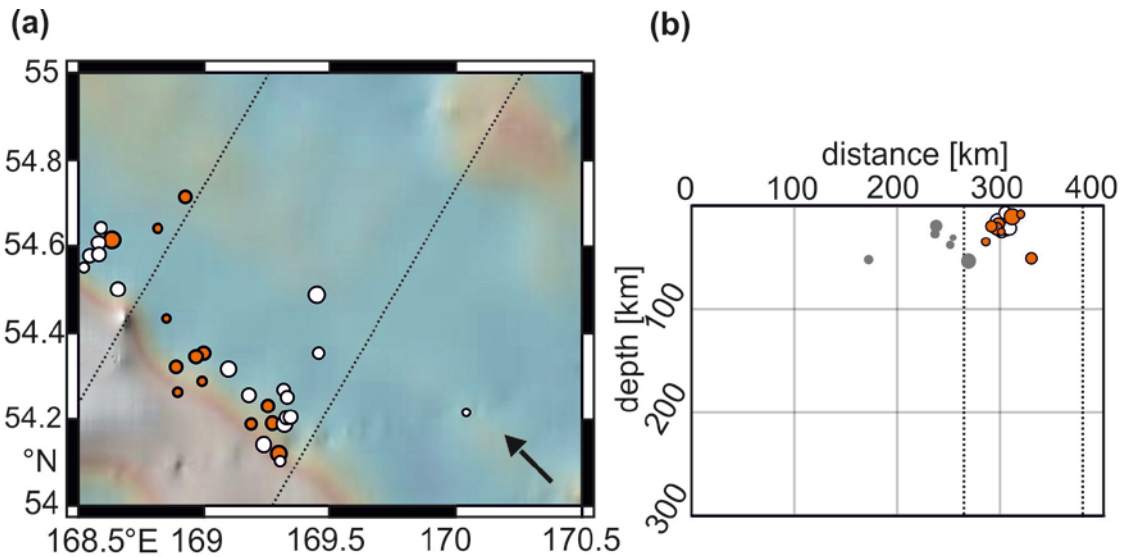

Fig. 29. Seafloor morphology and tectonic position of the area 2 in Aleutian volcanic arc. (a) Map showing seafloor morphology of the studied area. (b) Seismic cross-section showing the tectonic position of the studied area. Symbol description – see Fig. 28.

7.2. Kuril Arc

The Kuril volcanic arc is situated in the western part of the Pacific Ocean between Kamchatka and Japan. The arc comprises 74 volcanoes, 17 of which were active in the period between 1964 and 2008. Four volcanoes are submarine. The volcanic arc results from the subduction of the Pacific Plate under the Okhotsk Plate along the Kuril-Kamchatka Trench. The velocity of the convergent movement reaches 8 cm/yr (Bird, 2003). The 1,200 km long trench extends from a triple junction with the Ulakhan Fault and the Aleutian Trench in the northeast to the intersection with the Japan Trench in the southwest (Addicott and Richards, 1984).

The EHB database contains over 7,200 earthquakes occurring in the region. Most of the earthquakes (nearly 99 %) belong to the Wadati-Benioff zone and to the horizontal part of the Pacific plate in front of the trench. Only 1 % (less than 100 earthquakes) occurred in the overlying wedge beneath the volcanic arc. Due to the small number of earthquakes in the wedge, the results obtained are too inaccurate for any assessments.

7.3. Ryukyu Arc

The Ryukyu volcanic arc is situated in the western Pacific Ocean south of the Japan Islands. It consists of 16 volcanoes, four of which were active between 1964 and 2008. Three of the volcanoes are submarine. The volcanic arc results from the subduction of the Philippine Sea Plate under the Okinawa Plate, a part of the Eurasian plate, along the Ryukyu Trench. Over 1,200 km long trench extends from the Boso Triple Junction in the north to the Taiwan Island in the south. Velocity of the convergent movement reaches 8 cm/yr (Addicott and Richards, 1984; Bird, 2003).

The EHB database contains over 2,400 earthquakes occurring within the Ryukyu region. About 79 % of earthquakes belong to the Wadati-Benioff zone and to the horizontal part of the Philippine Sea Plate in front of the trench. 21 % of earthquakes (nearly 500 events) occurred in the overlying wedge beneath the volcanic arc.

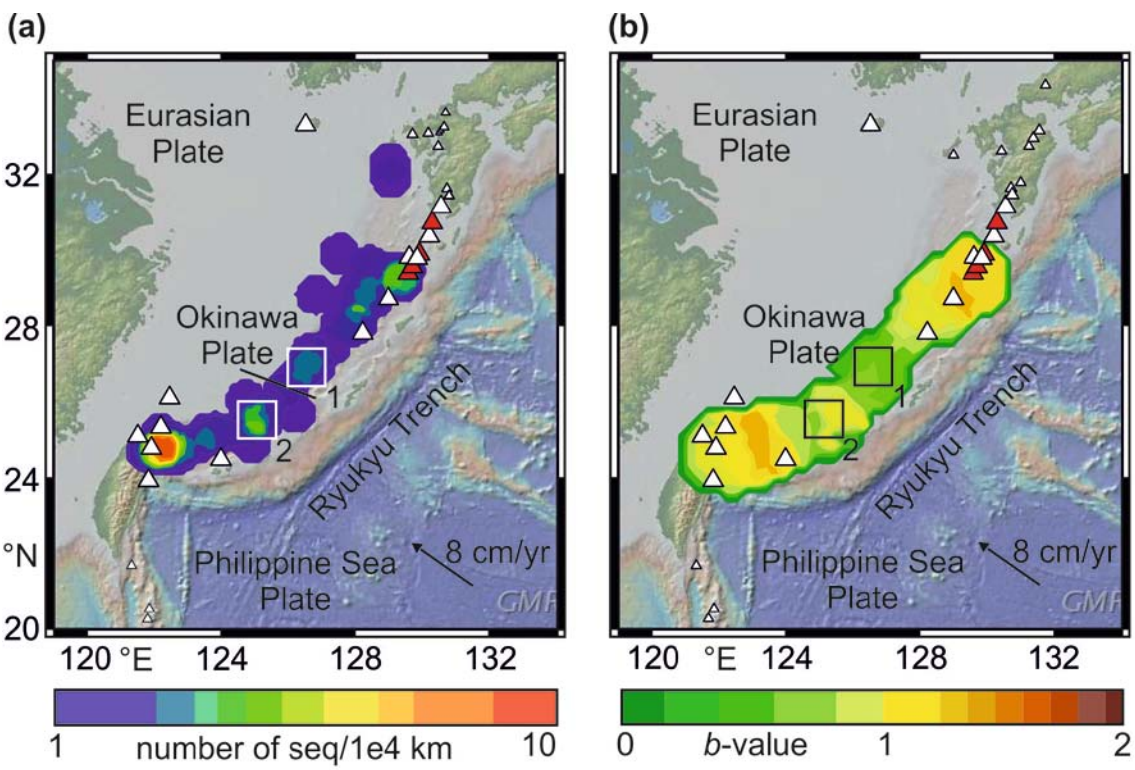

Fig. 30. Results of analyses for Ryukyu volcanic arc. (a) Analysis of seismic sequences density. (b) Environment heterogeneity analysis. The areas 1, 2 highlighted by rectangles are presented in detail in Figs. 31 and 32, respectively. Symbol description – see Fig. 27.

The seismic sequence density analysis (Fig. 30a) shows five spots of increased value of this parameter along the volcanic arc. Two spots of high *b*-value are situated in the northern and the southern edge of the arc (Fig. 30b). Both analyses show increased values in the

southern part of the arc, namely in the area where several dormant volcanoes are located. The ongoing detailed study, conducted by Špičák and Vaněk (2013c), explains this particular seismicity in the area by recent magma ascent through the lithospheric wedge. The two spots of increased sequence density occur in the middle part of the volcanic arc without any direct link to particular volcanoes. The local morphology in the area 1 is indistinct (Fig. 31a). Eruptions of magma at the seafloor are thus highly improbable, though the earthquake foci in the lithospheric wedge above the subducting slab are situated in a position that corresponds to potential subduction-generated magma migration in the wedge (Fig. 31b).

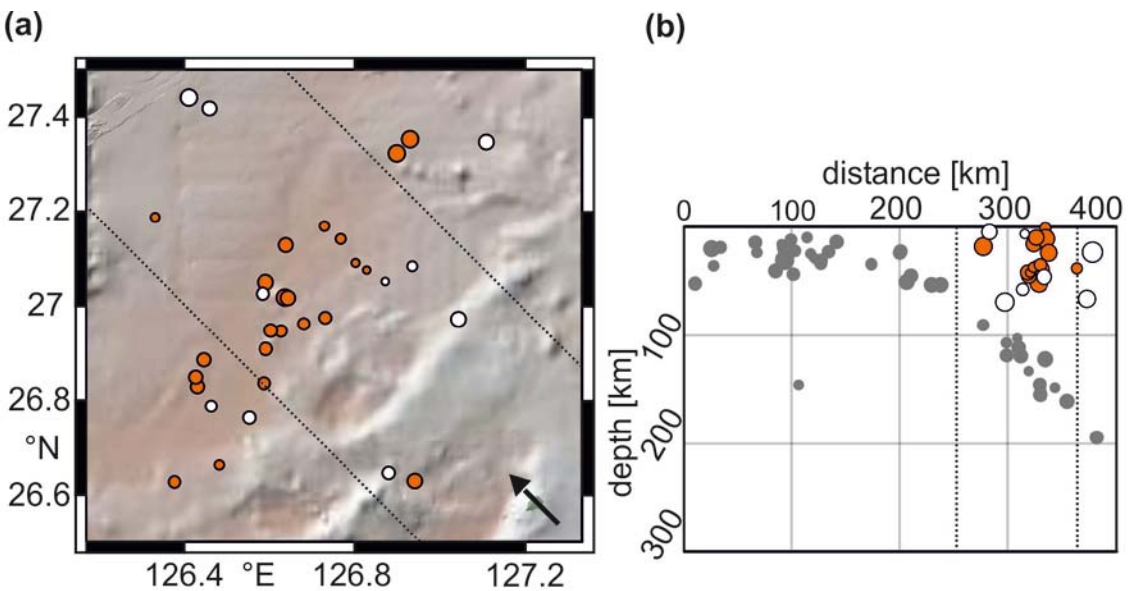

Fig. 31. Seafloor morphology and tectonic position of the area 1 in Ryukyu volcanic arc. (a) Map showing seafloor morphology of the studied area. (b) Seismic cross-section showing the tectonic position of the studied area. Symbol description – see Fig. 28.

An elongated seamount was found in the area 2, reaching about 1,000 meters above the seafloor, with the summit of about 1,000 m below the sea level (Fig. 32a). Epicenters of earthquakes in the lithospheric wedge correlate with the position of the seamount. Area 2 may be a site of recent magmatic/volcanic activity.

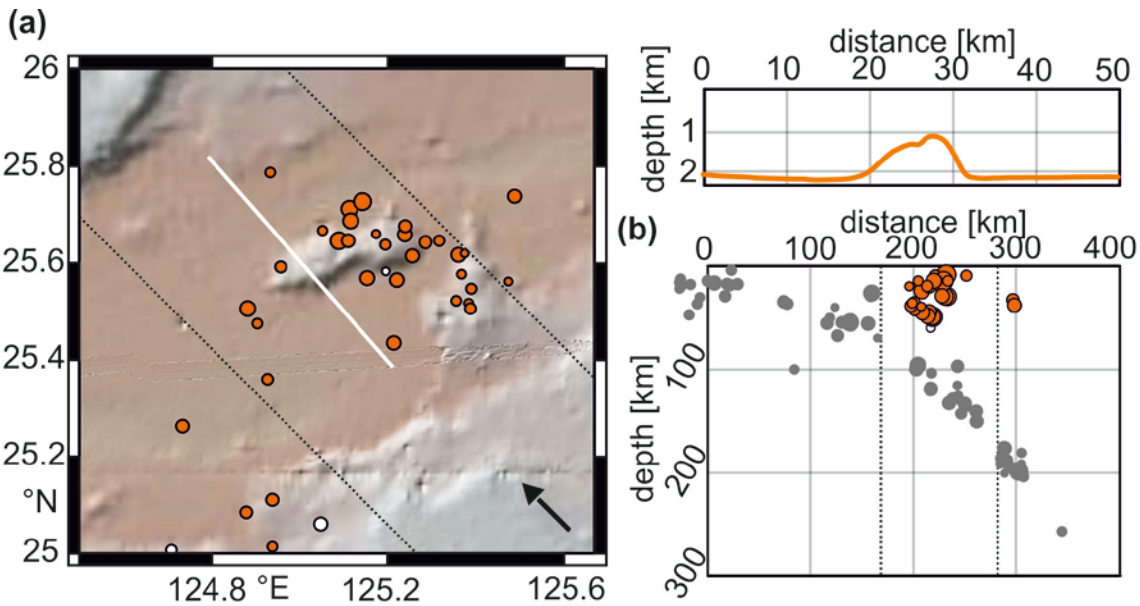

Fig. 32. Seafloor morphology and tectonic position of the area 2 in Ryukyu volcanic arc. (a) Map showing seafloor morphology of the studied area and the profile showing the topography of the present seamount. The position of the profile in the map is denoted by white line. (b) Seismic cross-section showing the tectonic position of the studied area. Symbol description – see Fig. 28.

7.4. Izu-Bonin Arc

The Izu-Bonin volcanic arc is situated in the western Pacific Ocean south of Japan. The arc comprises 30 volcanoes; 11 of the volcanoes are submarine. Eighteen volcanoes were active between 1964 and 2008. The volcanic arc results from the subduction of the Pacific Plate under the Philippine Sea Plate along the Izu-Ogasawara Trench. The 1,200 km long trench extends from the Boso Triple Junction in the north to the south where it merges into the Mariana Trench. The velocity of the convergent movement reaches about 5 cm/yr (Addicott and Richards, 1984; Bird, 2003).

The EHB database contains over 5,100 earthquakes in the Izu-Bonin region. About 82 % of earthquakes belong to the Wadati-Benioff zone and to the horizontal part of the Pacific plate. 17 % of earthquakes occurred in the overlying wedge beneath the volcanic arc.

Seismicity beneath the volcanoes is strong enough to be analyzed and the results of both analyses show discrete spots of elevated values. All the spots of the increased values are situated in the vicinity of the volcanoes of the arc and are not analyzed in detail. The

strongest anomalies can be found namely in the area around the Suiyo, Mokuyo and Doyo volcanic seamounts at latitude 28°N. The space-time analysis of seismicity in this area brought evidence of recent magma transport beneath the volcanic seamounts (Špičák et al., 2009).

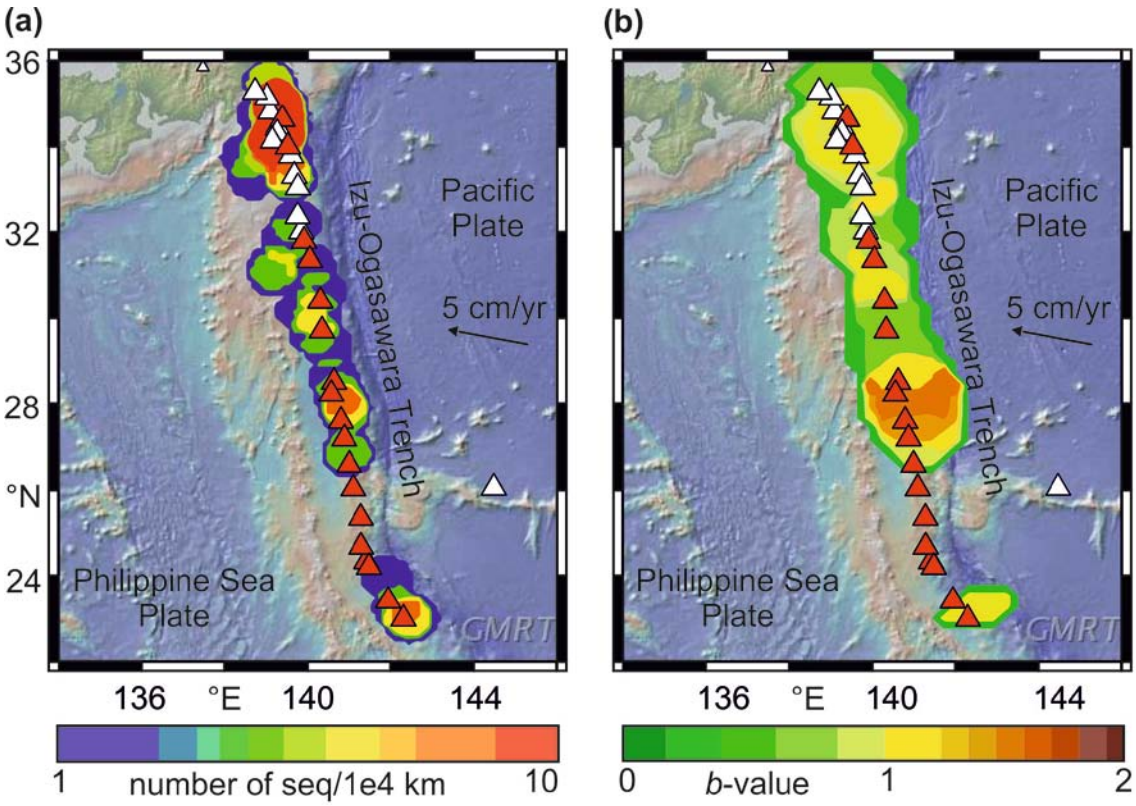

Fig. 33. Results of analyses for Izu-Bonin volcanic arc. (a) Analysis of seismic sequences density. (b) Environment heterogeneity analysis. Symbol description – see Fig. 27.

7.5. Mariana Arc

The Mariana volcanic arc is situated in the western Pacific Ocean south from the Izu-Bonin volcanic arc. The arc consists of 25 volcanoes, 21 of which are submarine. 11 volcanoes were active between 1964 and 2008; the volcanic arc results from the subduction of the Pacific Plate under the Mariana Plate, derived from the Philippine Sea Plate, along the Mariana Trench. The 2,300 km long Mariana Trench is the deepest part of the world's ocean. In the north it merges into the Izu-Ogasawara Trench, in the south it is followed by the Yap Trench. The velocity of the convergent movement reaches about 4 cm/yr (Addicott and Richards, 1984; Bird, 2003).

The EHB database contains over 5,000 earthquakes in the Mariana arc region. 86 % of the earthquakes belong to the Wadati-Benioff zone and the horizontal part of the Pacific plate in front of the trench. More than 14 % of earthquakes occurred in the overlying wedge beneath the volcanic arc.

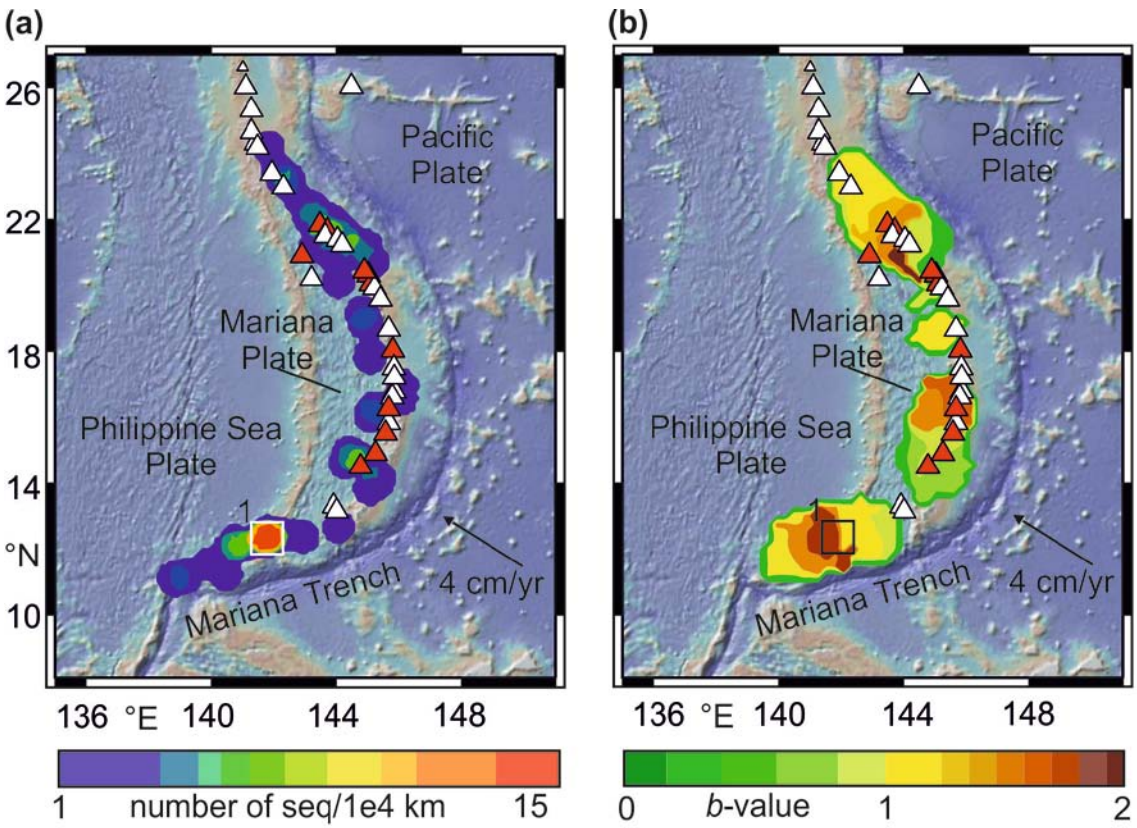

Fig. 34. Results of analyses for Mariana volcanic arc. (a) Analysis of seismic sequences density. (b) Environment heterogeneity analysis. Symbol description – see Fig. 27. The area 1 highlighted by rectangle is presented in detail in Fig. 35.

The results of both analyses show several discrete spots of increased values (Fig. 34). Most of the spots are situated in the vicinity of some of the arc volcano. One spot of increased values of the seismic sequence density and the increased *b*-value without any direct link to any volcano is situated in the southern tip of the volcanic arc.

A remarkable seamount was found on the seafloor in the area 1 (Fig. 35a). The seamount reaches height of approximately 1,500 meters above the seafloor, with the summit more than 1,000 m below the sea level. Epicenters of earthquakes occurring in the lithospheric wedge are situated about 40 km southwest from the seamount and do not correlate with the position of the seamount. Due to the absence of remarkable seamount above the seismicity pattern, eruptions of magma at the seafloor are improbable.

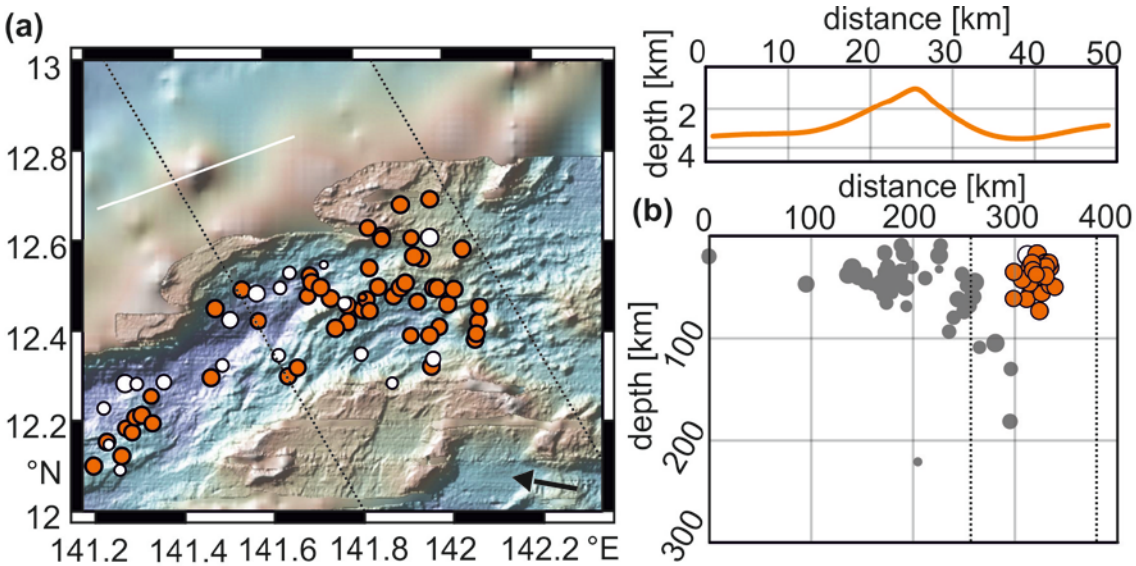

Fig. 35. Seafloor morphology and tectonic position of the area 1 in Mariana volcanic arc. (a) Map showing seafloor morphology of the studied area and the profile showing the topography of the present seamount. The position of the profile in the map is denoted by white line. (b) Seismic cross-section showing the tectonic position of the studied area. Symbol description – see Fig. 28.

7.6. Andaman-Nicobar Arc

The Andaman-Nicobar volcanic arc is located east of the Bay of Bengal. The volcanic arc comprises only 2 subaerial volcanoes, one of them being active between 1964 and 2008. The volcanic arc results from the subduction of Indo-Australian Plate under the Burma Plate, derived from the Sunda Plate, along the Andaman-Nicobar Trench. The Burma Plate is detached from the Sunda Plate by a north-south situated transform fault. The convergence velocity reaches about 7 cm/yr (Addicott and Richards, 1984; Bird, 2003).

Nearly 2,800 earthquakes of the EHB database occurred in the region during the studied period. Seismicity is strongly influenced by the large M 9.1 Dec. 26, 2004 Sumatra-Andaman earthquake that induced huge aftershock activity in the region. The amounts of earthquakes observed during the period 1964 - December 25, 2004 and during the year December 26, 2004 - December 25, 2005 were equal. Only 55 % of earthquakes occurred in the WBZ or in the horizontal part of the Indo-Australian Plate. 45 % of events belong to the overlying wedge. Most of the earthquakes in the wedge occurred at the transform fault between the Burma and Sunda Plates.

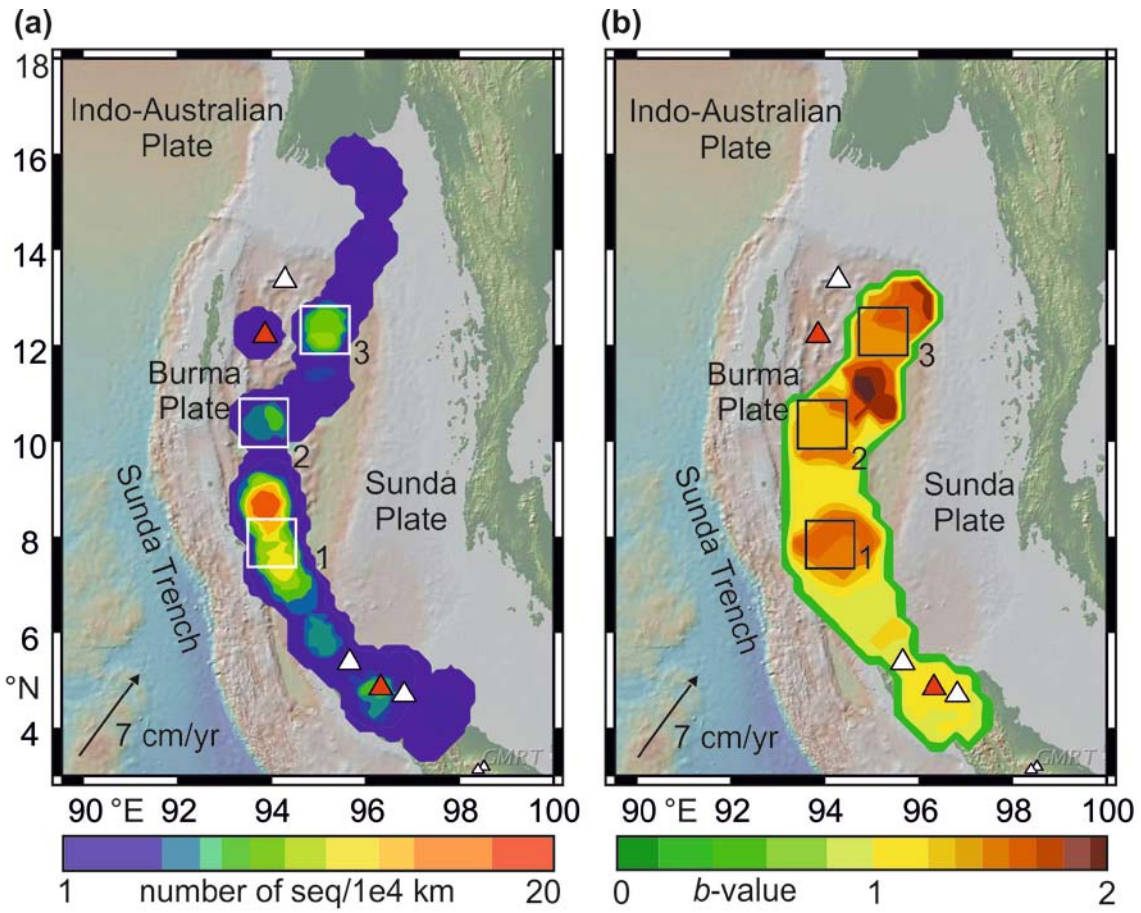

Fig. 36. Results of analyses for Andaman-Nicobar volcanic arc. (a) Analysis of seismic sequences density. (b) Environment heterogeneity analysis. The areas 1, 2, 3 highlighted by rectangles are presented in detail in Figs. 37, 38 and 39, respectively. Symbol description – see Fig. 27.

The results of the analysis of seismic sequence density (Fig. 36a) show four spots of increased values. Two spots are located in the northern part of the arc; one spot is situated beneath the Peuet Sague volcano in the southern part of the arc. The most remarkable one is situated approximately in the middle of the studied region at latitude 7.5 °N marked as area 1 in the Fig. 36. The *b*-value analysis shows increased values namely in the northern part and in the middle of the explored area.

An approximately 2,000 m high seamount is situated in area 1 (Fig. 37 a, b). The summit of the seamount is about 500 m below the sea level. It is situated at the edge of the Sunda Plate in the vicinity of the transform fault. The earthquake foci in the lithospheric wedge above the subducting slab are situated in a position that corresponds to potential subduction-generated magma migration in the wedge. A large seismic sequence occurred beneath the seamount in the period between December 26, 2004 and March, 2005

counting nearly 600 earthquakes in the EHB database. This remarkable earthquake occurrence motivated Kamesh Raju et al. (2012) to a detailed investigation of the area. Geochemical analyses of rock samples and detailed bathymetry detected a well-developed crater at the summit of the seamount and indicate that the seamount is most probably a recently active submarine stratovolcano.

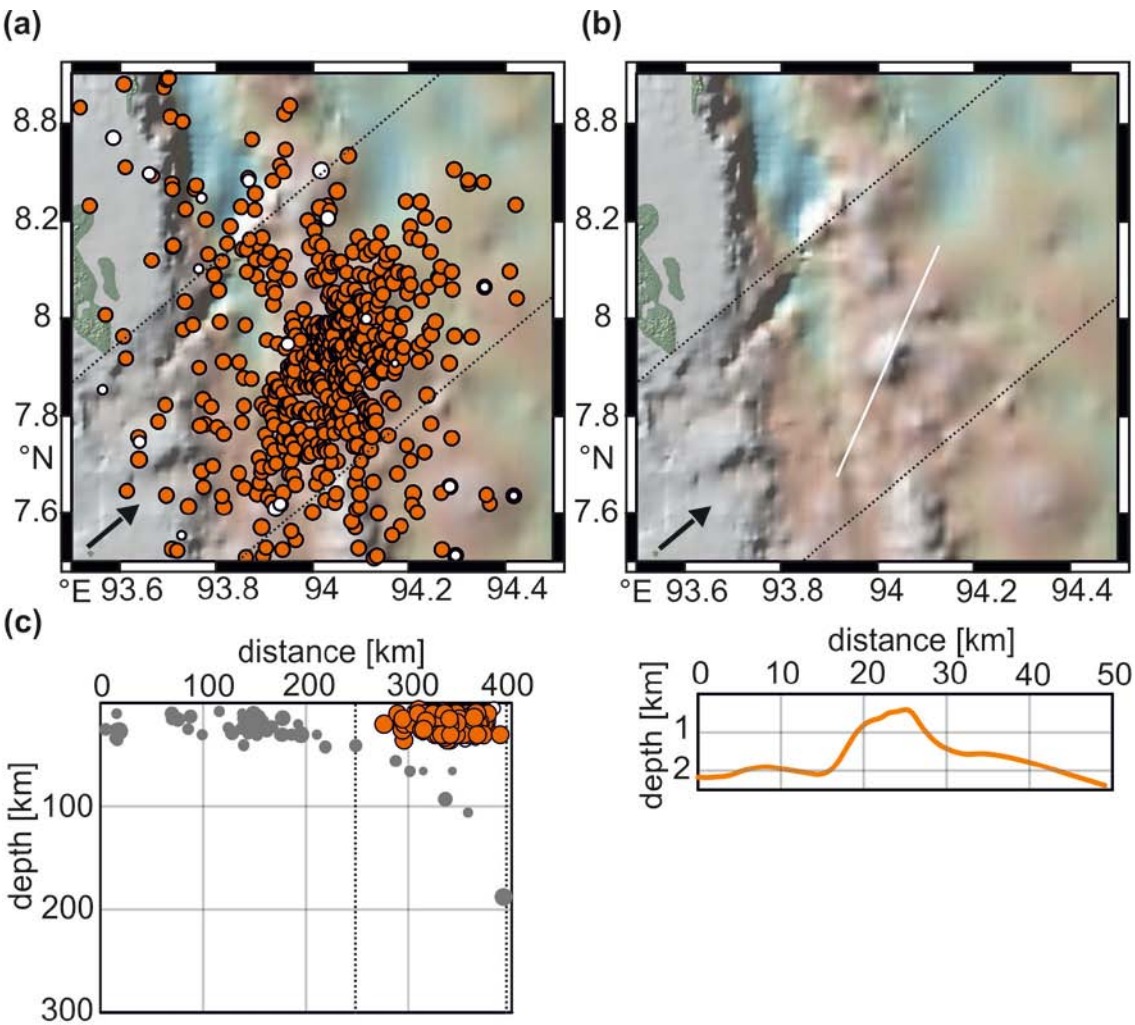

Fig. 37. Seafloor morphology and tectonic position of the area 1 in Andaman-Nicobar volcanic arc. (a) Epicentral map of the area. (b) Map showing seafloor morphology of the studied area and the profile showing the topography of the present seamount. The position of the profile in the map is denoted by the white line. (c) Seismic cross-section showing the tectonic position of the studied area. Symbol description – see Fig. 28.

A remarkable seamount is situated in the area 2, too (Fig. 38). It reaches the height of about 2,500 m above the seafloor; its summit is about 1,000 m below the sea level. The position of the seamount in relation to the subducting plate and the transform fault is the same as the position of the seamount in the area 1. Repeated earthquake occurrence in the

area in the form of earthquake swarms may reflect recent magmatic as well as volcanic activity beneath the seamount.

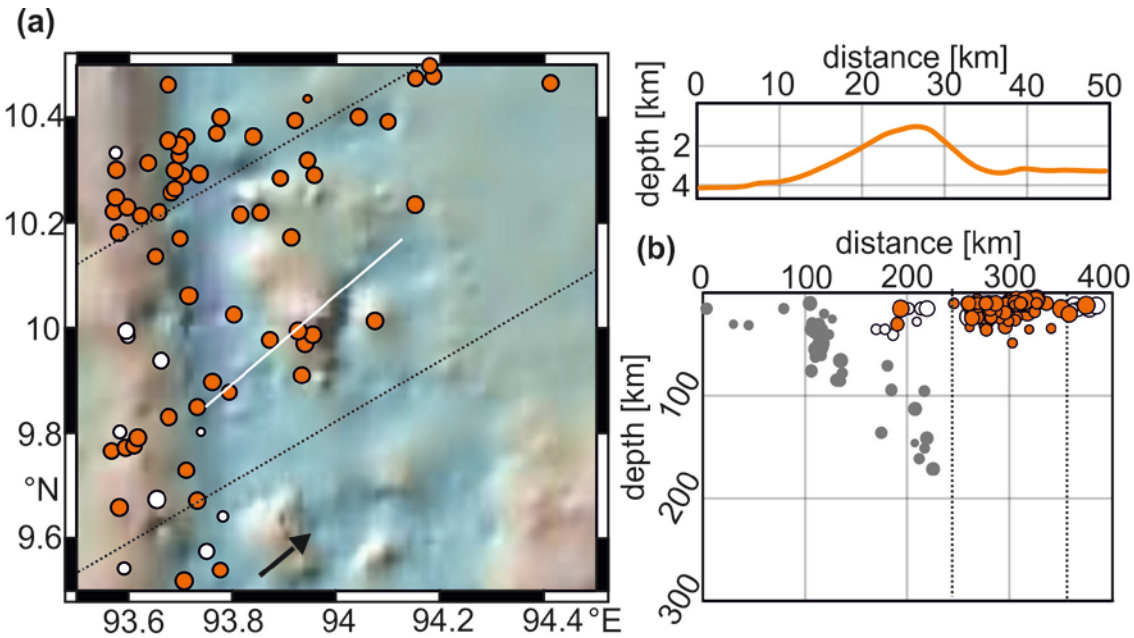

Fig. 38. Seafloor morphology and tectonic position of the area 2 in Andaman-Nicobar volcanic arc. (a) Map showing seafloor morphology of the studied area and the profile showing the topography of the present seamount. The position of the profile in the map is denoted by the white line. (b) Seismic cross-section showing the tectonic position of the studied area. Symbol description – see Fig. 28.

A morphological depression is situated in the area 3 (Fig. 39). The depression belongs to the north-south transform fault with the rift segments separating the Burma Plate from the Sunda Plate. Though the tectonic position of the area is inconvenient for the occurrence of the subduction-related magmatic processes, the specific seismicity pattern may reflect the movements of magma generated in the spreading center.

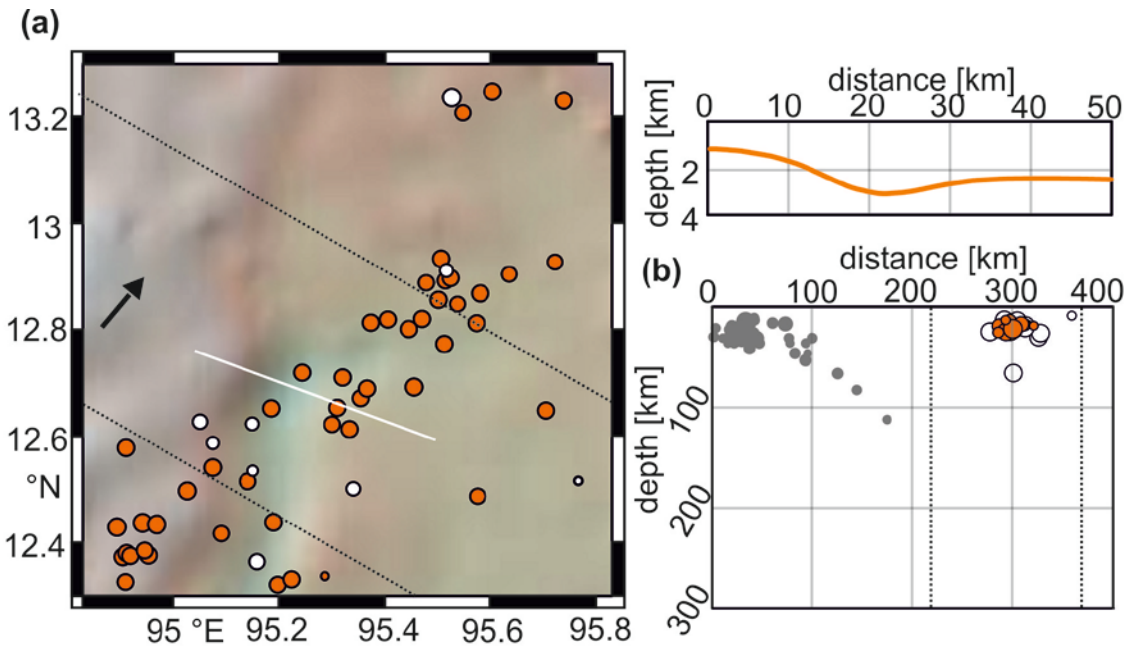

Fig. 39. Seafloor morphology and tectonic position of the area 3 in Andaman-Nicobar volcanic arc. (a) Map showing seafloor morphology of the studied area and the profile showing the topography of the depression. The position of the profile in the map is denoted by the white line. (b) Seismic cross-section showing the tectonic position of the studied area. Symbol description – see Fig. 28.

7.7. Philippine-Halmahera Arc

The Philippine-Halmahera volcanic arc is situated in the western Pacific Ocean south of the Mindanao Island. The arc consists of 10 volcanoes, 2 of which are submarine. Five volcanoes were active between 1964 and 2008. Structure and dynamics of the region is complicated. In the south, the Sunda Plate subducts under the Bird's Head Microplate (derivative of the Pacific and the Caroline Plates), in the north the Philippine Sea Plate subducts beneath the Sunda Plate (Addicott and Richards, 1984; Bird, 2003).

The EHB database contains nearly 4,300 earthquakes occurring within the region. About 93 % of earthquakes belong to the subducting plates and 7 % of events occurred within the overlying wedges. The region is of complex structure. Earthquakes occurring in the lithospheric wedges are spread in a wide area and the results of the analyses obtained for this region are unreliable.

7.8. Banda and Seram Arcs

The Banda and Seram volcanic arcs are situated in the eastern Indonesia. The area comprises two volcanic arcs belonging to two subduction zones. The Banda volcanic arc comprises six volcanoes; one of them was active between 1964 and 2008. The arc resulted from subduction of the Indo-Australian Plate under the Sunda Plate. Velocity of convergence is about 7 cm/yr. The Seram volcanic arc comprises only one recently active volcano; the rest of the arc is formed by dormant volcanoes of Pliocene age (Honthaas, 1999). The volcanic arc is related to the subduction of the Birds Head Microplate, derived from the Philippine Sea Plate and the Caroline Plate, under the Eurasian Plate. Both volcanic arcs have overall length of about 900 km (Addicott and Richards, 1984; Bird, 2003).

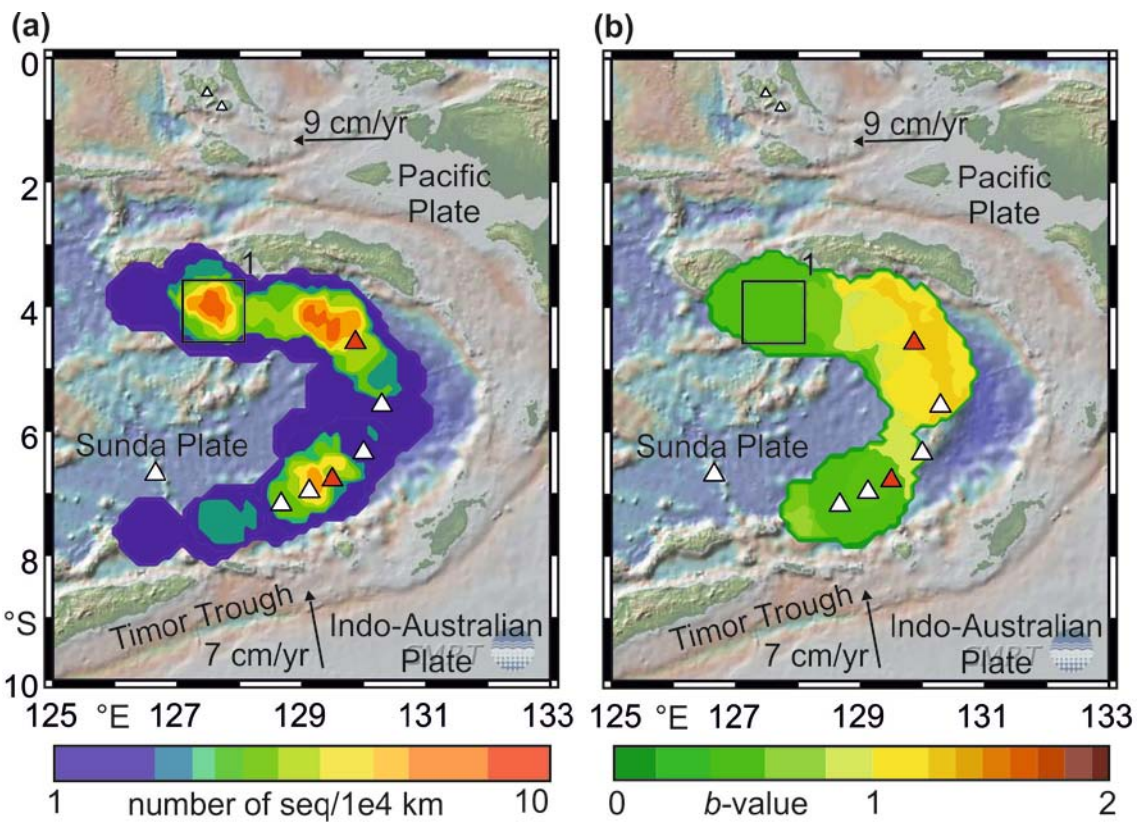

Fig. 40. Results of analyses for Banda and Seram volcanic arcs. (a) Analysis of seismic sequences density. (b) Environment heterogeneity analysis. The area 1 highlighted by rectangle is presented in detail in Fig. 41. Symbol description – see Fig. 27.

The EHB database contains over 2,500 earthquakes occurring in the Banda and Seram regions. 86 % of earthquakes belong to the Wadati-Benioff zone and to the horizontal

parts of the Indo-Australian Plate and the Birds Head Microplates. 14 % of earthquakes (over 350 events) occurred in the overlying wedge beneath the volcanic arc.

The results of the seismic sequence density analysis show three discrete spots of increased values (Fig. 40a). The results of the *b*-value analysis show slightly increased values in the eastern part of the Seram volcanic arc in the vicinity of the recently active Banda Api volcano (Fig. 40b). The first spot of increased values of sequence density is situated beneath the Teon and Nila volcanoes (VEI 1 eruption, 1968) in the Banda volcanic arc. The second spot is located in the vicinity of the Banda Api volcano belonging to the Seram arc. The third spot is situated in the western part of the Seram volcanic arc that was considered to be of Pliocene age, inactive in Holocene (Honthaas, 1999). It is an area without any volcano listed in the Catalogue of Active Volcanoes of the World. This area, marked in Fig. 40a as the area 1, is shown in detail in Fig. 41.

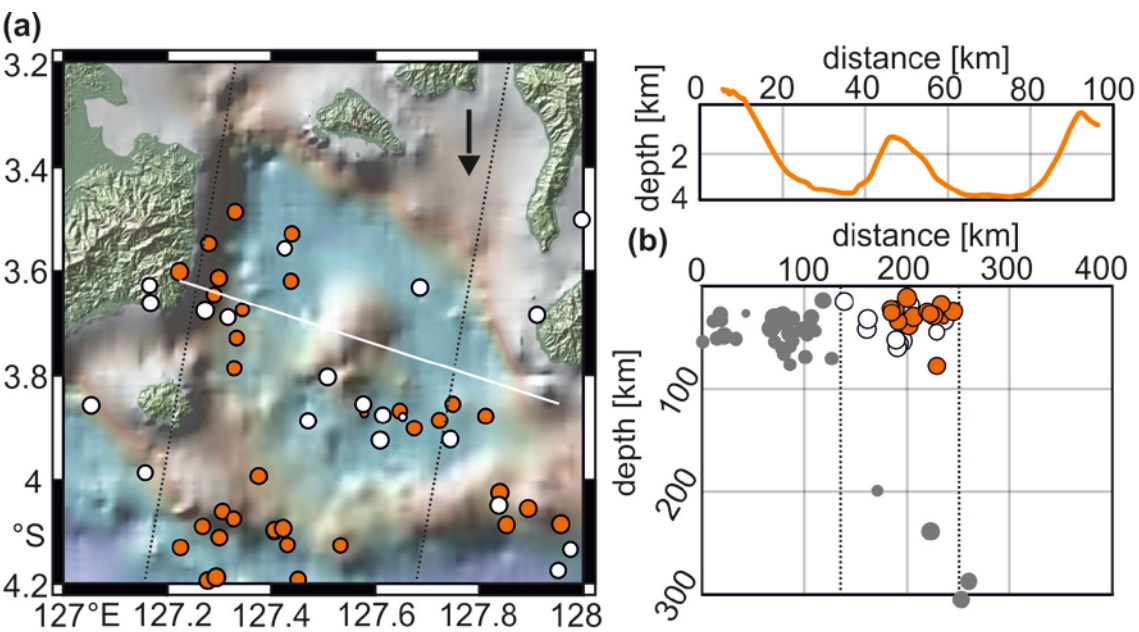

Fig. 41. Seafloor morphology and tectonic position of the area 1 in Banda and Seram volcanic arc. (a) Map showing seafloor morphology of the studied area and the profile showing the topography of the present seamount. The position of the profile in the map is denoted by the white line. (b) Seismic cross-section showing the tectonic position of the studied area. Symbol description – see Fig. 28.

A caldera-like structure with a seamount in the middle is clearly visible in the detailed bathymetry image. The seamount reaches height of about 2,000 meters above the seafloor, with the summit 1,500 m below the sea level. The detailed study of the seismicity in the area was done by Špičák et al. (2013a) and Špičák et al. (2013b). According to these studies

and results described above, the specific seismicity beneath the seamount might be induced by recent magmatic processes.

7.9. Solomon Arc

The Solomon volcanic arc is situated in the equatorial area of the western Pacific Ocean. It consists of 39 volcanoes, 4 of which are submarine. Eleven volcanoes were active between 1964 and 2008. The region is of complex structure and recent geodynamics. In the northern part, the Solomon Sea Plate subducts northward under the South Bismarck Plate. In the southeastern part, of the volcanic arc the Indo-Australian Plate subducts beneath the Pacific Plate. The margin has overall length about 2,000 km. The velocity of the convergent movement varies around 7 cm/yr (Addicott and Richards, 1984; Bird, 2003).

The earthquake database contains nearly 6,000 earthquakes occurring in the region. 86 % of all events are related to the subducting plates. About 850 earthquakes (14%) occurred beneath the volcanic arc and belong to the overlying wedge.

The seismic sequence density analysis shows several discrete spots of increased values, whereas the results of the *b*-value analysis are without particular anomalies. All the spots of increased sequence density occur in the vicinity of the arc volcanoes. Because the evaluation was pointed to the submarine portions of volcanic arcs, where no active volcano is tabulated in the Smithsonian database, these spots of increased sequence density were not studied in detail.

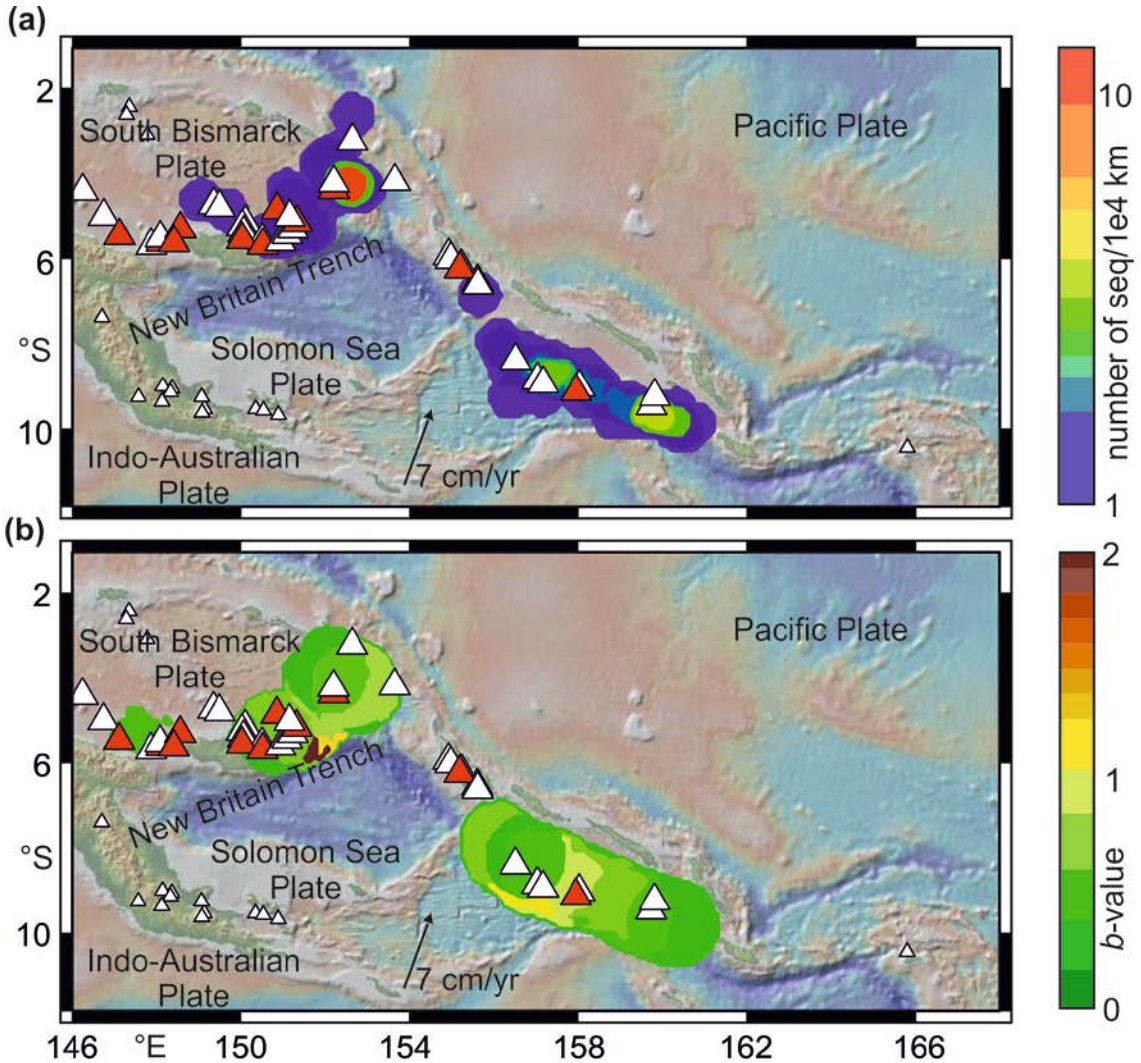

Fig. 42. Results of analyses for Solomon volcanic arc. (a) Analysis of seismic sequences density. (b) Environment heterogeneity analysis. Symbol description – see Fig. 27.

7.10. New Hebrides Arc

The New Hebrides volcanic arc is situated in the southwest Pacific Ocean. It consists of 18 volcanoes, 2 of them are submarine. Eleven volcanoes were active between 1964 and 2008. The volcanic arc results from the subduction of the Indo-Australian Plate under the Pacific and the New Hebrides Plates along the New Hebrides Trench. The velocity of the convergent movement reaches 8 cm/yr. The arc has an overall length of about 1 600 km (Addicott and Richards, 1984; Bird, 2003).

The EHB database contains over 5,200 earthquakes in the New Hebrides region. About 92 % of earthquakes belong to the Wadati-Benioff zone and to the horizontal part of the Indo-Australian plate in front of the trench. 8 % of earthquakes occurred in the overlying wedge beneath the volcanic arc.

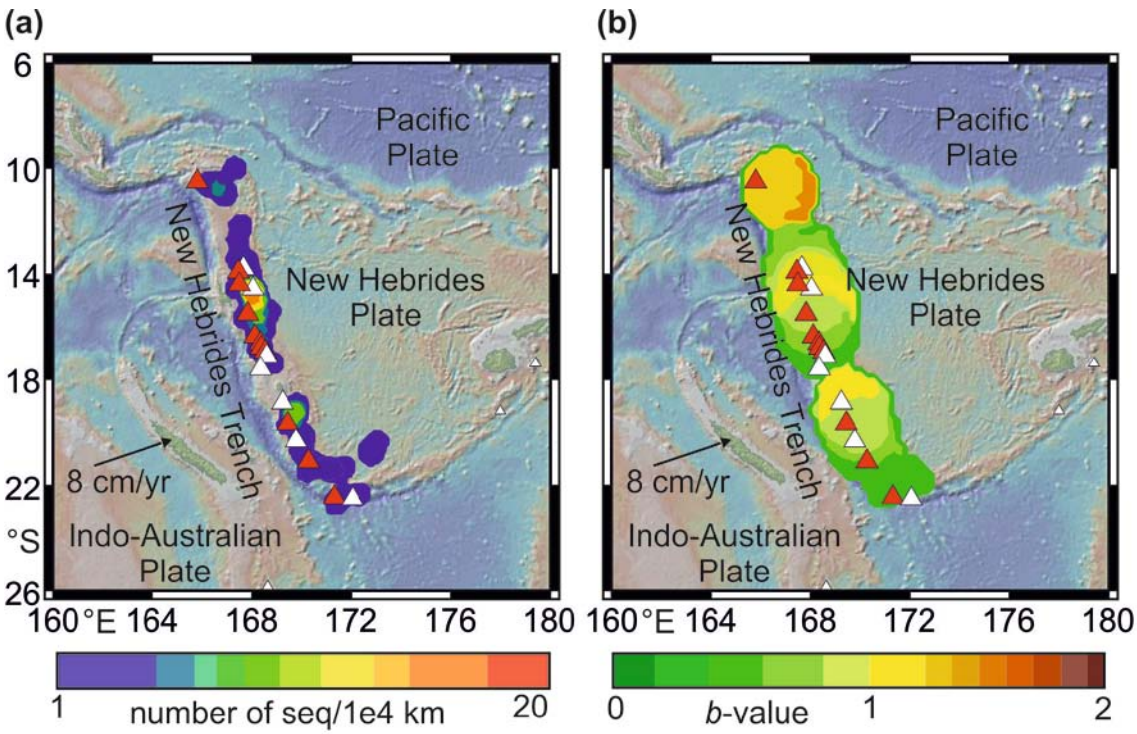

Fig. 43. Results of analyses for New Hebrides volcanic arc. (a) Analysis of seismic sequences density. (b) Environment heterogeneity analysis. Symbol description – see Fig. 27.

Both the *b*-value and the seismic sequence density analyses show several spots of increased values. Because all these spots are situated in the vicinity of the arc volcanoes, they are not studied in detail.

7.11. Tonga Arc

The Tonga volcanic arc is situated in the southeastern Pacific. It consists of 20 volcanoes, 9 of them are submarine. Twelve volcanoes were active between 1964 and 2008. The volcanic arc results from the subduction of the Pacific Plate under the Tonga Plate, derived from the Indo-Australian Plate, along the Tonga Trench. The 1,400 km long trench extends from the north, where it turns west and becomes a transform fault zone, to the

south, where it merges into the Kermadec Trench. The velocity of the convergent movement reaches 8 cm/yr (Addicott and Richards, 1984; Bird, 2003).

The EHB database contains over 10,000 earthquakes in the Tonga region. Most of them (over 97 %) belong to the Wadati-Benioff zone, including rich deep (500 – 670 km) seismicity and to the horizontal part of the Pacific plate. Only less than 3 % of events occurred in the overlying wedge beneath the volcanic arc.

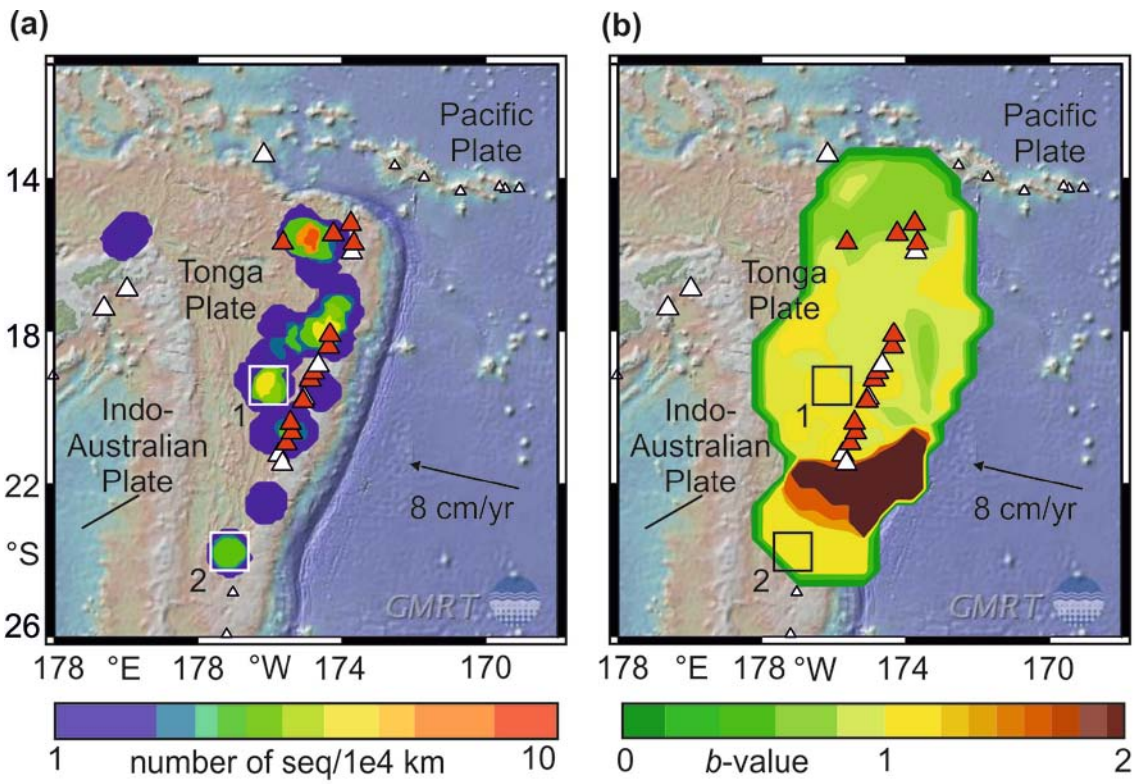

Fig. 44. Results of analyses for Tonga volcanic arc. (a) Analysis of seismic sequences density. (b) Environment heterogeneity analysis. The areas 1, 2 highlighted by rectangles are presented in detail in Figs. 45 and 47, respectively. Symbol description – see Fig. 27.

The area of increased *b*-value occurs south of the southernmost volcano of the arc. The results of seismic sequence analysis show five spots of increased values. Three of them are situated in the vicinity of arc volcanoes and they are not investigated in detail. One spot of the increased values, denoted as area 1 in Fig. 44, is situated approximately 100 km west from the volcanic arc. About 1000 meters deep roughly circular structure is situated in the area 1 (Fig. 45). The depression is probably related to the transform fault segment of the boundary between the Tonga Plate and the Indo-Australian Plate. The specific seismicity pattern probably reflects movements at the transform fault and the relation to magmatic

processes is improbable. The last spot of increased sequence density, marked as area 2, is affiliated to the Kermadec arc region (chapter 7.12.).

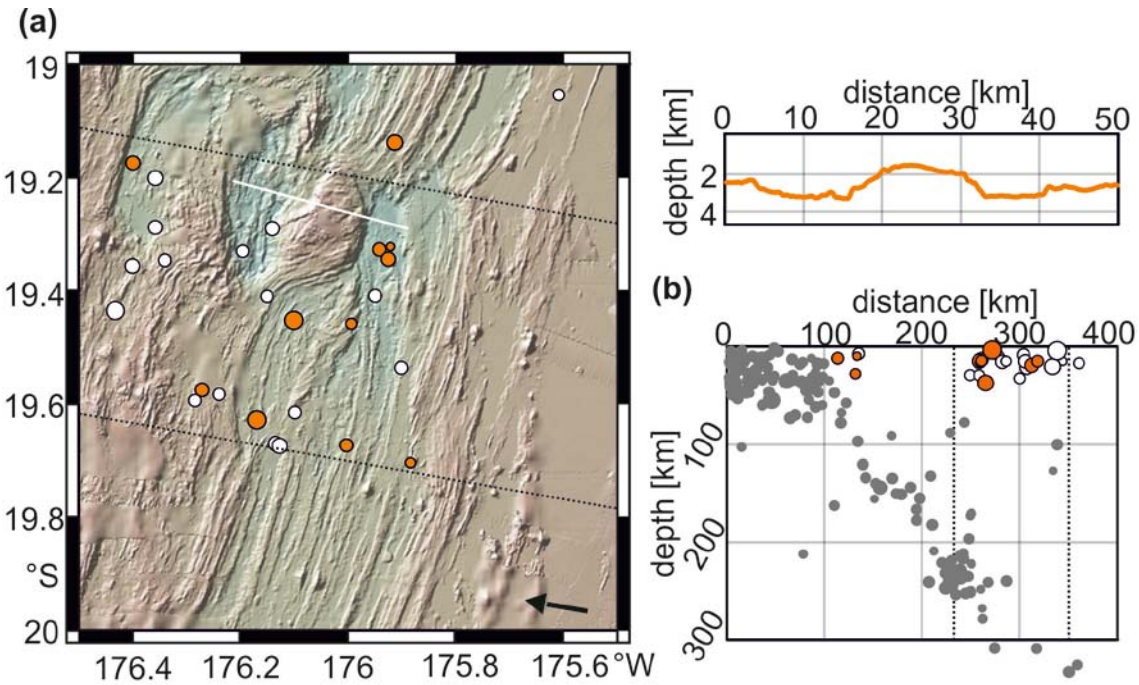

Fig. 45. Seafloor morphology and tectonic position of the area 1 in Tonga volcanic arc. (a) Map showing seafloor morphology of the studied area and the profile showing the topography of depression. The position of the profile in the map is denoted by the white line. (b) Seismic cross-section showing the tectonic position of the studied area. Symbol description – see Fig. 28.

7.12. Kermadec Arc

The Kermadec volcanic arc is situated in the southwestern Pacific and represents a southward continuation of the Tonga arc. The arc comprises 23 volcanoes, 13 of them are submarine. Five volcanoes were active between 1964 and 2008. The volcanic arc results from the subduction of the Pacific Plate under the Kermadec Plate a derivative of the Indo-Australian Plate, along the 1,600 km long Kermadec Trench. In the north, the trench merges into the Tonga Trench and reaches the New Zealand's New Island in the south. The velocity of convergent movement is about 5 cm/yr (Addicott and Richards, 1984; Bird, 2003).

The EHB database contains over 6,300 earthquakes in the Kermadec region. Most of the earthquakes (over 96 %) belong to the Wadati-Benioff zone and to the horizontal part of

the Pacific plate in front of the trench. Only about 4 % occurred in the overlying wedge beneath the volcanic arc.

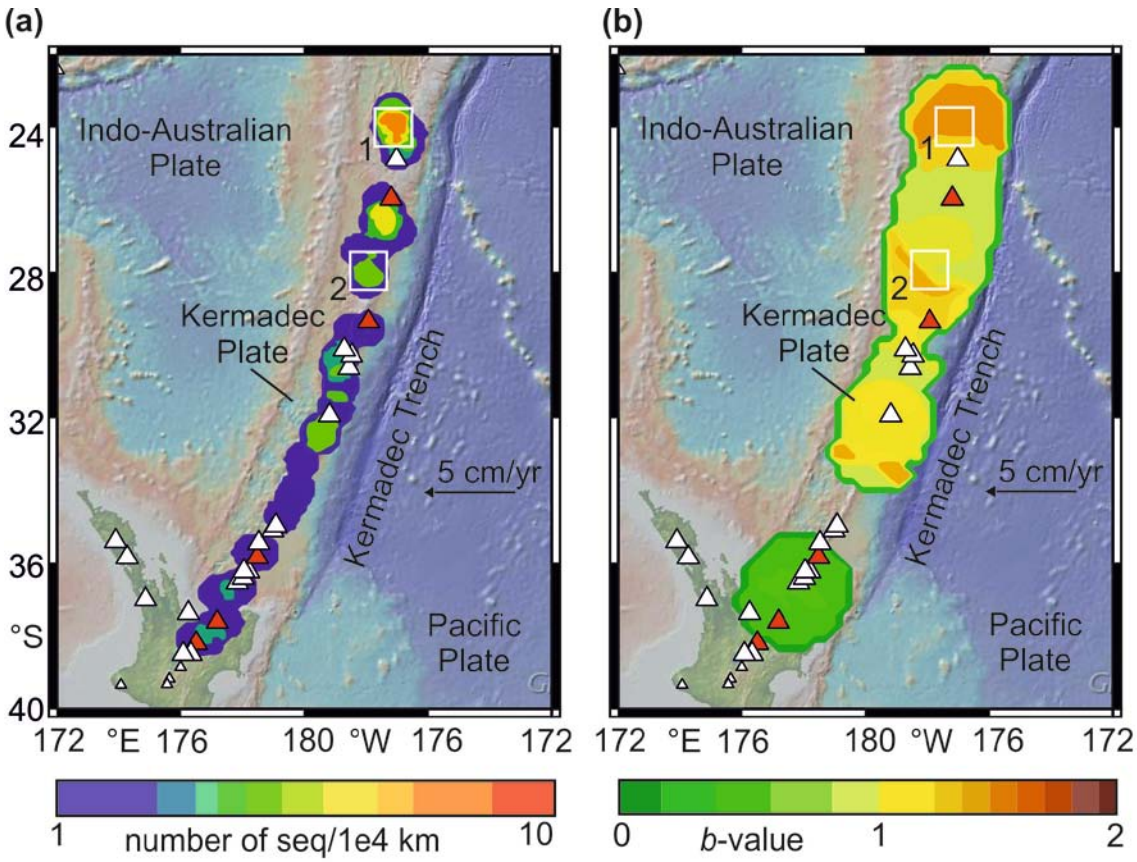

Fig. 46. Results of analyses for Kermadec volcanic arc. (a) Analysis of seismic sequences density. (b) Environment heterogeneity analysis. The areas 1, 2 highlighted by rectangles are presented in detail in Figs. 47 and 48, respectively. Symbol description – see Fig. 27.

The results of the seismic sequence density and the *b*-value analyses show several spots of increased values. Two of them are situated in the northern part of the volcanic arc, away of volcanoes tabulated in the Smithsonian database. In the northernmost anomalous spot denoted as area 1, a caldera-like seamount was found on the seafloor (Fig. 46). The seamount reaches the height about 900 meters above the seafloor, with the summit about 500 m below the sea level. Most of the earthquake epicenters are situated north of the seamount and do not correlate with the position of the seamount. Eruptions of magma at the seafloor are thus improbable.

Eruptions of magma at the seafloor are improbable in the area 2, where no remarkable seafloor morphology occurs.

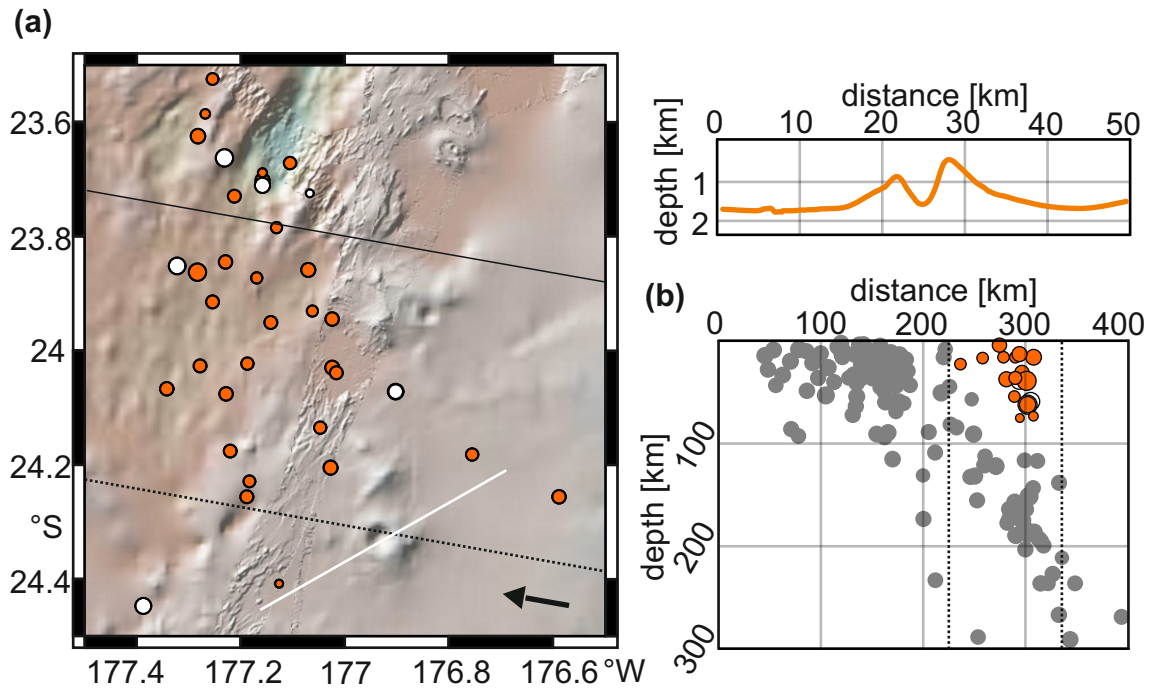

Fig. 47. Seafloor morphology and tectonic position of the area 1 in Kermadec volcanic arc. (a) Map showing seafloor morphology of the studied area and the profile showing the topography of the present seamount. The position of the profile in the map is denoted by white line. (b) Seismic cross-section showing the tectonic position of the studied area. Symbol description – see Fig. 28.

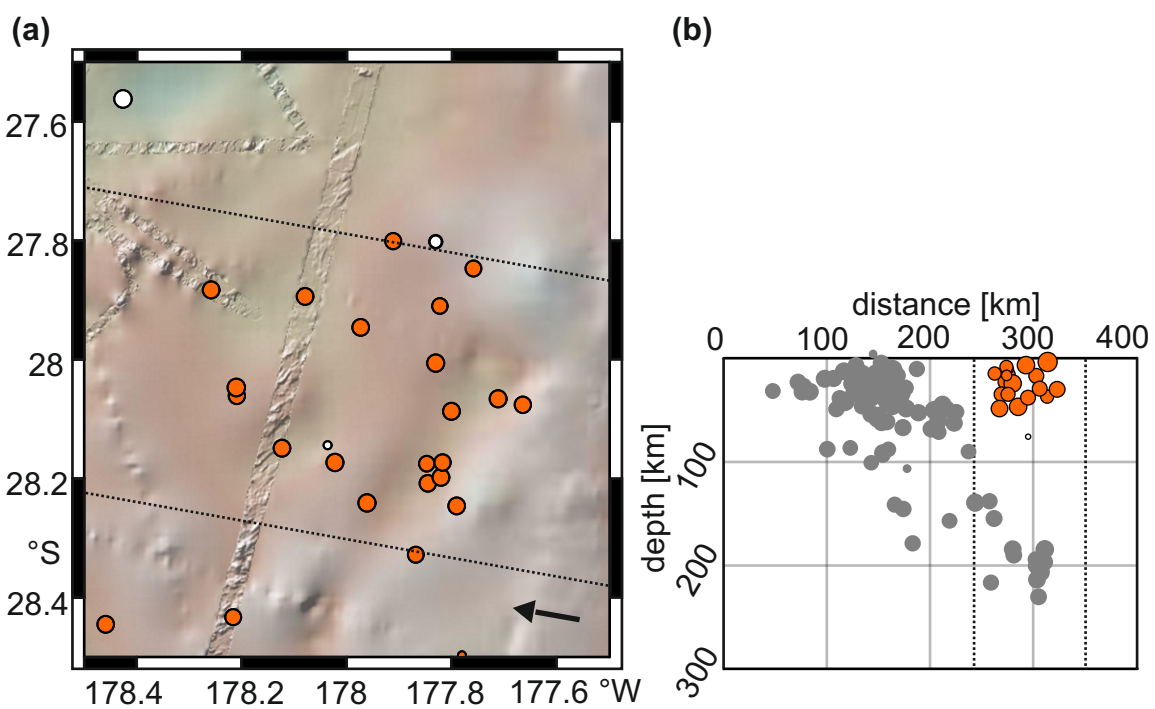

Fig. 48. Seafloor morphology and tectonic position of area 2 in Kermadec volcanic arc. (a) Map showing seafloor morphology of the studied area. (b) Seismic cross-section showing the tectonic position of the studied area. Symbol description – see Fig.

7.13. Scotia Arc

The Scotia arc is situated in the southeastern Pacific Ocean south of the South America mainland. It is formed by 9 volcanoes, 3 of which were active between 1964 and 2008. One volcano is submarine. The volcanic arc results from the subduction of the South American Plate beneath the Scotia Plate, a derivative of the South Sandwich Plate. The length of the trench is approximately 900 km and the convergence velocity reaches about 6 cm/yr (Addicott and Richards, 1984; Bird, 2003).

The EHB database contains approximately 1,900 earthquakes occurring in the Scotia arc region. More than 93 % of earthquakes belong to the Wadati-Benioff zone and to the horizontal part of the South American plate in front of the trench. 7 % of earthquakes (over 120 events) occurred in the overlying wedge beneath the volcanic arc. Such a small dataset does not enable to perform a reliable data analysis.

7.14. Lesser Antilles Arc

The Lesser Antilles volcanic arc is situated in the Caribbean Sea. It consists of 16 volcanoes, one of which is submarine. Five volcanoes were active between 1964 and 2008. The volcanic arc results from the subduction of the North American Plate under the Caribbean Plate along the Lesser Antilles Trench. The velocity of the convergent movement reaches about 2 cm/yr. The length of the trench is about 1,000 km. The trench extends from the Puerto Rico Trench in the north to the intersection with transform faults (e.g. El Pilar, Bocono faults) in the south (Addicott and Richards, 1984; Bird, 2003).

Less than 800 EHB earthquakes occurred within this region. About 87 % of earthquakes belong to the Wadati-Benioff zone and to the horizontal part of the North American Plate. 13 % (less than 100 earthquakes) occurred in the overlying wedge beneath the volcanic arc. Due to the innumerous seismicity the results obtained by the analyses are too inaccurate for any assessments.

8. Conclusions

The EHB database of hypocentral determinations was used to analyze space-time distribution of earthquake foci. The analysis of the combined space-time correlation dimension led to definition of seismic sequences, both in the time and space domains. In the space domain, the analysis reveals earthquakes triggered by the co-seismic stress transfer. In the time domain, the analysis sets the limits of long-range post-seismic stress transfer. Seismic sequences were identified by means of these analyses. The analysis of *b*-value from the Gutenberg-Richter law was done to estimate the heterogeneity of rock environment.

Seismicity patterns beneath subduction-related volcanoes at 14 island arcs were studied by means of seismic sequence density analysis and the *b*-value analysis. Submarine portions of volcanic arcs where little information on volcanic structures and processes is available, were investigated in order to constrain areas with specific seismicity pattern. Detailed analysis of bathymetry data accompanied the seismo-statistical analyses with the aim to find potential volcanic structures on the seafloor.

Three areas with specific seismicity pattern and pronounced seafloor morphology were found in the Andaman-Nicobar volcanic arc (Fig. 49a), one area in the southern part of the Ryukyu volcanic arc (Fig. 49b) and one in the Seram volcanic arc (Fig. 49c). Geographical parameters of these areas are listed in Tab. 6. It is highly probable that specific seismicity patterns in areas with pronounced seafloor morphology reflect recently active magmatic and even volcanic processes.

Tab. 6. Areas with recently active magmatic and volcanic processes.

#	Volcanic arc	Latitude	Longitude	Elevation	Related to
1	Andaman-Nicobar	12.66 °N	95.27 °E	- 3080 m	rift zone
2	Andaman-Nicobar	10.02 °N	93.97 °E	- 1050 m	subduction
3	Andaman-Nicobar	7.92 °N	94.03 °E	- 380 m	subduction
4	Ryukyu	25.62 °N	125.11 °E	- 1000 m	subduction
5	Banda and Seram	3.72 °S	127.55 °E	- 1300 m	subduction

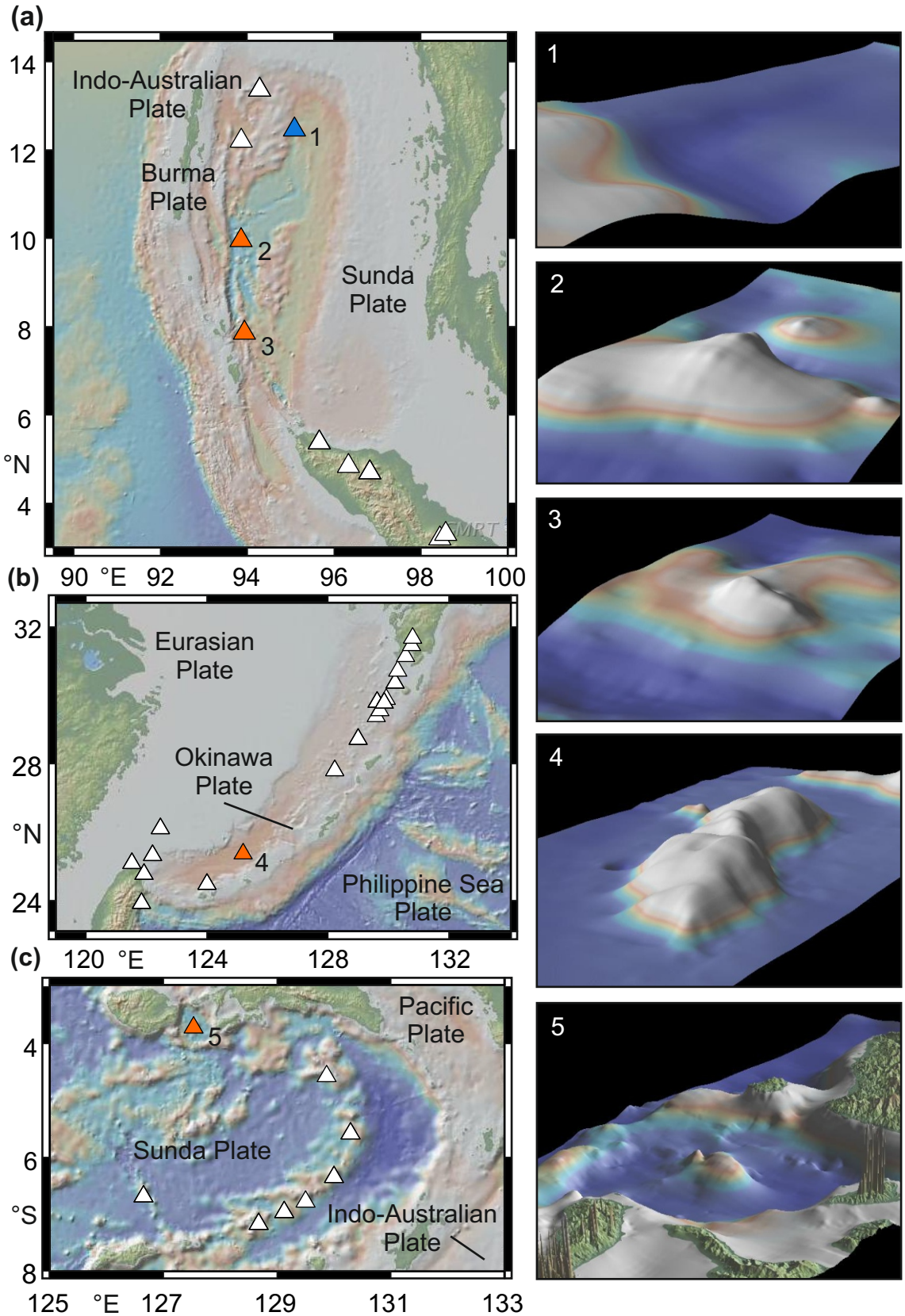

Fig. 49. Areas with recently active magmatic and volcanic processes and related morphological structures. (a) Andaman and Nicobar arc. The areas of subduction-related magmatic processes are denoted by orange triangles, the area with magmatism induced by rifting is marked by blue triangle. Volcanoes tabulated in the Smithsonian database are colored in white. (b) Ryukyu arc. (c) Banda and Seram arc.

9. References

- Addicott, W. O., Richards, P. W., 1984. Plate-tectonic map of the Circum-Pacific region. The American Assotiation of Petroleum Geologists, Tulsa, Oklahoma.
- Bayrak, Y., Bayrak, E., 2012. Regional variations and correlations of Gutenberg-Richter parameters and fractal dimension for the different seismogenic zones in Western Anatolia, *Journal of Asian Earth Sciences, Elsevier,* **58**, 98-107.
- Bhattacharyya, P., Chakrabarti, B. K., et al., 2006. Modelling Critical and Catastrophic Phenomena in Geoscience, Springer, Berlin Heidelberg, 525 pages, ISBN-10: 3540353739.
- Bird, P., 2003. An updated digital model of plate boundaries, Geochemistry, Geophysics, Geosystems, 4(3), 1027.
- Condie, K. C., 1997. Plate Tectonics and Crustal Evolution. New Mexico Institute of Mining and Technology Socorro, New Mexico, ISBN 0-7506-3386-7.
- Conrad, C., Lithqow-Bertelloni, C., 2002. How Mantle Slabs Drive Plate Tectonics. *Science*, **4**, 207-209.
- Davidson, J. P., 1991. Continental and island arcs, Encyclopedia of Earth Systems Science, Academic Press, San Diego, ISBN-10: 0122267192.
- De Rubeis, V., Dimitriu, P., Papadimitriou, E., Tosi, P., 1993. Recurrent patterns in the spatial behavior of Italian seismicity revealed by the fractal approach. *Geophysical Research Letters*, **20**, 1911-1914.
- Engdahl, E. R., Van der Hilst, R., Buland, R., 1998. Global teleseismic earthquake relocation with improved travel times and procedures for depth determination, *Bull. Seism. Soc. Am.* **88**, 722-743.
- Feder, J., 1988. Fractal dimension of the surface of the human brain, Plenum Press, New York.
- Gouyet, J. F., 1996. Physics and fractal structures. Masson Springer, Paris/New York, ISBN-10: 0387941533.
- Grassberger, P., Procaccia, I., 1983. Measuring the strangeness of strange attractors, *Physica D*, **9**, 189-208.

- Gutenberg, B., 1945. Magnitude determination for deep focus earthquakes, *Bull. Seismol. Soc. Am.*, **35**, 117–130.
- Gutenberg, B., Richter, C. F., 1945. Seismicity of the Earth, *Geological Society of America Bulletin*, **56**, 603-668.
- Hanks, C., Kanamori, H., 1979. A Moment Magnitude Scale*, Journal of Geophysical Research*, **84**, B5.
- Hanuš, V., Vaněk, J. and Špičák, A., 2000. Seismically active fracture zones and distribution of large accumulations of metals in the central part of Andean South America, *Mineralium Deposita*, **35**, 2-20.
- Hanuš, V., Vaněk, J., 1985. Structure of Wadati-Benioff zones and volcanism produced by the process of subduction, *Tectonophysics*, **112**, 51–67.
- Harris, R.A., 1998. Introduction to special section: Stress triggers, stress shadows, and implications for seismic hazard, *Journal of Geophysical Research – Solid Earth*, **103**, 24347-24358
- Heinicke, J., Fischer, T., Gaupp, R., Gotze, J., Koch, U., Konietzky, H., Stanek, K. P., 2009. Hydrothermal alteration as a trigger mechanism for earthquake swarms: the Vogtland/NW Bohemia region as a case study, *Geophysical journal international*, **178**, 1-13.
- Heuret, A., Lallemand, S., 2005. Plate motions, slab dynamics and back-arc deformation, *Physics of The Earth and Planetary Interiors*, **149(1-2)**, 31-51.
- Hill, D.P., Reasenberg, P.A., Michael, A., Arabaz, W.J. et. al., 1993. Seismicity remotely triggered by the magnitude 7.3 Landers, Clifornia, earthquake. *Science*, **260**, 1617-1623.
- Honthaas, Ch., Maury, R. C., Priadi, B., Bellon, H., Cotten, J., 2008. The Plio–Quaternary Ambon arc, Eastern Indonesia. *Tectonophysics*, **301**, 261–281.
- Kagan, Y.Y., Knopoff, L., 1980. Spatial distribution of earthquakes – the 2-point correlation function, *Geophysical Journal of the Royal Astronomical Society*, **62**, 303-320.
- Kamesh Raju, K. A., Ray, D., Mudholkar, A., et al., 2012. Tectonic and volcanic implications of a cratered seamount off Nicobar Island, Andaman Sea, *J. Asian Earth Sci.*, **56**, 42-53.
- Kapelner, A., Schupack, V., Golomshtok, M, Alicea, J., 2002. Fractal Dimension of Broccoli, The Physics Factbook, http://hypertextbook.com/facts/2002), 17.6.2013.

- Konstantinou, I. K., Schlindwein, V., 2002. Nature, wavefield properties and source mechanism of volcanic tremor: a review, *Journal of Volcanology and Geothermal Research*, **119**, 161-187.
- Kornreich, D., 1999. What is a dimension?, Cornell University, New York, United States, http://curious.astro.cornell.edu/, 18.7.2013.
- Lowrie W., *(Ed.),* 2007. Fundamentals of Geophysics, Cambridge University Press, Cambridge, United Kingdom, ISBN-10: 0521675960.
- Mandelbrot, B. B., 1982. The fractal geometry of nature. Macmillan, United States, ISBN-10: 0716711869.
- Mandelbrot, B. B., 2004. Fractals and Chaos, Springer, Berlin, ISBN 10: 0387201580.
- McCartney, M., Abernethy, G., Gault, L., 2010. The Divider Dimension of the Irish Coast, *Irish Geography*, **43**, 277-284.
- Michelson, A. A., 1917. The Laws of Elastico-Viscous Flow, *Proc Natl Acad Sci USA*, **3(5)**, 319–323.
- Mogi, K., 1967. Earthquakes and fractures. *Tectonophysics*, **5**, 35-55.
- Murru, M., Montuori, C., Console, R., Lisi, A., 2005. Mapping of the b value anomalies beneath Mt. Etna, Italy, during July-August 2001 lateral eruption, *Geophysical Research Letters*, **32**, 5.
- Neumann Van Padang, M., 1951. Catalogue of the Active Volcanoes of the World Including Solfatara Fields (1951-1967). International Assotiation of Volcanology, Rome.
- Newhall, C. G., Self, S., 1982. The volcanic explosivity index (VEI) an estimate of explosive magnitude for historical volcanism, *Journal of Geophysical Research: Oceans*, **87**, 1231–1238.
- Park, R. G., 1983. Foundations of Structural Geology, Blackie & Son Ltd, London, England, ISBN-10: 074875802X.
- Reid, H.F., 1910. The Mechanics of the Earthquake, The California Earthquake of April 18, 1906, Report of the State Investigation Commission, Carnegie Institution of Washington, Washington, D.C., **2**, 16-28.
- Richter, C. F. 1935. An instrumental earthquake magnitude scale. *Bull. Seismol. Soc. Am.*, **25**, 1–32.
- Roman, D. C., Cashman, K. V., 2006. The origin of volcano-tectonic earthquake swarms, *Geology*, **34**, 457–460.

- Sapoval, B., 2001. Universalités et fractales, Flammarion-Champs, ISBN 2-08-081466-4.
- Schmidt, M. X., Poli, S., 1998. Experimentally based water budgets for dehydrating slabs and consequences for arc magma generation, *Earth Planetary Sci. Lett.* **163,** 361–379.
- Siebert, L., Simkin, T., 2002-. Volcanoes of the World: an Illustrated Catalog of Holocene Volcanoes and their Eruptions. Smithsonian Institution, Global Volcanism Program Digital Information Series, GVP-3, (http://www.volcano.si.edu/world/).
- Sigurdsson, H., Houghton, B., McNutt, S. R., Rymer, H., Stix, J., 1999. Encyclopedia of Volcanoes, Academic Press, A Harcourt Science and Technology Company, ISBN-10: 012643140X.
- Špičák, A., Hanuš, V., Vaněk J., 2002. Seismic activity around and under Krakatau volcano, Sunda arc: Constraints to the source region of island arc volcanics, *Stud. Geophys. Geod.*, 46, 545– 565.
- Špičák, A., Hanuš, V., Vaněk J., 2004. Seismicity pattern: an indicator of source region of volcanism at convergent plate margins. *Physics of the Earth and Planetary Interiors*, **141**, 303-326.
- Špičák, A., Hanuš, V., Vaněk J., 2005. Seismotectonic pattern and the source region of volcanism in the central part of Sunda Arc. *Journal of Asian Earth Sciences*, **25**, 583-600.
- Špičák, A., Hanuš, V., Vaněk, J., Běhounková, M., 2007. Internal tectonic structure of the Central American Wadati-Benioff zone based on analysis of aftershock sequences, *Journal of geophysical research-solid earth*, **112**.
- Špičák, A., Horálek, J., 2001. Possible role of fluids in the process of earthquake swarm generation in the West Bohemia/Vogtland seismoactive region, *Tectonophysics*, **336**, 151.
- Špičák, A., Kozák, J., Vaněk J., Hanuš, V., 2008. The Krakatau volcano 125 years after the catastrophic eruption (August 27, 1883), Studia Geophysica et Geodaetica, 52(3), 449-454.
- Špičák, A., Kuna, V., Vaněk, J., 2013b. Earthquake occurrence reveals magma ascent beneath volcanoes and seamounts in Banda region, *Bull. Volc.,* submitted.

- Špičák, A., Vaněk J., Hanuš, V., 2011. Recent plumbing system of the Krakatau volcano revealed by teleseismic earthquake distribution, International Journal of Earth Sciences, 100(6), 1375-1381.
- Špičák, A., Vaněk, J., 2013a. Earthquake clustering in the tectonic pattern and volcanism of the Andaman Sea region, *Tectonophysics*, submitted.
- Špičák, A., Vaněk, J., 2013c. April 2013 earthquake swarm, southern Ryukyu: consequence of magma ascent, *in preparation.*
- Špičák, A., Vaněk, J., Hanuš, V., 2009. Volcanic plumbing system and seismically active column in the volcanic arc of the Izu-Bonin subduction zone, *Geophys. J. Intern.*, **179**, 1301-1312.
- Syracuse, E. M., Abers, G. A., 2006. Global compilation of variations in slab depth beneath arc volcanoes and implications, *Geochem. Geophys. Geosyst.*, **7**, 1525-2027.
- Uyeda, S., 1982. Subduction zones: an introduction to comparative subductology. *Tectonophysics*, **81**, 133-159.
- Uyeda, S., Kanamori, H., 1979. Back-arc opening and the mode of subduction. *Journal Geophys. Res.,* **84**, 1049-1061.
- Vaněk, J., Špičák, A., Hanuš, V., 2000. Position of the disastrous 1999 Puebla earthquake in the seismotectonic pattern of Mexico. *Bull. Seis. Soc. Amer.*, **90**, 786-789.
- Venzke, E., Wunderman, R. W., McClelland, L., Simkin, T., Luhr, J. F., Siebert, L., Mayberry, G. and Sennert, S., 2002-. Global Volcanism, 1968 to the Present. Smithsonian Institution, Global Volcanism Program Digital Information Series, GVP-4, http://www.volcano.si.edu/reports/.
- Yuasa, M., Murakami, F., Saito, E., Watanabe K, 1991. Submarine topography of seamounts on the volcanic front of the Izu-Ogasawara (Bonin) Arc, *Bull. Geol. Surv. Japan*, **42**, 703-743.